SYNTHESIS AND STRUCTURAL CHARACTERIZATION OF MULTIFUNCTIONAL TI ALLOY: GUM METAL

A THESIS SUBMITTED TO
THE GRADUATE SCHOOL OF NATURAL AND APPLIED SCIENCES
OF
MIDDLE EAST TECHNICAL UNIVERSITY

BY

ORKUN ELÇİN

IN PARTIAL FULFILLMENT OF THE REQUIREMENTS
FOR
THE DEGREE OF MASTER OF SCIENCE
IN
METALLURGICAL AND MATERIALS ENGINEERING

JANUARY 2020

Approval of the thesis:

SYNTHESIS AND STRUCTURAL CHARACTERIZATION OF MULTIFUNCTIONAL TI ALLOY: GUM METAL

submitted by **ORKUN ELÇİN** in partial fulfillment of the requirements for the degree of **Master of Science** i**n Metallurgical and Materials Engineering, Middle East Technical University** by,

Prof. Dr. Halil Kalıpçılar
Dean, Graduate School of **Natural and Applied Sciences** _____

Prof. Dr. Hakan Gür
Head of the Department, **Met. and Mat. Eng.** _____

Prof. Dr. M. Vedat Akdeniz
Supervisor, **Met. and Mat. Eng., METU** _____

Prof. Dr. Amdulla Mekhrabov
Co-Supervisor, **Met. and Mat. Eng., METU** _____

Examining Committee Members:

Prof. Dr. Rıza Gürbüz
Metallurgical and Material Eng., METU _____

Prof. Dr. M. Vedat Akdeniz
Metallurgical and Material Eng., METU _____

Prof. Dr. Amdulla Mekhrabov
Metallurgical and Material Eng., METU _____

Prof. Dr. Cevdet Kaynak
Metallurgical and Material Eng., METU _____

Assist. Prof. Dr. Mehmet Yıldırım
Metallurgical and Material Eng., KTUN _____

Date: 31.01.2020

I hereby declare that all information in this document has been obtained and presented in accordance with academic rules and ethical conduct. I also declare that, as required by these rules and conduct, I have fully cited and referenced all material and results that are not original to this work.

Name, Last name : Orkun Elçin

Signature :

ABSTRACT

SYNTHESIS AND STRUCTURAL CHARACTERIZATION OF MULTIFUNCTIONAL TI ALLOY: GUM METAL

Elçin, Orkun
Master of Science, Metallurgical and Materials Engineering
Supervisor: Prof. Dr. M. Vedat Akdeniz
Co-Supervisor: Assoc. Prof. Dr. Amdulla Mekhrabov

January 2020, 82 pages

Gum metal (Ti-23Nb-0.7Ta-2Zr-1.2O at%), a newly discovered titanium alloy, is considered as a suitable unique alloy for structural applications in aerospace, sports equipment, industrial, and especially in biomedical areas because of their outstanding properties such as high yield strength (up to 2000 MPa) with low elastic modulus (50 GPa), and biocompatibility. Furthermore, in the heavily deformed state, it still possesses an ultra-low elastic modulus, ultra-high-strength, large elasticity (up to 2.5%), Elinvar, and Invar properties. These exclusive mechanical and physical properties are mainly attributed to their extraordinary deformation mechanism. However, alloy design and production of gum metal are quite difficult since it consists of raw materials that are difficult to work with and tend to oxidize quite easily. In addition, these raw materials are quite challenging to forge an alloy with a homogeneous structure. Therefore, it is generally produced by powder metallurgy, a very laborious, sensitive, and troubled production. It is important to develop a new production process since this method is not suitable for mass production.

This thesis focuses on three main subjects: (i) to develop the candidate alloys exhibit gum metal properties with the help of the theoretical calculations, (ii) to be able to produce alloys successfully by using the arc melting furnace which is suitable for mass production, easier and conventional production method rather than powder metallurgy, and (iii) to investigate the effects of alloying elements on deformation mechanism, structural and mechanical properties of $Ti_{71.8+n}Nb_{25-n}Zr_2O_{1.2}$ base alloy and approval of the validity of theoretical estimations proposed for single-phase gum metal alloy.

According to theoretical calculations, three different forms, (S1) Ti-23.8Nb-2Zr-1.2O (at%), (S2) Ti-23Nb-0.93V-2Zr-1.2O (at%) and (S3) Ti-25Nb-0.7Ta-2Zr-2Al-1.2O (at%), were determined and casted successfully in an atmosphere-controlled arc melting furnace. The chemical characterization, mineralogical analyses, and mechanical properties of these alloys were investigated by using XRD, DSC, SEM, EDS, microhardness, and compression test instruments.

It has been observed that these three alloys were prepared composing of only a single phase with homogeneous morphology and elemental composition. On account of the incorporation of various elements to the base composition, from alpha to beta phase transition temperature were reduced as much as 100 degrees C and mechanical properties were improved significantly. Around 85% reduction in thickness with the compression tests were obtained with no apparent crack formation. Also, no noticeable increase in hardness emerged with this deformation. In the end, these mechanical and structural investigations suggest that all the prepared compositions within the scope of this work could be in the gum metal family.

Keywords: Ti Based Alloy, Gum Metal, Arc Melting, Deformation Mechanism

ÖZ

ÇOK FONKSİYONLU Tİ ALAŞIM: SAKIZ METAL'İN SENTEZLENMESİ VE YAPISAL KARAKTERİZASYONU

Elçin, Orkun
Yüksek Lisans, Metalurji ve Malzeme Mühendisliği
Tez Yöneticisi: Prof. Dr. M. Vedat Akdeniz
Ortak Tez Yöneticisi: Prof. Dr. Amdulla Mekhrabov

Ocak 2020, 82 sayfa

Son yıllarda keşfedilen bir titanyum alaşım türü olan sakız metal (Ti-23Nb-07Ta-2Zr-O) sahip olduğu olağanüstü düşük elastik modülü (50 GPa), yüksek akma dayanımı (2000 MPa'ya kadar), ve biyouyumluluk gibi özellikleri sayesinde spor malzemeleri, havacılık, endüstriyel ve özellikle biyomedikal alanlarda kullanılabilecek benzersiz bir alaşım türü olarak düşünülebilir. Ayrıca, bütün bu ayırt edici özellikleri şiddetli deformasyon halinde dahi koruyabilmesi ve Elinvar-Invar özelliklerine sahip olması sakız metali eşsiz bir malzeme haline getirmektedir. Sakız metalin sahip olduğu üstün mekanik ve fiziksel özellikler olağandışı deformasyon mekanizması ile ilişkilidir. Fakat, sakız metalin çalışılması zor olan ve oldukça kolay oksitlenme eğilimi gösteren hammaddelerden oluşması, yapının homojen bir şekilde üretilmesini zorlaştırmaktadır. Bu nedenle, üretimi için oldukça hassas, zahmetli ve sorunlu bir yöntem olan toz metalurjisi yöntemi kullanılmaktadır. Toz metalurjisi seri üretime uygun bir yöntem olmadığı için yeni bir üretim methodu geliştirmek önemlidir.

Bu tez üç ana konuya odaklanmaktadır: (i) teorik hesaplamalar yardımıyla sakız metal özellikleri sergileyen farklı alaşımları geliştirmek, (ii) seri üretime uygun, toz metalurjisinden daha kolay ve geleneksel bir yöntem olan ark ergitme fırınını kullanarak alaşımları başarılı bir şekilde üretmek ve (iii) alaşım elementlerinin $Ti_{71.8+n}Nb_{25-n}Zr_2O_{1.2}$ temel alaşımının deformasyon mekanizması, yapısal ve mekanik özellikleri üzerindeki etkilerini araştırmak, ve tek fazlı sakız metal alaşımı için önerilen teorik tahminlerin geçerliliğinin onaylamak.

Teorik hesaplamalara göre, üç farklı yapı, (S1) Ti-23.8Nb-2Zr-1.2O (at%), (S2) Ti-23Nb-0.93V-2Zr-1.2O (at%) ve (S3) Ti-25Nb-0.7Ta-2Zr-2Al-1.2O (at%) belirlenmiş ve atmosfer kontrollü ark eritme fırınına başarıyla dökülmüştür.

Bu alaşımların kimyasal karakterizasyonu SEM, EDS, termal kararlılığı DSC, mineralojik analizleri XRD ve mekanik özellikleri ise mikro sertlik ve basma testi metodları kullanılarak araştırılmıştır.

Hazırlanan üç alaşımın, tek fazlı, homojen morfolojiye ve elementel kompozisyona sahip olduğu gözlenmiştir. Temel alaşıma çeşitli elementlerin dahil edilmesi ile alfa fazından beta fazına geçiş sıcaklığı 100 °C' ye kadar düşürülmüş ve mekanik özelliklerin önemli ölçüde iyileştirildiği gözlemlenmiştir. Basma testlerinde numune kalınlığı %85 oranında azaltılmasına rağmen, görünür bir çatlak oluşmamaktadır. Ayrıca, bu deformasyon sonucunda dahi sertlikte belirgin bir artış ortaya çıkmamıştır. Sonuç olarak, elde edilen mekanik ve yapısal bulgular, bu çalışma kapsamında hazırlanan tüm bileşimlerin sakız metal ailesinde olabileceğini düşündürmektedir.

Anahtar Kelimeler: Ti Alaşımı, Sakız Metal, Ark Ergitme, Deformasyon Mekanizması

To my family, who made it all worthwhile…

ACKNOWLEDGMENTS

The study, which is the subject of this thesis, was conducted at the Department of Metallurgical and Materials Engineering of Middle East Technical University. I am grateful to the Department of Metallurgical and Materials Engineering of Middle East Technical University for giving me the opportunity to conduct a Master of Science study.

Firstly, I would like to express my gratitude to my supervisor Prof. Dr. M. Vedat Akdeniz, and my co-supervisor, Prof. Dr. Amdulla Mekhrabov, for their support, guidance, and encouragement during this independent research.

I would like to thank Nasuh Arık, Esra Babür, Ragıp Kızıltaş, Duygu Keleş, Beyza Nur Kuru, and colleagues working for BOREN for their help and support in my studies.

This study would not be present without the support, endless understanding and contribution of friends who are members of NOVALAB and my friends Muammer Demiralp and Muhammed Juneyd Aslam. I also thank Yusuf Yıldırım, Serkan Yılmaz, and Nilüfer Özel for their continuous help and understanding.

My sincerest thanks go to my entire family for their regardless, lifelong support, particularly to my parents Zehra and Erkan Elçin.

Finally, I would like to thank BOREN for giving me an opportunity to succeed in this study.

TABLE OF CONTENTS

LIST OF TABLES

TABLES

LIST OF FIGURES

FIGURES

LIST OF SYMBOLS AND ABBREVIATIONS

β	Body centered cubic
α	Hexagonal closed packed
α’	Hexagonal closed packed
α″	Orthorhombic crystal system
ω	Non close hexagonal crystal system
SIM	Stress-induced martensitic transformation
BCC	Body centered cubic
HCP	Hexagonal closed packed
C.W.	Cold worked
Md	D orbital energy
Bo	Bond order value
e/a	Valance electron number
XRD	X-ray Diffraction
SEM	Scanning electron microscope
TEM	Transmission electron microscope
EDX	Energy dispersive X-ray spectroscopy
DSC	Differential scanning calorimeter

CHAPTER 1

INTRODUCTION

Titanium alloys are unique materials for structural applications in automotive, aerospace, and biomedical industrial areas because of their high yield strength, low elastic modulus, low density, biocompatibility, and superior corrosion resistance. For the industrial regions mentioned above, continuous efforts are ongoing for the development of various microstructure and mechanical properties of titanium alloys by different alloying and processing methods. As a result of these studies, especially beta phase titanium alloys have gained popularity in recent times due to their following properties; high yield strength with the low elastic modulus (superelasticity), shape memory manner, and biocompatibility. [1-8]. Nonetheless, beta-titanium alloys produced up to recent years have not reached the satisfactory requirements since elastic modulus and yield strength values can change with the changing of heat and the plastic deformation as a result of dislocation activity.

Fortunately, a new beta titanium alloy called “Gum Metal” was developed by Saito and his team in Toyota R&D in 2003. [9]. This alloy is a band of multi-component titanium alloys with the combination of V-A and IV-A elements, which stabilize β-phase and reduce elastic modulus without changing the yield strength in titanium alloys, and oxygen which inhibits the dislocation activity by forming a cluster with zirconium. When the alloy is exposed to severe cold working, deformation occurs by twinning, stress-induced martensite, and most importantly, nano disturbed slip bands, which is called “Giant Fault” instead of dislocation aid activity [9-11]. Consequently, cold work hardening does not occur in this alloy under the presence of nano-disturbed slip bands [10-14]. The deformation mechanism of Gum Metal is mentioned in more detail in Chapter 2.2.2.

Gum Metal alloys can be easily distinguishable from the ordinary beta phase titanium alloys from their Invar property (temperature-independent expansion and contraction) and Elinvar property (temperature invariant elasticity) from -200 to +250 ^{o}C, high yield strength (up to 2000MPa) with low elastic modulus (50GPa), large elastic deformation (2,5%), super cold-workability (up to 99%), extra-ordinary deformation mechanism and the accompanying defect structure [15-17]. Furthermore, it has been shown to possess many interesting properties such as superplasticity at room temperature without extensive work hardening. In the heavily deformed state, it still possesses an ultra-low elastic modulus, ultra-high-strength, and large elasticity. These exclusive mechanical and physical properties are mainly attributed to their extraordinary deformation mechanism. However, it is complicated to determine the suitable composition of the alloy that exhibits gum metal properties because complex and difficult theoretical calculations are required to decide the composition. Moreover, the production of gum metal is quite difficult. Raw materials tend to oxidize and are challenging in terms of structural and compositional homogeneity in the alloy formation. For gum metals, it is also a challenge to form a desired shape during the casting process due to high viscosity. Therefore, it is generally produced by a very laborious, sensitive, and troubled production method such as powder metallurgy.

This study aims to develop new alloy compositions which are considered as gum metals with the help of theoretical calculations regarding the difficulties mentioned above, ark melting furnace techniques has been adopted within the scope of this work to produce this alloy which can be suitable for mass production in the future due to its easier and conventional nature by comparison to powder metallurgy. Also, one of the main objectives is to examine the effect of V, Ta, and Al on deformation mechanism, structural, and mechanical properties of $Ti_{71.8+n}Nb_{25-n}Zr_2O_{1.2}$ base alloy. The approval of the validity of theoretical estimations proposed for single-phase gum metal alloy is tried to understand in detail as well.

Furthermore, a direct correlation between microstructure and melting point has been attempted to provide in order to increase castability. In this certain point, the major

focus was directed toward which alloying element addition on the base alloy provides the high casting ability without spoiling the gum metal properties.

With respect to theoretical calculation, the alloy (S1) Ti-23.8Nb-2Zr-1.2O, likely to have gum metal property, was determined as the base alloy.

During the melting of S1, the molding was not obtained presumably due to the high viscosity. Hence, the melt was solidified as a button shape.

In order to increase the casting ability and the final mechanical properties, V has been added to the base alloy (S1), resulting in S2 (Ti-23Nb-0.93V-2Zr-1.2O) composition. Melting of S2 revealed that molding was not possible nonetheless. Nevertheless, mechanical properties and beta phase stability was increased as anticipated. Also, the effect of V has been studied in terms of deformation mechanism, which is one of the crucial parameters for the reveling of the gum metal aspect of any alloy composition.

The last approach was taken as the addition of Al and Ta's combination resulting in S3 composition (Ti-25Nb-0.7Ta-2Zr-2Al-1.2O). Once more, shaping was not achieved even though by suction molding technique was employed. However, the elastic modulus was decreased with respect to increased yield strength. Beta stability was increased due to change in the phase transition of alpha to beta and change in the relative amount of Nb.

This thesis begins with giving the basic information about titanium alloys, gum metal alloys, and theoretical calculation used to obtain the gum metal composition in Chapter 2. The experimental procedure used for the production and characterization of the candidate alloys is given in Chapter 3. In Chapter 4, the effect of alloying elements addition on solidification characteristic and phase transition temperature of $Ti_{71.8+n}Nb_{25-n}Zr_2O_{1.2}$ base alloy were examined. This study continues with the investigation of the mechanical properties and deformation mechanisms of candidate alloys. Finally, within the scope of this work, conclusion and future work have been given in Chapter 5.

CHAPTER 2

LITERATURE REVIEW

A newly discovered beta-type titanium alloy ((Ti-23Nb-0.7Ta-2Zr-1.2O at%) is called “Gum Metal” since the elastic deformation is quite extensive, and cold work hardening does not occur [15-17]. Experiments and observations of microstructures of severe cold-worked alloy support the assumption that ideal shear mechanism under the deformation process occurs mostly by nano-disturbed slip band “Giant Fault.” Deformation behavior is related to the primary alloying elements and microstructure. Moreover, phase transformation during the deformation process can also occur. To help understand the results presented in this study, this section begins with a concise overview of the phase classifications of titanium alloys and then continued with the general information of gum metal and its deformation mechanism.

2.1 Classification of Titanium Alloys

In general, the crystal structure has a significant effect on the mechanical and physicochemical properties of materials such as yield strength, ductility, corrosion resistance, weldability, wearing resistance, creep and fatigue properties, etc. For example, the deformation capability of the BCC structure is higher than the densely packed HCP structure due to the higher number of active slip systems. Pure titanium has two allotropic crystal structures: hexagonal closed packed (HCP) and body-centered cubic (BCC) structure. Alpha-“α”-(HCP), the phase is stable up to 882±2 ^{o}C and above that temperature, it is transformed into the beta-“β”-(BCC) phase [18, 19]. The crystal structures of alpha (HCP) and beta (BCC) titanium are schematically shown in Figure 2.1 [20]. Alloying elements addition to pure titanium could affect the crystal structure and phase transformation temperature, as shown in Figure 2.2.

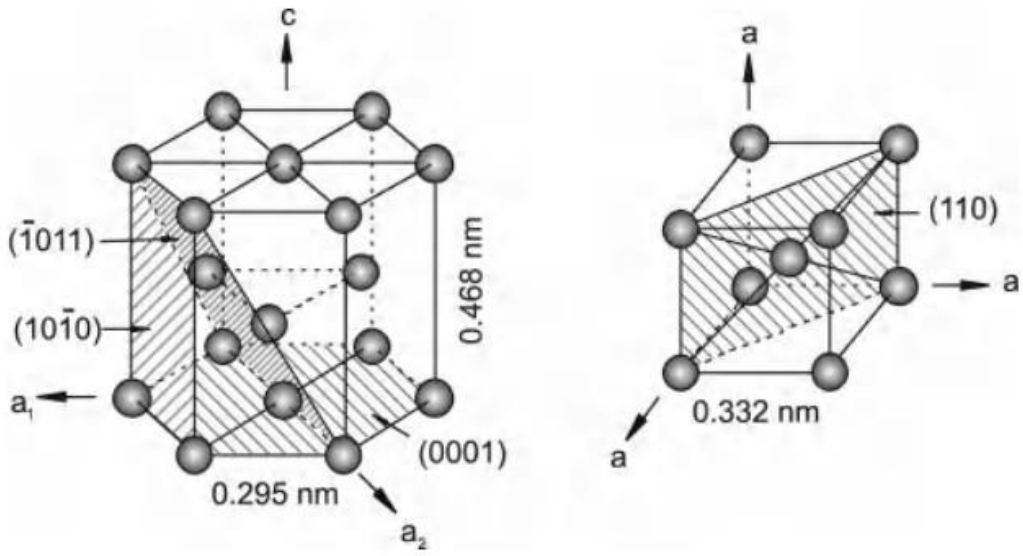

Figure 2.1 Crystal structure of HCP and BCC phase [20].

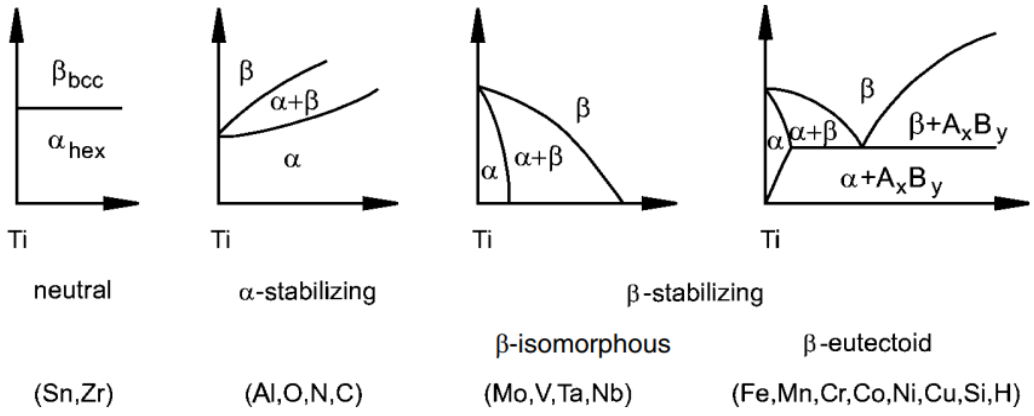

Figure 2.2 The effects of alloying elements on the phase diagram of titanium alloys [20].

According to this effect, elements are classified as alpha, beta, or neutral stabilizers [20].

- Sn and Zr are one of the neutral elements. The neutral stabilizer elements almost have no effect on the alpha-beta transition line; however, they strengthen the alpha phase at first [21].

- The α (alpha) stabilizer elements extend the higher temperature phase area for the alpha phase. Aluminum, nitrogen, oxygen, and carbon are essential interstitial

elements among the alpha stabilizers. Although it is useful to add low-density aluminum to titanium, though it cannot be put in more than 8% by weight because alloy becomes exceptionally brittle. The addition of oxygen increases the strength and elastic modulus [21].

- The β (beta) stabilizer elements depress the alpha-beta transition temperature. Beta stabilizer elements can be subdivided into two categories: beta-isomorphous and beta-eutectic [21].

  - Beta-isomorphous elements (molybdenum, vanadium, tantalum, niobium) have complete solubility in pure titanium [20].

  - Beta-eutectic elements (iron, manganese, chromium, cobalt, nickel, copper, silicon, hydrogen) have limited solubility in titanium; thus, intermetallic compounds can be formed by the addition of these elements [20].

In this respect, titanium alloys are usually categorized as α, α + β and β alloys, with further subsections, such as near α, near β, and metastable β based on the proximity of the composition to the α-β transition line, as shown in Figure 2.3 [21]. α (HCP) titanium alloys comprise entirely or mostly the HCP phase, and they are alloyed with alpha stabilizers or neutral elements. Even after the addition of β (BCC) stabilizing elements to the alpha titanium, the alloy continues to exist in the HCP phase/crystal, and this alloy is categorized as near α alloy. α + β alloys occur when both HCP and BCC phase exist in the structure. The volume percentage of the beta phase ranges from 5 to 40 percent in α + β alloys. If the sufficient β stabilizing elements are added to pure titanium, the β phase does not show martensitic transformation during quenching to room temperature yet it still lies in the α+β field, this alloy is considered as metastable β titanium. The metastable β titanium alloy remains appear to be existing at the right of the martensitic start (Ms) line at room temperature, but it still lies within the two-phase region. Stable β alloys lie in the β field region at room temperature. Stable β alloys can be classified as beta-isomorphous and beta-eutectic. Beta-isomorphous elements are entirely soluble in the titanium; on the other hand, beta-eutectic elements have limited solubility in the titanium [20-21].

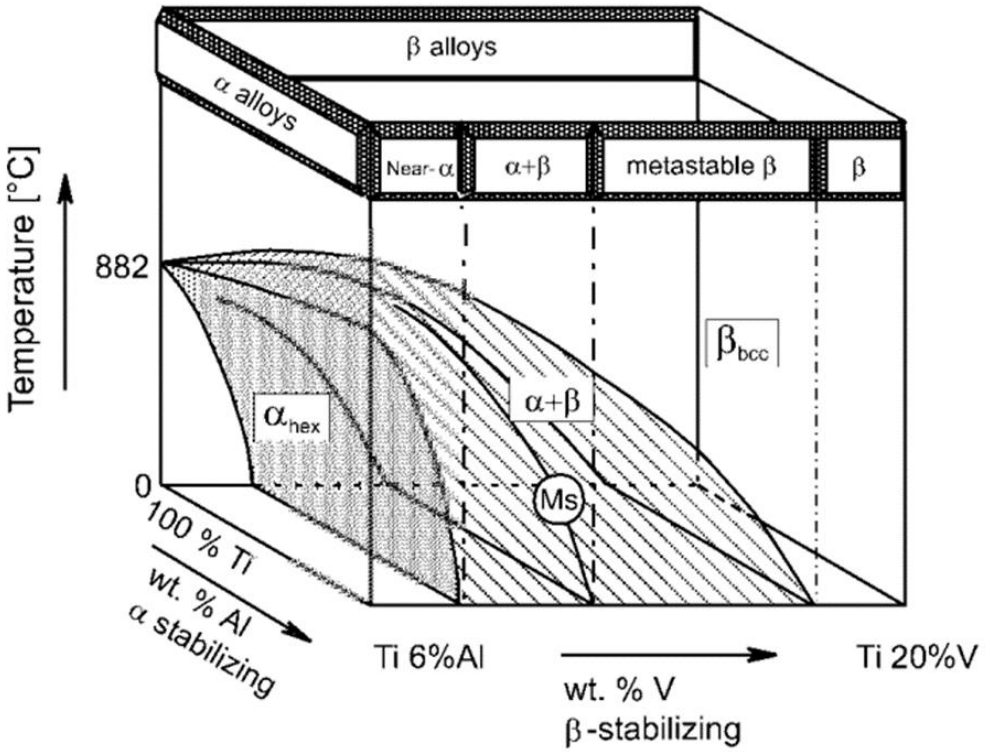

Figure 2.3 3D phase diagram of titanium alloy [21].

Each phase of titanium alloys has specific characteristic properties which are listed below, and they are listed in Table 2.1:

- Pure titanium and Alpha alloys α (HCP) have good weldability. However, they are non-heat treatable in nature. Further, they possess low to medium yield strength, good toughness, optimum ductility, and remarkable mechanical properties at an ultra-low temperature [19].

- Beta alloys β (BCC) have medium to high yield strength up to intermediate temperature, good toughness, and high ductility. The noticeable differences between beta alloys β (BCC) than alpha alloys are being less weldable, more heat treatable, and remarkable formable [20].

- Alpha + Beta alloys are metastable, and their mechanical properties are in between alpha and beta alloys. For example, although the ductility of these alloys is more excellent than the α phase's; however, it is lower than the β alloys. They have excellent hot workability, but their cold workability is limited [21].

Table 2.1 *Properties of alpha, beta, and alpha-beta titanium alloys [21].*

Type of Travel	α	β	$\alpha + \beta$
Density	+	-	+
Strength	-	++	+
Ductility	-/+	+/-	+
Fracture Toughness	+	+/-	-/+
Creep Strength	+	-	+/-
Corrosion Behavior	++	+/-	+
Oxidation Behavior	++	-	+/-
Weldability	+	-	+/-
Cold Formability	--	-/+	-

Gum Metal is also considered as a metastable beta alloy since it is an utterly beta phase at room temperature after proper heat treatment. However, gum metal is slightly different from conventional metastable beta alloys in terms of its mechanical properties and, more importantly, in the deformation mechanism.

2.2 General View of Gum Metal

Gum metal has a cold formable ability up to 90%, and surprisingly it does not undergo hardening despite this rate of deformation. In addition, it has been shown to be more potent than conventional Ti alloys due to its extraordinary mechanical properties [22-24]. The mechanical properties of conventional Ti alloys and Gum Metal are compared in Figure 2.4 and Table 2.2. Also, in Table 2.2, the comparison of gum metal and Ti-6Al-4V, which is used mainly in biomedical implants, razors, disc, airplane bodies, is listed. Gum Metal is a special titanium alloy with a body-centered cubic structure (BCC) and expressed mainly as at 75% Ti – 25% (Ta, Nb, V) + (Zr, Hf, O) indicating ultra-high-strength (up to 2 GPa), low Young's modulus (up to 50 GPa), super-elasticity (without martensitic transformation), and exceptional cold workability ability (up to 99%). High strength and low modulus of elasticity make the gum metal alloy to be a good candidate material for the implants (since alloying elements of gum metal are non-toxic), aerospace industry, and special sports equipment such as tennis rackets, golf clubs, and hockey rackets. In addition to the superior mechanical properties mentioned above, the super-elastic (up to 2.5%) and super-plastic (up to 8.1%) behavior are other prominent features of gum metal [24]. Some of these properties could be achieved by cold working.

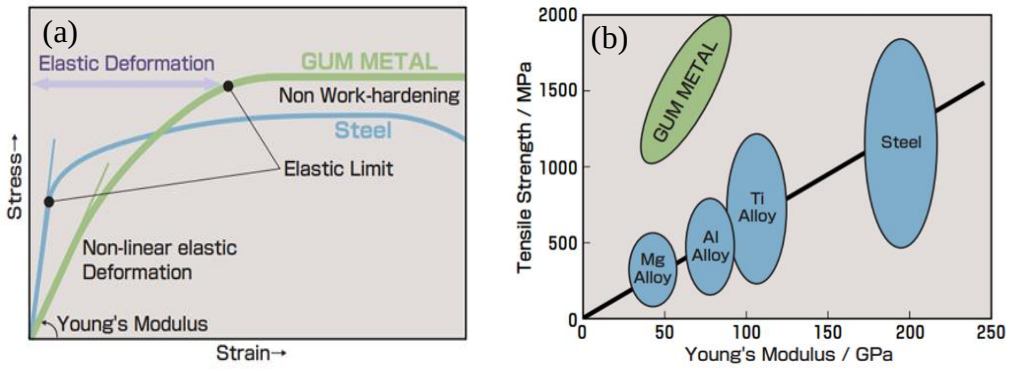

Figure 2.4 Stress-strain behavior of gum metal and steel (a) and representative comparison of stress-strain behavior of traditional metals and gum metal (b).

Table 2.2 *Comparison of mechanical characteristics of Pure Ti (Cp-Ti gr. 2), α+β type Ti (Ti-6Al-4V), and gum metal [23-24].*

Alloy	Elastic Limit (MPa)	UTS (MPa)	Elongation at Rupture (%)	Young's Modulus (GPa)	Recoverable, strain (%)
CP-Ti (gr.2)	330	360	27	110	0,25
Gum Metal	850	900	19	65	1,2
Ti-6Al-4V	790	860	15	114	-

Cold work significantly decreases the elastic modulus, increases the yield strength, and confirms nonlinearity in the elastic range (Figure 2.5). Thanks to the cold working process, elastic strain reaches 2.5% [25]. Before cold working, the elastic strain is limited (approximately 1%). When cold working ratio reaches 90%, elastic modulus decreases to 40 GPa with the increase in elastic strain up to 2.5%; on the other hand, hardness value does not change with the change of cold working ratio. These properties indicate that this alloy has superplasticity at room temperature (Figure 2.6) [9,25].

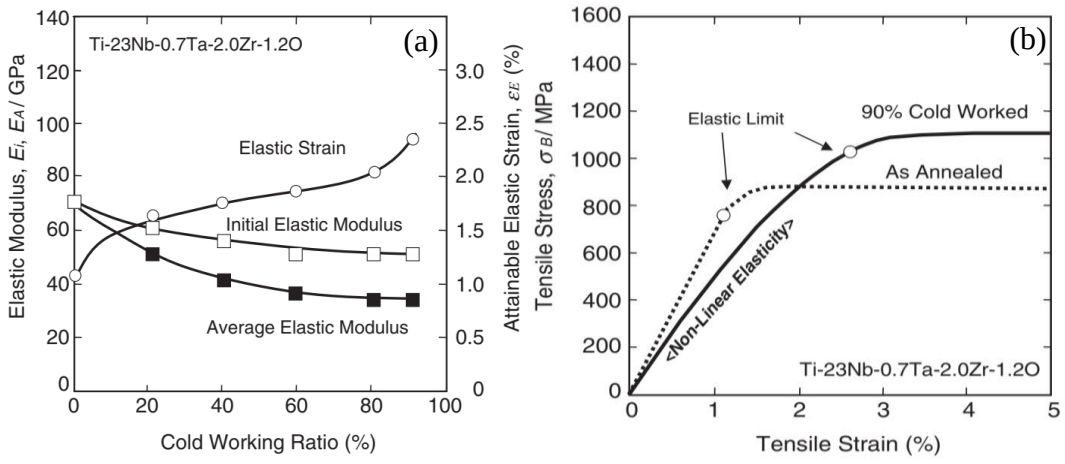

Figure 2.5 Changes in elastic strain and elastic modulus with cold working ratio (a) and stress-strain curve with 90% cold working (b) [25].

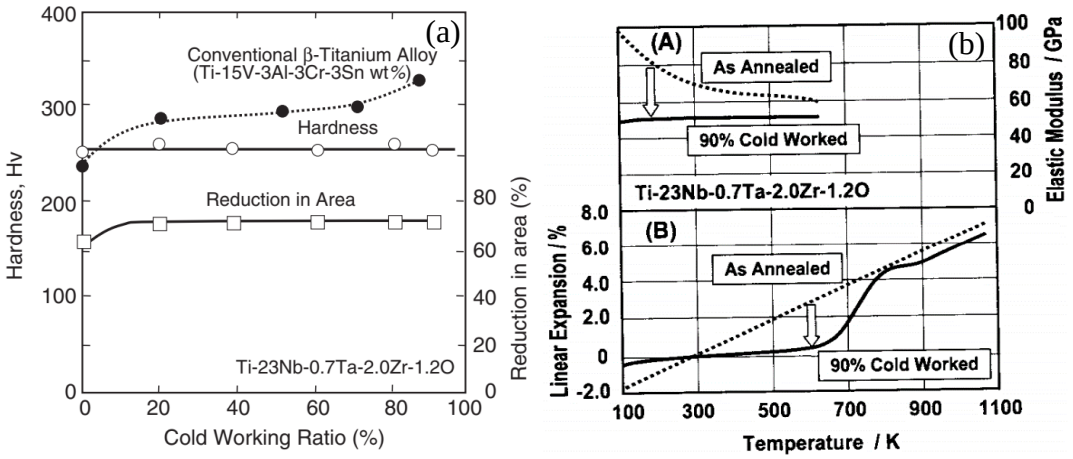

Figure 2.6 Effect of cold working on hardness value (a) and temperature dependence of elastic modulus and linear expansion with 90% cold working (b) [9, 25].

Furthermore, with the help of the cold working process, elastic modulus can not be affected by temperature variations (Figure 2.6). In conventional titanium metals as well as as-cast gum metal (non-cold worked) elastic modulus decreases with increasing temperature, but elastic modulus of cold-worked gum metal stays constant between 100K and 600K. This temperature range is far away from the standard Elinvar alloys. Moreover, the Linear expansion coefficient of common alloys and as-cast gum metal increases linearly with increasing temperature; on the other hand, in the cold worked gum metal, it is extremely low and remains constant from 100K to 500K. This is also a higher range than conventional Invar alloys [26-27]. Besides the cold working, oxygen is also an effective parameter in the mechanical properties of gum metal. Increase in the oxygen content to 1.2 mol%, elastic strain increases from 1% to 2.5% as well as the elastic modulus. Tensile strength is also linked with the oxygen content like conventional titanium alloys, and it reaches 1.6 GPa at 2.9 mol% oxygen content (Figure 2.7) [28]. Except for those, in the conventional titanium alloy, increasing the amount of oxygen causes the alloy to become more brittle since they inhibit dislocation activity; on the other hand, in the gum metal even at high oxygen content, alloy maintains extraordinary ductility because of its dislocation-free deformation mechanism.

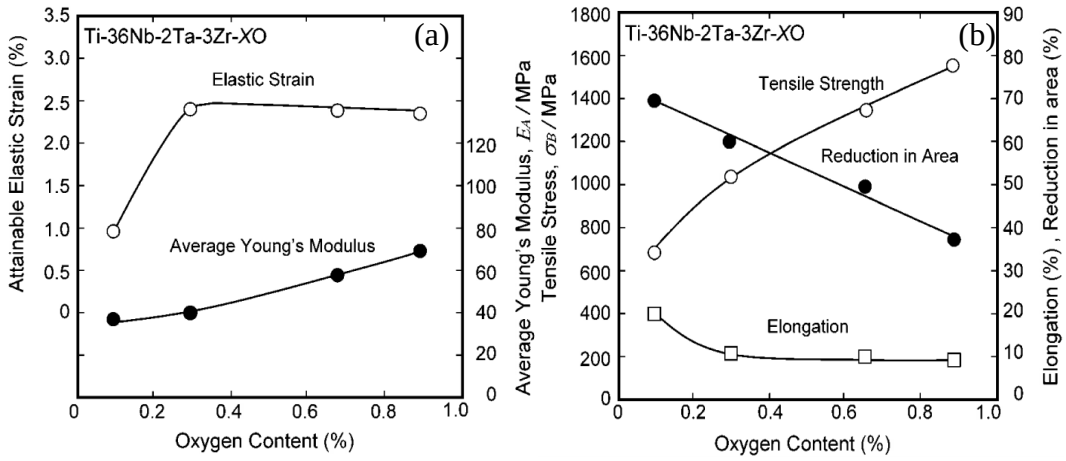

Figure 2.7 Changes in elastic strain and elastic modulus with oxygen content (a) and the effect of oxygen content on tensile stress, elongation, and reduction area (b) [28].

2.2.1 The Parameters Required to Produce Gum Metal

As mentioned previously, the alloy is called gum because not only this alloy does not undergo cold work hardening during the deformation process so that it can be formed, bent, and shaped evermore, rather it can also be elastically deformable up to 2,5%. The condition required to prevent cold work hardening and to obtain gum metal properties is that plastic deformation should occur with the dislocation-free mechanism "Giant Fault." For the giant fault mechanism to have occurred, the ideal shear strength should be close to zero, and the dislocation movement should be inhibited. In order to inhibit dislocation activity, oxygen must be present in the alloy. Furthermore, oxygen hinders the secondary phases (α', α", ω), which elevates the ideal shear strength. When ideal shear strength is close to zero, a dislocation-free nano-disturbed slip mechanism (Giant Fault) becomes stable. For the ideal shear stress to be close to zero (C_{11}-$C_{12}\approx 0$), the elastic modulus should be as low as possible, and the main structure of titanium alloy should be in beta "β" phase. Therefore, this alloy should be composed of IV and V elements (V, Nb, Ta, Db, Zr, Hf, Rf), which stabilize the beta phase and decrease the elastic modulus. Ikehata [29] has compared the effect of IV and V elements on Young's modulus in beta-phase titanium alloys and showed that the lowest elastic modulus is obtained in $T_{0,75}M_{0,25}$

alloys (M: IV and V elements). The results of the studies are shown in Figure 2.8 and Table 2.3. In order to meet all these conditions, theoretical calculations (Pseudopotential method with density functional theory) are used, and these calculations are called "magic numbers." Magic numbers are composed of 3 different alloying parameters: valence electron number (e/a), bond order (Bo), and M-d orbital level (Md).

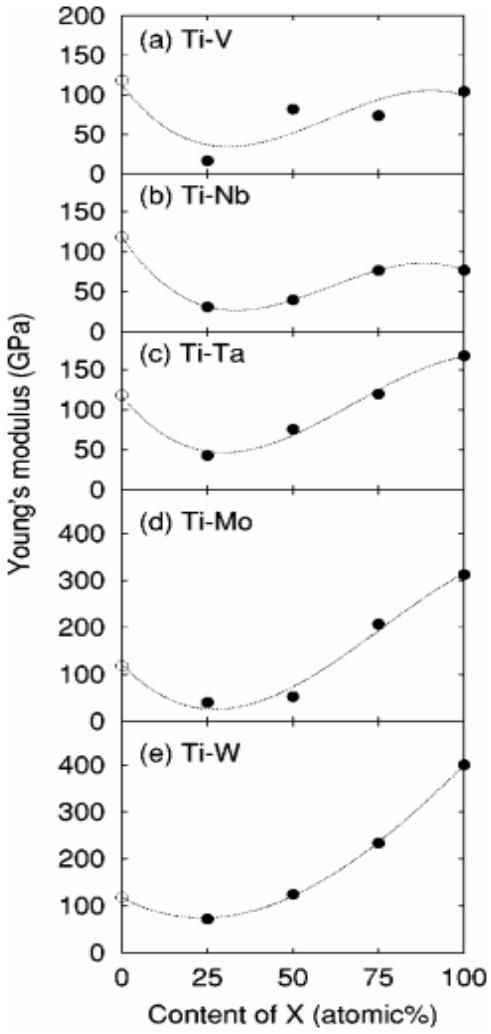

Figure 2.8 Estimated Young's modulus of Ti-M alloys, where M is V, Nb, Ta, Mo, and W [29].

Table 2.3 *Empirical lattice constant an elastic constants C_{11}, C_{12}, and C_{44}, and ideal shear stress (C_{11}-C_{12}) of bcc Ti-X (X=V, Nb, Ta, Mo, and W) Zr-Nb, and Zr-Mo binary alloys [29].*

Composition $M_{1-x}X_x$	Structure	a (Å)	C_{11} (GPa)	C_{12} (GPa)	C_{44} (GPa)	$C_{11}-C_{12}$ (GPa)
$Ti_{0.75}V_{0.25}$	$D0_3$	3.273	123.9	116.9	36.3	7.0
$Ti_{0.5}V_{0.5}$	$B2$	3.280	169.6	122.3	33.6	47.3
$Ti_{0.25}V_{0.75}$	$D0_3$	3.306	213.0	132.2	29.6	80.8
$Ti_{0.75}Nb_{0.25}$	$D0_3$	3.273	128.5	115.5	14.9	13.0
$Ti_{0.5}Nb_{0.5}$	$B2$	3.280	155.4	124.7	12.8	30.7
$Ti_{0.25}Nb_{0.75}$	$D0_3$	3.306	203.5	126.8	21.3	76.8
$Ti_{0.75}Ta_{0.25}$	$D0_3$	3.271	129.9	121.6	38.6	8.2
$Ti_{0.5}Ta_{0.5}$	$B2$	3.278	163.4	132.8	39.0	30.6
$Ti_{0.25}Ta_{0.75}$	$D0_3$	3.302	207.0	145.3	55.6	61.7
$Ti_{0.75}Mo_{0.25}$	$D0_3$	3.273	160.5	125.6	34.1	34.8
$Ti_{0.5}Mo_{0.5}$	$B2$	3.280	224.0	146.6	10.4	77.5
$Ti_{0.25}Mo_{0.75}$	$D0_3$	3.306	363.6	151.5	62.0	212.2
$Ti_{0.75}W_{0.25}$	$D0_3$	3.217	169.2	134.2	32.4	35.0
$Ti_{0.5}W_{0.5}$	$B2$	3.184	239.9	165.9	50.9	73.9
$Ti_{0.25}W_{0.75}$	$D0_3$	3.179	374.8	184.2	81.7	190.6
$Zr_{0.75}Nb_{0.25}$	$D0_3$	3.508	112.8	98.3	19.8	14.5
$Zr_{0.5}Nb_{0.5}$	$B2$	3.447	144.4	108.3	18.3	36.1
$Zr_{0.25}Nb_{0.75}$	$D0_3$	3.382	196.2	118.5	17.9	77.7
$Zr_{0.75}Mo_{0.25}$	$D0_3$	3.451	138.4	104.2	16.6	34.2
$Zr_{0.5}Mo_{0.5}$	$B2$	3.349	208.5	124.3	29.2	84.2
$Zr_{0.25}Mo_{0.75}$	$D0_3$	3.244	342.4	134.5	49.7	207.9

Valence electron number (e/a) is related to the elastic properties of Ti alloys. Elastic modulus and ideal shear strength (C_{11}-C_{12}) increase as valence electron increases. When the valence electron number is 4.24, it is found that the ideal shear strength approached to zero since the elastic modulus is very low (Figure 2.9) [29-36]. Moreover, the work hardening ratio approaches the lowest value when the valance electron number is 4.24. Therefore, the e/a value of candidate alloys should be 4.24 or close to that value.

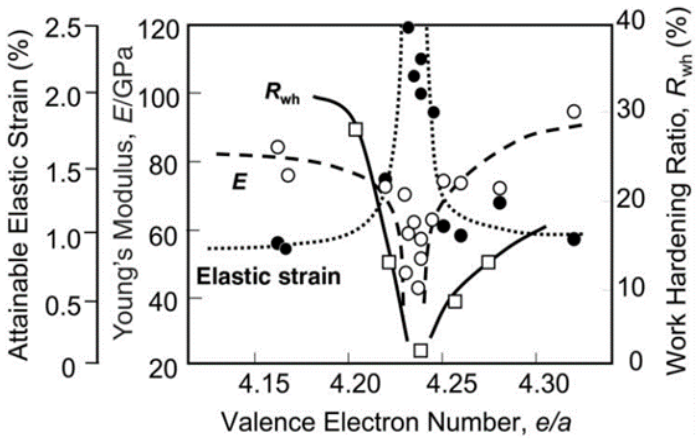

Figure 2.9 Elastic properties with cold working ratio versus the valance electron number per atom (e/a) [30].

Bond order value (Bo) is related to the covalent bond of transition metal and base metal. An increase in the bond order value increases the chemical bond strength of base metal and alloying elements [31]. Furthermore, the Bond order helps determine the corrosion resistance characters. Corrosion resistance increases as bond order value increases. In the β phase Ti alloy, the bond order value is also related to the work hardening ratio and Young's modulus seen from Figure 2.10 [37]. As can be seen, when the bond value is 2.87, the elastic modulus and work hardening ratio reach the minimum value. Hence, the bond order value of candidate alloy should be 2.87 or close to that value.

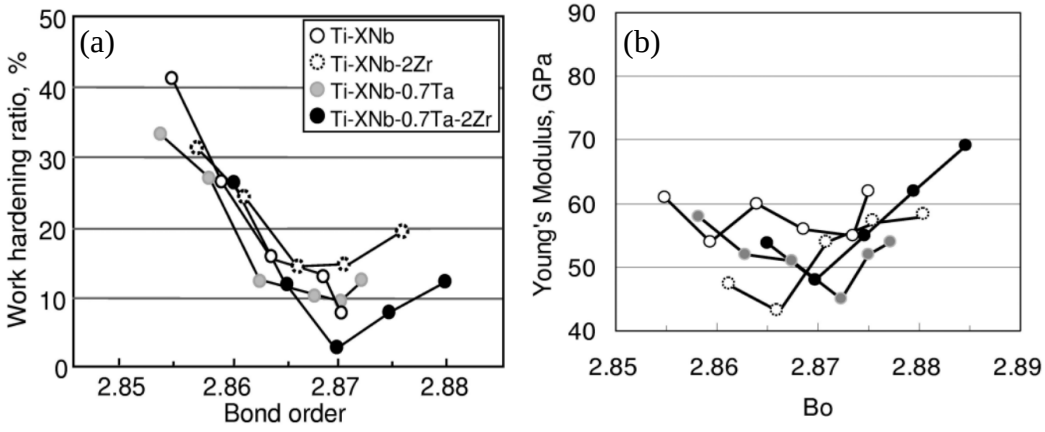

Figure 2.10 Relationship between bond order and work hardening ratio (a) and Young's modulus (b) [37].

Except for those, bond order value (Bo) with the help of valance electron number (e/a) can determine the characteristic feature of the plastic deformation mechanism (SIM α", dislocation glide, or peculiar plastic deformation) (Figure 2.11) [32]. According to the determined e/a and Bo values, possible deformation mechanism can be identified with peculiar plastic deformation.

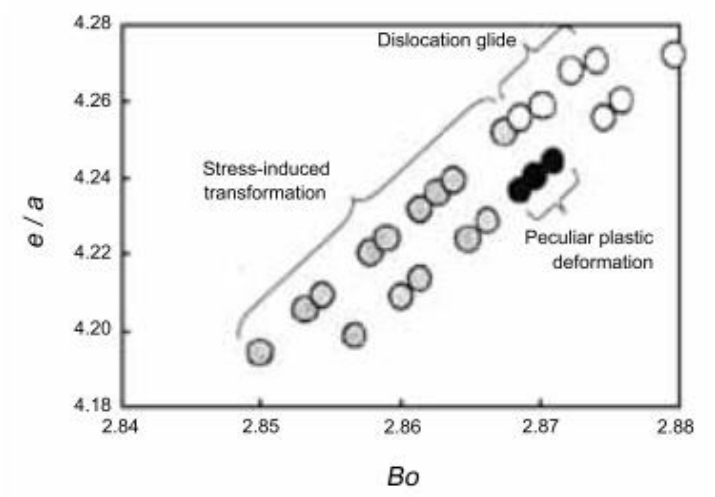

Figure 2.11 Correlation of Plastic deformation mechanism with e/a and Bo values [32].

Md value is related to electronegativity and atomic radius. Md value is are directly proportional to the atomic radius (Figure 2.12) [31] and inversely proportional to electronegativity.

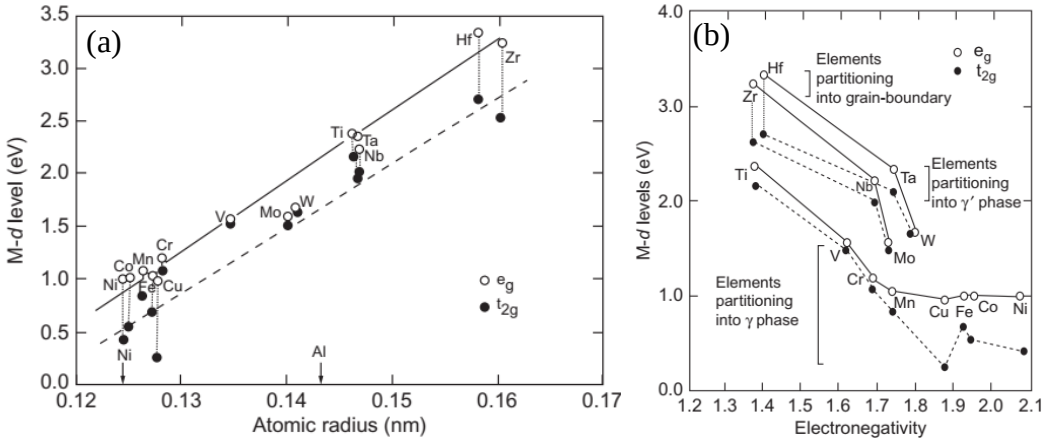

Figure 2.12 Correlation of M-d values with atomic radius (a) and electronegativity (b) [31].

D orbital (Md) with the bond order (Bo) determines not only the phase of the alloy but also determines whether the plastic deformation will be a slip or twin (Figure 2.13) [33, 34]. Deformation mechanism changes from SIM α" to slip with an increase in bond order (Bo) value or decrease in D orbital (Md) value. Since the agreed Bo value is 2.87, it is suggested that Md value should be lower than 2.456 to inhibit SIM α" deformation mechanism. Furthermore, the Md value should be near to 2.45 for the alloy to be stable in the metastable beta phase (Figure 2.14).

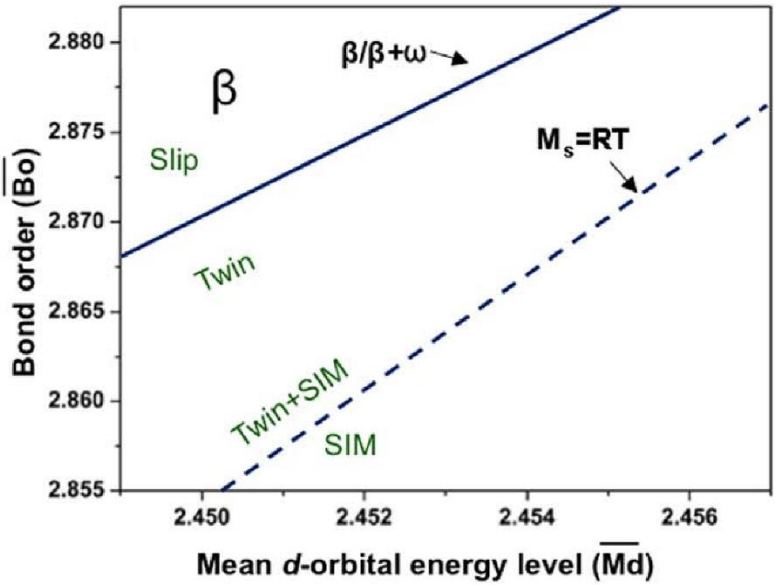

Figure 2.13 Bo-Md diagram corresponding to deformation mechanisms [33].

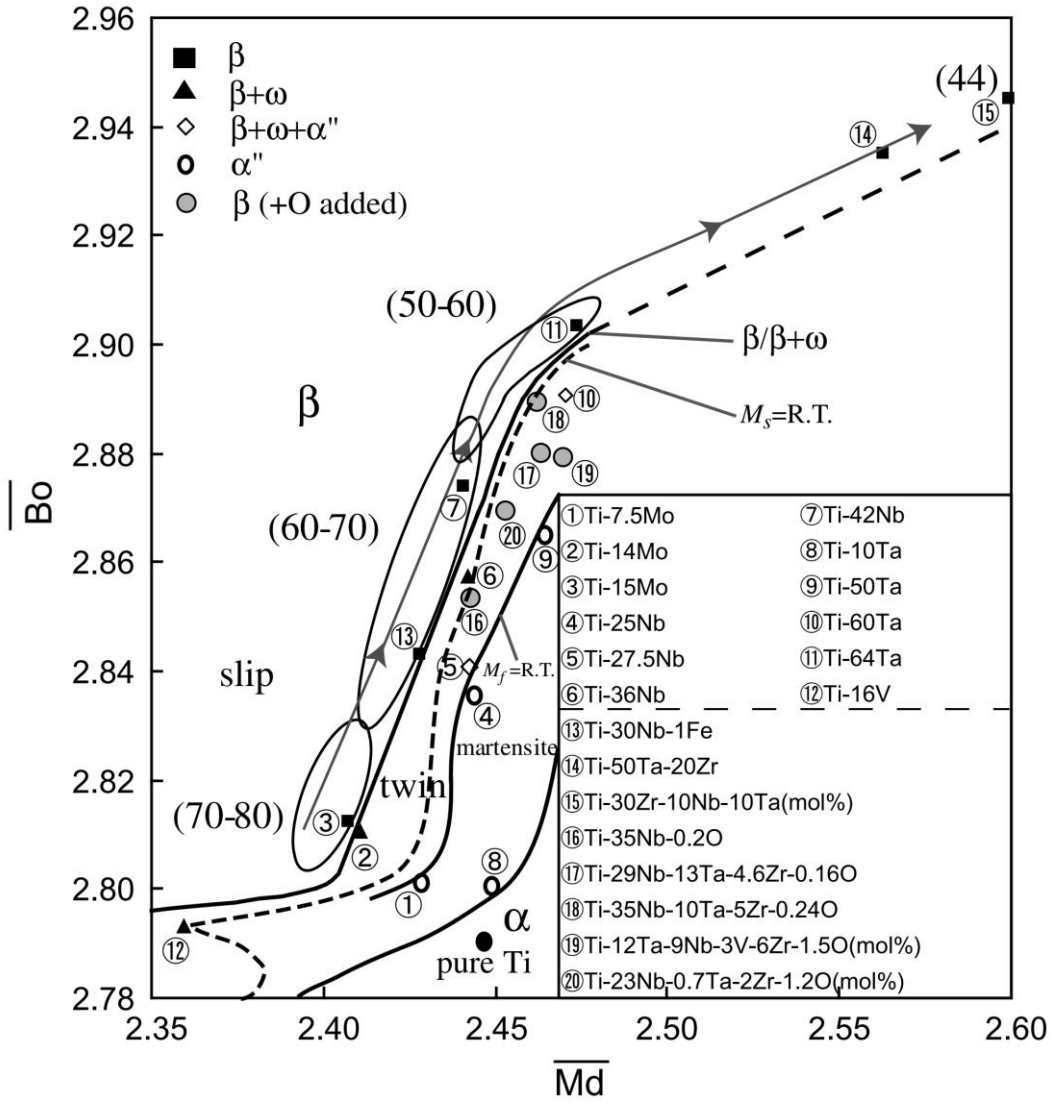

Figure 2.14 Bo-Md diagram in which the β/β+ω phase boundary is shown together with the boundaries. Young's modulus (GPa) is given in parentheses for typical alloys [34].

Therefore, in order to obtain the gum metal properties, it is suggested that d orbital (Md), bond order (Bo), and valence electron (e/a) values should be close to 2.45, 2.87, and 4.24, respectively.

These magic numbers (Md, Bo and e/a) are defined as the following equation,

$$\underline{Md} = \sum_{i=1}^{n} X_i \times (Md)_i = 2.45$$

$$\underline{Bo} = \sum_{i=1}^{n} X_i \times (Bo)_i = 2.87 \qquad (2.1)$$

$$\underline{e/a} = \sum_{i=1}^{n} X_i \times (e/a)_i = 4.24$$

Where Xi is the atomic ratio of the alloying elements and (Md)i, (Bo)i, and (e/a)i are the specific number of alloying elements which are listed in Table 2.4 [34].

Table 2.4 *List of the Bo and Md values for different alloying elements in the β phase Titanium [34].*

3d	Bo	Md (eV)	4d	Bo	Md (eV)	5d	Bo	Md (eV)	Other	Bo	Md (eV)
Ti	2.790	2.447	**Zr**	3.086	2.934	**Hf**	3.110	2.975	**Al**	2.426	2.200
V	2.805	1.872	**Nb**	3.099	2.424	**Ta**	3.144	2.531	**Si**	2.561	2.200
Cr	2.779	1.478	**Mo**	3.063	1.961	**W**	3.125	2.072	**Sn**	2.283	2.100
Mn	2.723	1.194	**Tc**	3.026	1.294	**Re**	3.061	1.490			
Fe	2.651	0.969	**Ru**	2.704	0.859	**Os**	2.98	1.018			
Co	2.529	0.807	**Rh**	2.736	0.561	**Ir**	3.168	0.677			
Ni	2.412	0.724	**Pd**	2.208	0.347	**Pt**	2.252	0.146			
Cu	2.114	0.567	**Ag**	2.094	0.196	**Au**	1.953	0.258			

2.2.2 Deformation Mechanism of Gum Metal

The plastic deformation mechanism is significantly affected by the phase stability and initial microstructure of the beta phase titanium alloys. Conventional alloys in which martensitic transformation is unstable deforms by deformation twin or stress-induced martensite (SIM). The means of martensitic transformation unstable alloy is that alloys still include a non-equilibrium phase, even though the quenching process

is done appropriately. Non-equilibrium phase in the structure prevents the slip deformation or acts as a nucleation site for the stress-induced martensitic phase. Therefore, these alloys deform by twinning or stress-induced martensite (SIM α") phase. Deformation mechanism shifts from twinning to slip as the ratio of beta stabilizer element in alloy increases [38]. This is the case for ordinary beta titanium alloys. However, gum metal is different from the conventional titanium alloy. Although gum metal alloy is placed on the border of the beta phase field, it does not include a non-equilibrium phase; in other words, it is not an unstable alloy in the quenched state. Although oxygen acts as an alpha stabilizer element in pure titanium, it can be said that it acts as a beta phase stabilizer element in gum metal since oxygen inhibits secondary phases such as the stress-induced martensite (SIM α") and ω phase [14, 39]. This is just one of the reasons why gum metal differs from normal beta titanium alloy. The other reason is that increased beta stability in the conventional titanium alloy is known to reduce yield strength along with yield modulus [40]. However, although the gum metal is considered as a metastable beta phase alloy, the elastic modulus is relatively low with respect to high yield strength. Another factor of the difference of gum metal is that the mechanism of plastic deformation in metals is explained by the displacement of the atoms by dislocation activity, while this theory could not explain the plastic deformation of gum metal. The deformation mechanism of gum metal is unusual. Shear stress of deformed gum metal alloy approaches to its theoretically calculated ideal value 0.11 G in <111> direction, which is lower than the critical shear stress of the dislocation slip [41, 42]. Thus, an exceptional dislocation free mechanism is possible instead of slip deformation. Some articles have mentioned that the reason for the critical shear stress of the dislocation slip is higher than the ideal shear stress is nano pinning defects, which could be caused by ZrO clusters or ω phase. [10, 11]. However, recent studies have shown that more traditional deformation mechanisms are still effective in gum metals such as the presence of ½ <111> dislocation [41-48], orthorhombic α″ [49-53]. Furthermore, {1 1 2} <1 1 1> or {3 3 2}<1 1 3> twins, which have not observed in conventional titanium alloy [54, 55], as well as secondary phases such as "stress-

induced hexagonal ω plates" [15], have been observed. Except those, some articles have mentioned that a reversible stress-induced martensitic transformation (SIM) from β to α″ could be responsible for superelasticity of gum metal [55]. The deformation mechanism of the gum metal is still contradictory and unclear.

The deformation mechanism and phase stability of gum metal are determined by using some empirical rule, which is mentioned in Chapter 2.2.1. Pseudopotential method [56, 57] with density functional theory [58, 59] are used to estimate the elastic constant of binary alloys comprising titanium and V-a group elements such as Nb, Ta, and V. According to these theories, when a valance electron number (e/a) of the gum metal is approach to 4.24, Young's modulus becomes extremely low and elastic constant (C_{11} and C_{12}) are almost the same for this alloy. In fact, in BCC phase, Young's modulus are almost zero in <100> direction, shear modulus also approaches to zero in <111> direction, $C = (C_{11}-C_{12})/2 \sim 0$ (Figure 2.15) [11]. This is the typical slip deformation mechanism in beta titanium alloys, and it advised that the ideal shear strength (elastic limit) of this alloy is exceptionally small [60]. Thus, the hardness value of gum metal does not change even if the cold work ratio increases in both the Vickers hardness test and tensile test. Furthermore, ideal strength is very close to theoretical strength during the deformation process. The lack of hardening and the idea that the gum metal deforms at ideal shear strength has introduced a novel concept of plastic deformation mechanism where deformation occurs by two planes shears to each other without the activity of dislocation motion seen from Figure 2.16 and Figure 2.17 and can be thought as a nanoscale planar mechanical melting coupled with recrystallization [61]. Atomic pillars on both sides of the nanoscopic shearing plane may not be arranged in subsequent recrystallization, and the resulting lattice shift is not dependent on the lattice parameter. In the literature, it was defined as "nanoscale dipoles of non-crystallographic partial dislocations with Burgers vector" or "nanodisturbance," [10]. Nanodisturbances, which is a planar nanoscopic area of shear, carry plastic deformation energy on the gum metal, and it differs from the common dislocation since slip displacement in <111> (112) which is lower than the (111) lattice spacing. According to another concept, nanodisturbances can occur

if only plastic deformation occurs under the ideal shear. The structure formed by the merger of nanodisturbances is called giant faults. Giant faults are a planar macroscopic area, as shown in Figure 2.18 [37, 62].

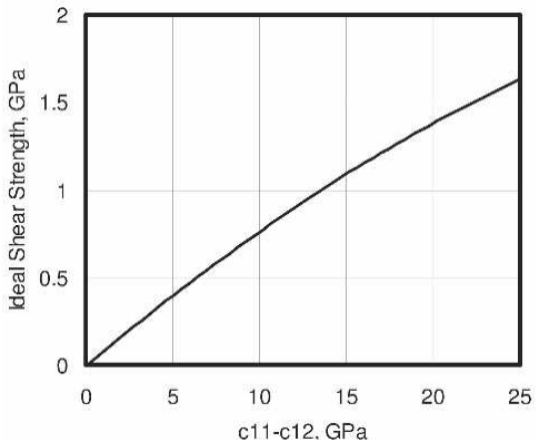

Figure 2.15 Ideal Shear Strength vs C_{11}-C_{12} graph [11].

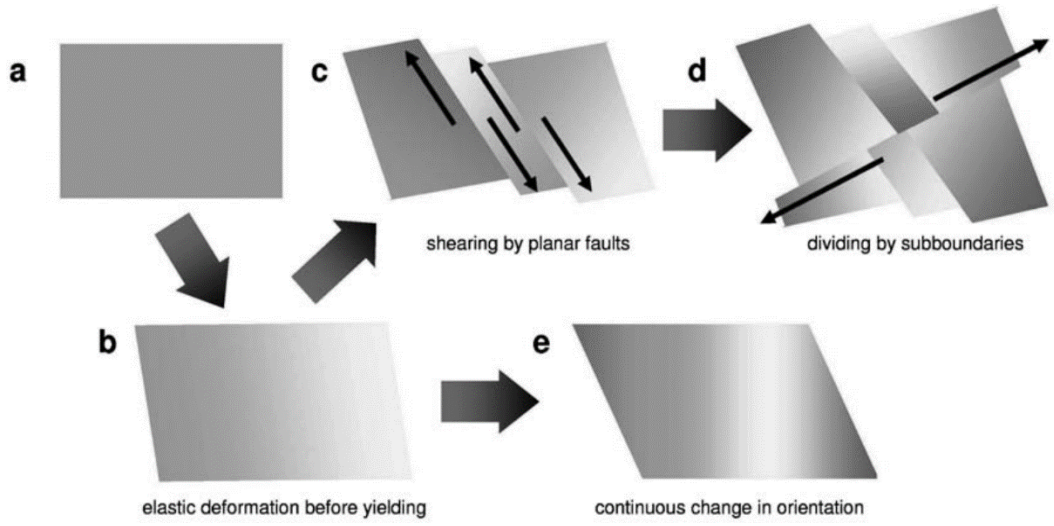

Figure 2.16 Plastic Deformation Mechanism of Gum Metal [61].

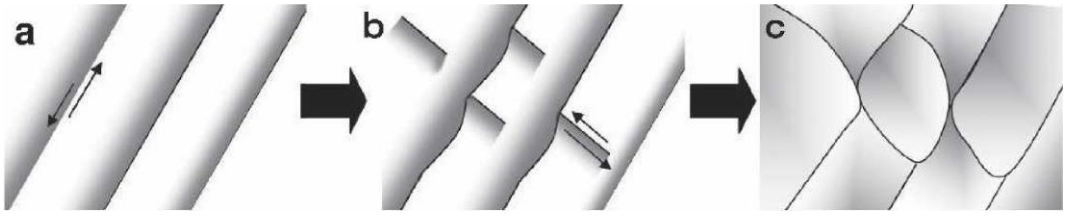

Figure 2.17 Subgrain (Giant fault) formation schema [11].

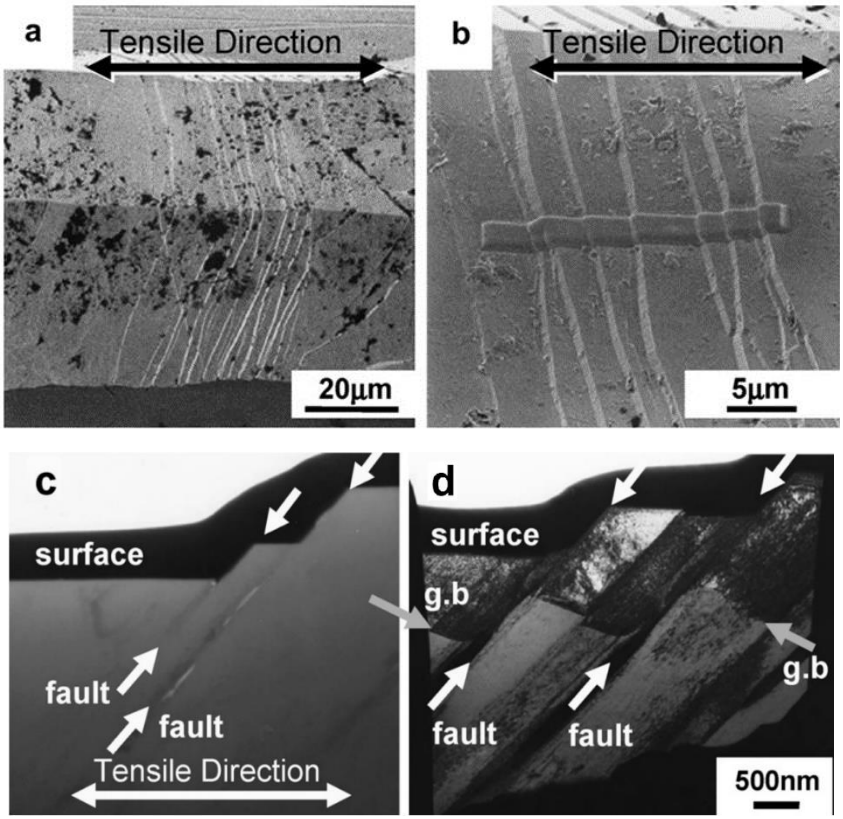

Figure 2.18 Giant Faults on the free surface (a, b) and longitudinal section (c, d) of the deformed surface of Gum metal [62].

Another idea about the lack of hardening and high yield strength during the deformation process is that dislocation in gum metals may be pinned by particles at high stress. The elements that pinned dislocation movement are considered as Zr and O. When the alloy is subjected to a high load, Zr atoms shift to <100> direction. <100> direction has very low interatomic bond strength. Oxygen atoms also move along with Zr atoms to form Zr-O clusters. This cluster is nano-sized and segregated around the Zr atoms. Since the distance between the atom and the cluster is almost 1 nm, it forms a dense cluster and strongly prevents dislocation activity. Elastic deformation occurs due to exceptionally low shear modulus in <111> direction. Finally, when the local stresses reach the "ideal shear stress" critical values, the shear

deformation can proceed immediately along the maximum shear stress plane without the activity of dislocation motion [9], so giant fault mechanism occurs.

Except for those, the effect of secondary "metastable" phases such as α' (hcp), α" (orthorhombic), and especially ω (non-closed packed hexagonal) on the physical properties and deformation mechanism is remarkable. Secondary phases in the gum metal are not desirable since they increase the elastic modulus and ideal shear strength of solution treated alloys, as presented in Figure 2.19 [63]. Thus, the deformation mechanism may not occur with nanodisturbed slip bands (Giant Faults), and cold work hardening could occur. However, the ω phase was detected in the gum metal [64]. Omega "ω" phase can be formed by two different types: thermally or mechanically. Thermally generated ω phase (ellipsoidal or cuboidal) homogeneously distributed on the β matrix; mechanically generated ω phase (plate-like) heterogeneously distributed on the β matrix. In the gum metal, the plate-like ω phase can be formed on the <111> direction (211) plane twin boundary. [64]. In the ordinary beta phase titanium alloy, the dislocation arrangement changes from inhomogeneous to homogenous distribution because of the advantageous presence of the ω particles [65]. The presence of the ω phase is thought to be highly effective in the deformation mechanism. However, the exact effect of the ω phase on the deformation mechanism is still unclear and unexplained.

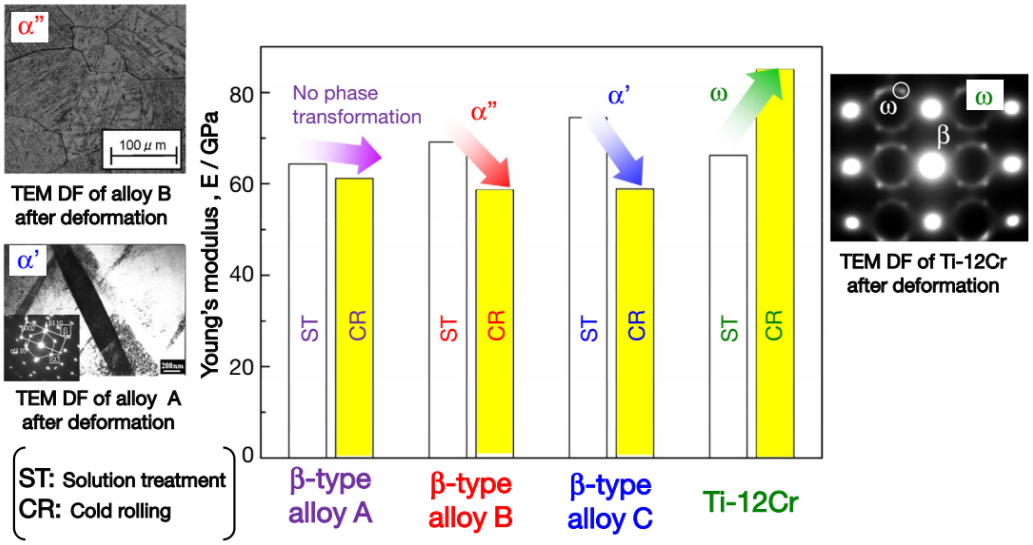

Figure 2.19 The effect of secondary phases on Young's modulus as a result of cold deformation [63].

As a result of the researches started in 2003, the Giant fault mechanism was described as carrying two-dimensional band-like structure local shear. It has been suggested that this structure is associated with certain crystallographic <111> directions. Previous studies have suggested that there is no dislocation activity in the alloy to support the dislocation-free giant fault mechanism, but recent studies describe that there is dislocation activity in gum metal [41-48]. Some research work claim that plastic deformation occurs with dislocation glide in <111> direction. The results of this contradiction raise a new question: If there is a dislocation mechanism, then why does strain hardening not occur during the tensile test; compression test takes the event to another dimension. Giant fault mechanism is generally seen in as-annealed tensile alloys, while dislocation activity is observed in cold swaged or cold compressed alloys. Nevertheless, the deformation mechanism of gum metal has not been adequately resolved and elucidated.

CHAPTER 3

EXPERIMENTAL PROCEDURE

In this section, characterization techniques, raw materials, and experimental procedures are given.

3.1 Raw Materials

The ratio of elements is critical in the production of gum metal, so pure elements were used to achieve a certain composition ratio. It is also essential in which form the raw materials will be because they should not be in powder form as they will be cast in the arc furnace. The purity percentage and forms of using elements obtained from Alfa Aesar are listed in Table 3.1.

Table 3.1 *Form and purity percentage of elements.*

ELEMENT	*FORM*	*PURITY (%)*
Ti	wire	99.90
Zr	pieces	99.95
V	pieces	99.85
Ta	wire	99.90
Nb	lumps	99.85
Al	shot	99.89
TiO2	pellet	99.95

3.2 Determination of Alloying Composition

In Chapter 2.2.1, the parameters required for the alloy composition that may have gum metal properties were mentioned. According to these parameters, (S1) $Ti_{73}Nb_{23.8}Zr_2O_{1.2}$, likely to have gum metal properties, was selected as the base alloy. However, during the melting of S1, the molding was not obtained presumably due to the high viscosity. Hence, the melt was solidified as a button shape.

In order to increase the casting ability and the final mechanical properties, V was decided to be added to the base composition (S1), resulting in (S2) $Ti_{72.87}Nb_{23}V_{0.93}Zr_2O_{1.2}$ composition. Melting of S2 revealed that molding was not possible nonetheless. Also, the effect of V addition was decided to be further studied with details in terms of deformation mechanism, which is one of the crucial parameters for the reveling of the gum metal aspect of any alloy composition.

The last approach was taken as the addition of Al and Ta's combination resulting in (S3) composition $Ti_{69.1}Nb_{25}Ta_{0.7}Zr_2Al_2O_{1.2}$.

The alloys and proportions suitable for making gum metal were listed in Table 3.2. For convenience, the alloys were named S1, S2, and S3.

Table 3.2 *Measured chemical composition (wt.%) and electronic parameters of candidate samples.*

	Ti	Nb	Zr	O	Ta	V	Al	e/a	Bo	Md
S1	59.15	37.43	3.09	0.32	-	-	-	4.238	2.869	2.451
S2	59.38	36.38	3.11	0.33	-	0.81	-	4.239	2.867	2.446
S3	55.01	38.63	3.03	0.32	2.11	-	0.90	4.277	2.868	2.446

3.3 Preparation of Candidate Samples

3.3.1 Arc Melting

In this study, Edmund Bühler GmbH arc melting device (Figure 3.1) was used for the casting process. Arc melting device has a water-cooled copper crucible mold with optional suction apparatus. The vacuum is supplied by Varian rotary (10^{-4} mbar) and diffusion (10^{-8} mbar) pumps. Generator power can reach 400 amperes.

Elements were added in pure and bulk metals form, except oxygen, introduced by titanium oxide (TiO_2) pellet form, to obtain the designed alloys. The prepared mixtures (10 g) were placed in the arc furnace. Ark melting furnace was evacuated to $<5x10^{-5}$ mBar and filled with %99,995 purity argon. The melting process was performed under 800 mbar argon pressure with 200 amperes power. The molten samples quickly cooled down on the copper mold. For the homogeneous mixing of these alloys, the melting process was repeated four times. The alloys were fabricated in the button shape (Figure 3.2) with a near diameter of 16 mm and a thickness of 8 mm. The weight loss after the melting process was nearly 0.3 wt.%

Figure 3.1 Edmund Bühler GmbH arc melting device and water-cooled copper crucible mold.

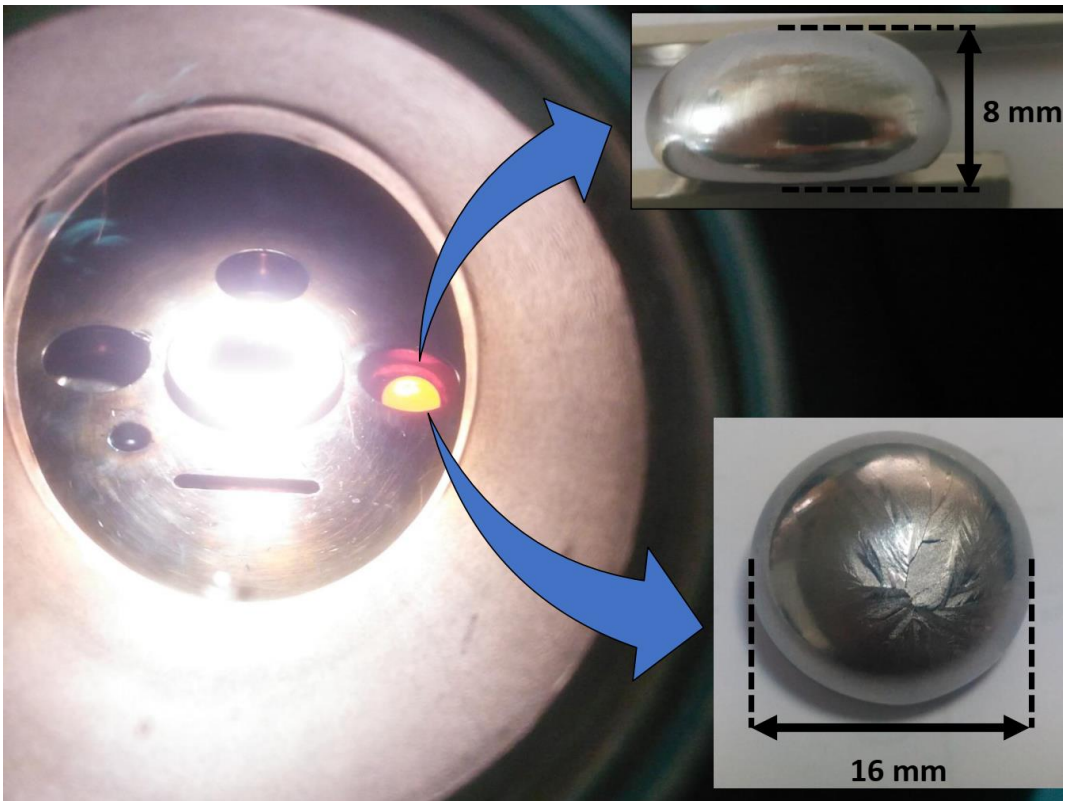

Figure 3.2 Button shaped alloy produced by arc melting furnace.

3.3.2 Wire Erosion Machine

Wire erosion is an electrothermal cutting process. This method uses the abrasive function of the electrical discharges between the two electrodes on the material. The workpiece immersed in an insulating liquid is processed by the wire with the tool electrode. As-cast samples were cut by wire erosion to give cylindrical shape to bring the alloys suitable for mechanical testing (Figure 3.3). Cylindrical specimens' dimensions were selected as 3 mm diameter and 6 mm length according to ASTM E9 standards (Standard Test Methods of Compression Testing of Metallic Materials at Room Temperature).

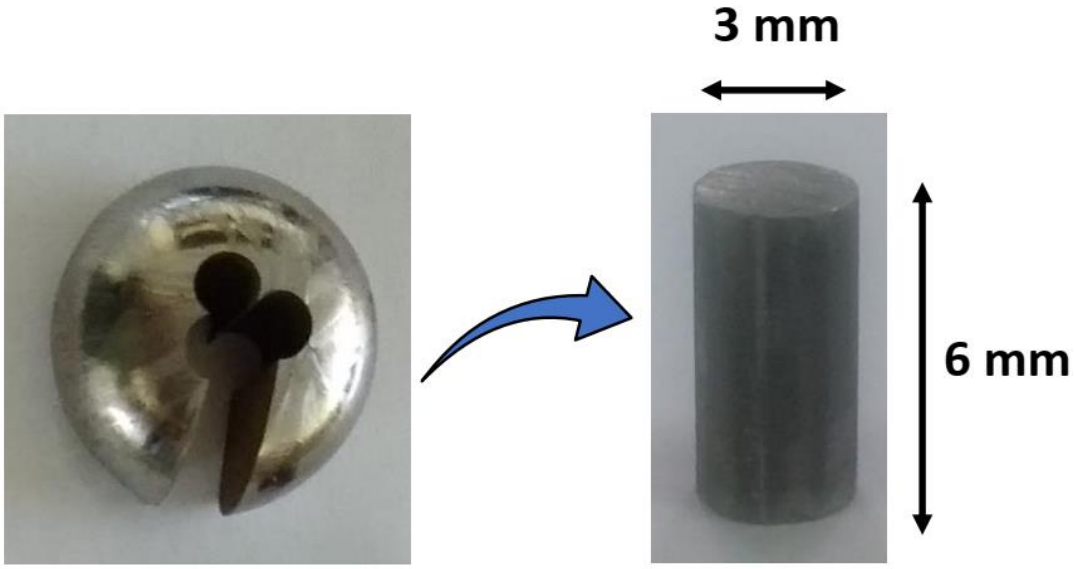

Figure 3.3 Cylindrical specimen after wire erosion.

3.4 Characterization of the Samples

3.4.1 X-Ray Diffractometry

Phase analysis of all prepared samples was done by Bruker D8 Advance XRD device with a copper (Kα) sealed tube at a wavelength of 1.540562 Å. Diffractograms were collected at diffraction angles (2θ) from 30^{o} to 90^{o} with a scanning rate of 0.2^{o}/minutes and a step size of 0.02 ^{o}. Samples to be analyzed for XRD were performed only grinding and polishing processes except chemical etching to prevent loss of secondary phases. Moreover, in-situ XRD analysis of these samples was performed to examine the interaction of the phases with temperature. For in-situ XRD analysis, temperatures have been chosen as; room temperature, 500, 600, 700, 800, and 900 ^{o}C.

3.4.2 Scanning Electron Microscope

FEI Nova Nano 430FEG field emission scanning electron microscope (FESEM) equipped with JOEL 2100F model energy dispersive spectroscopy (EDS) detector is used to examine the microstructure of prepared samples. The EDS apparatus is used to determine the phase of the structure by elemental analysis. SEM analyses were operated under an accelerating voltage of 20 kV, and the spot size was set to 3.5. For microstructural analysis, samples were ground until 2000 grit, polished by 20nm colloidal silica suspension, and etched in 5% HF, 10% HNO3, and 85% H2O solution. EDX analysis was performed under an accelerating voltage of 30KV, and spot size was set to 5. Mapping analysis alongside the EDX was performed to observe the homogeneity of samples.

3.4.3 Differential Scanning Calorimetry

Thermal analyses were performed with a Setaram Setsys 16/18 DSC device (Figure 3.4) with yttria oxide coated alumina crucible. 20mg sample was prepared, and the whole measurements are conducted as heated from room temperature to 1200 ^{o}C with a constant rate of 40 ^{o}C/minute, waited at that temperature for 10 minutes, then cooled to 300 ^{o}C with a rate of 40 ^{o}C/minute in a pure argon atmosphere.

Figure 3.4 Setaram Setsys–16/18 DSC device.

3.4.4 Microhardness Test

Shimadzu C227-E013C. HMV-2 Series Micro Hardness Tester (Figure 3.5) with Vickers probe under 9,8 N constant load for the 30s at room temperature is used to measure the hardness of all samples. The hardness measurement was made by looking at the average of the calculations taken from 9 different regions for each sample.

Figure 3.5 Shimadzu C227-E013C. HMV-2 Series Micro Hardness Tester.

3.4.5 Compression Testing

Compression testing is one of the essential mechanical testing types. It is used to determine material properties such as elastic limit, yield strength, compressive strength. Instron 5582 Universal Testing machine (Figure 3.6) was used to carry out a compression test for the mechanical characterization of the specimens. The capacity of the compression test machine is up to 100 kN. The cold working process of as-cast specimens was done by the hydraulic press at room temperature to reduce the thickness of specimens. Due to an elliptical cross-section of samples in the button form, the cold-worked ratio is not constant, so calculated thickness reduction is approximately 30% and 60%. The compression test was carried out at a strain rate

of 10^{-4} s^{-1} according to ASTM E9 standards. After the compression test, the average thickness of the samples decreased to nearly 85% in thickness. Three specimens of each alloy were conducted in the compression test. The final dimensions of the cold compressed samples were 7-8 mm in diameter and nearly 1 mm in height (Figure 3.7). The yield stress was determined as 0.2% proof stress in uniaxial compression.

Figure 3.6 Instron 5582 Universal Testing machine.

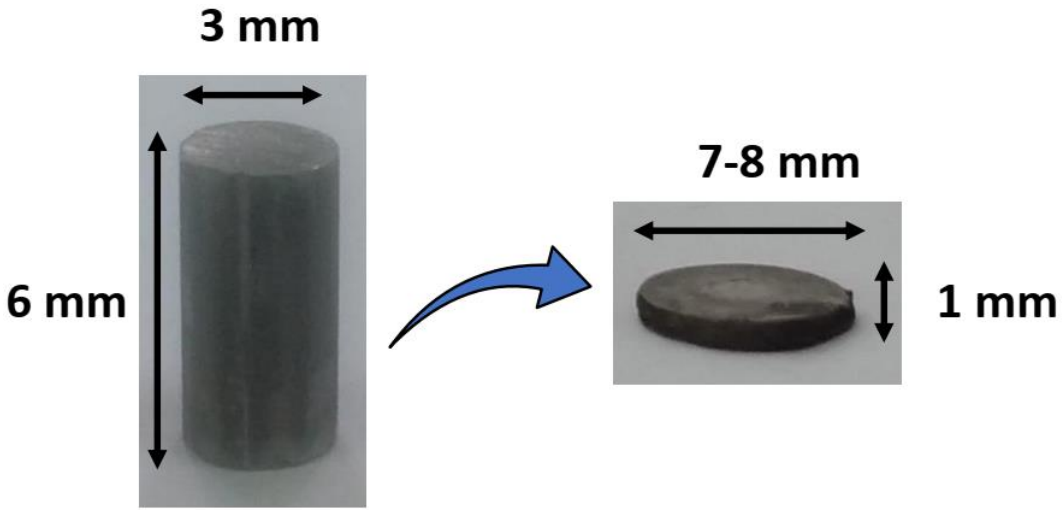

Figure 3.7 Cylindrical specimen whose thickness reduced by around 85% after compression test.

CHAPTER 4

RESULT AND DISCUSSION

Three different gum metal like alloys were prepared and cast to study microstructural examination, mechanical properties, and deformation mechanism. Before casting, the alloys compositions were determined according to the empirical rules, which were mentioned in Chapter 3.2. In this section, microstructural analysis, X-ray diffractometers, thermal analysis, mechanical properties, and deformation mechanisms of prepared alloys were investigated.

4.1 Characterization of As-Casted Alloys

As can be seen from optical micrographs given in Figure 4.1, microstructure consist of columnar and planar growth forms. Through thickness, solidification structures of the as-cast sample have shown that planar growth morphologies were observed in the region where samples were in contact with the copper mold and subjected to a high solidification rate. During solidification, the solid-liquid interface undergoes morphological instability because of the changing growth velocity; thus, there is a structural transition from planar growth to dendritic solidification as the solidification rate decreases moving away from the contact surface. Planar growth areas are slightly higher due to the effect of alloying element differences. Unlike the base alloy (S1), the second sample (S2) has a lower niobium and titanium content, while it contains vanadium alloying element additionally. The third sample (S3) has higher niobium content than S1 and S2. Furthermore, it contains extra tantalum and aluminum elements. The purpose of the production of the second (S2) and third sample (S3) is to increase mechanical properties and to reduce the viscosity in order to increase moldability, which is useful for mass production.

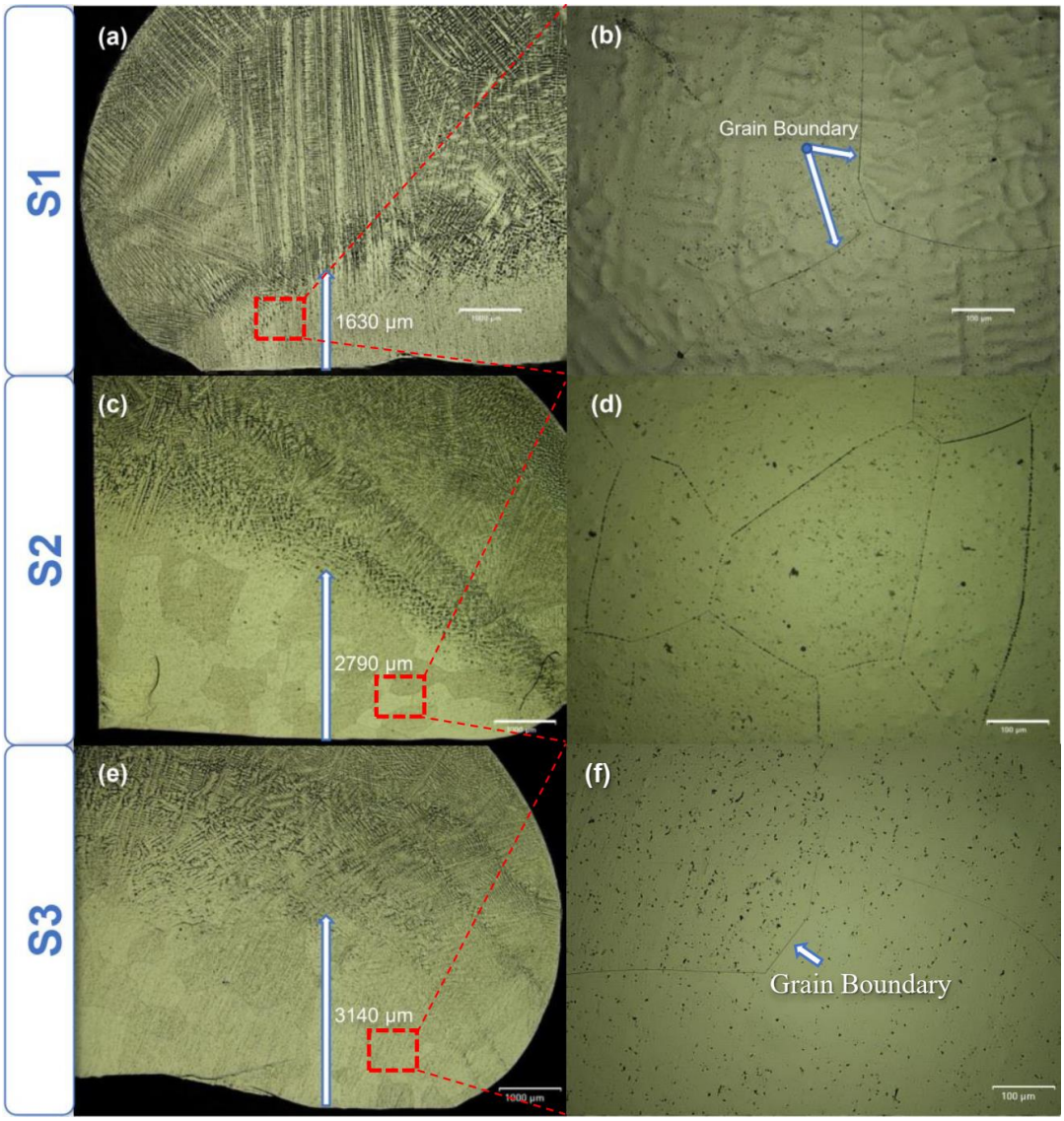

Figure 4.1 Optical micrographs of as cast (a, b) S1 (Ti-23.8Nb-2Zr-1.2O), (c, d) S2 (Ti-23Nb-0.93V-2Zr-1.2O) and (e, f) S3 (Ti-25Nb-0.7Ta-2Zr-2Al-1.2O) alloys.

Optical micrographs show that S3 has the highest planar growth area, while S1 has the lowest planar growth areas. It can be said that the addition of vanadium and aluminum-tantalum combination reduces the melting point of the alloy or increases the time required for the formation of planar growth.

Base alloy (S1) has very large grains (approximately 400-600 μm) with a thin boundary can be seen barely on the dendritic structures. The grain size of the second sample (S2) ranges from 150 to 300 microns, which are smaller than the S1. However, grain size distribution is not homogeneous. Grain size can reach up to 600 microns according to the cooling rate. Furthermore, the second alloy (S2) has more equiaxed grains than S1. The third alloy's (S3) grains are larger (800-1000mm), and grain boundaries are thinner than other S1 and S2 alloys.

As seen in the Optical micrograph results, the microstructure of all three samples consists of a single-phase, but SEM analyzes were performed to make a more accurate decision. If the alloy contained a second phase, there would be contrast differences in structure, and it would look like as in Figure 4.2 [66].

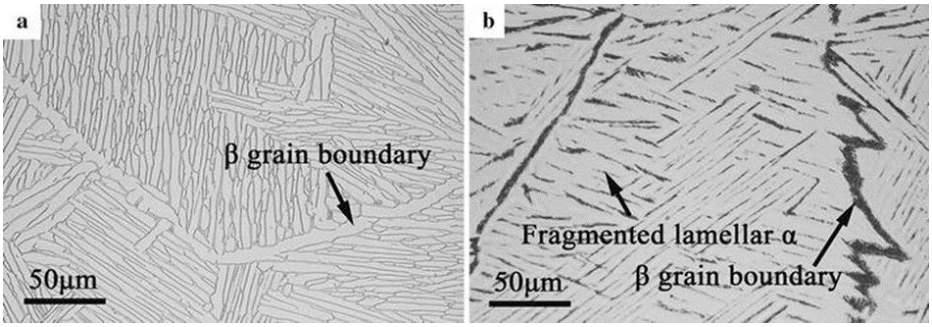

Figure 4.2 Lamella type microstructure of as-cast alloy, the white region represents α, and grey is the β phase [66].

It is challenging to reveal grain boundaries of single beta phase titanium alloys because of the too-thin grain boundary. As can be seen from Figure 4.1 and Figure 4.3, the structure has a dendritic form, and thin grain boundaries are seen in the dendritic form.

There is no contrast difference in the SEM images (Figure 4.3). EDS mapping (Figure 4.4) and line analysis, which was carried out on the surface shown in Figure 4.5, show that all three structures are in the form of a single-phase, and the alloying elements are homogeneously distributed. The reason for the small holes in the structure is the excess etch applied to see the very thin grain boundaries. Mapping analysis was done under 30 kV and 800x magnification for all three samples.

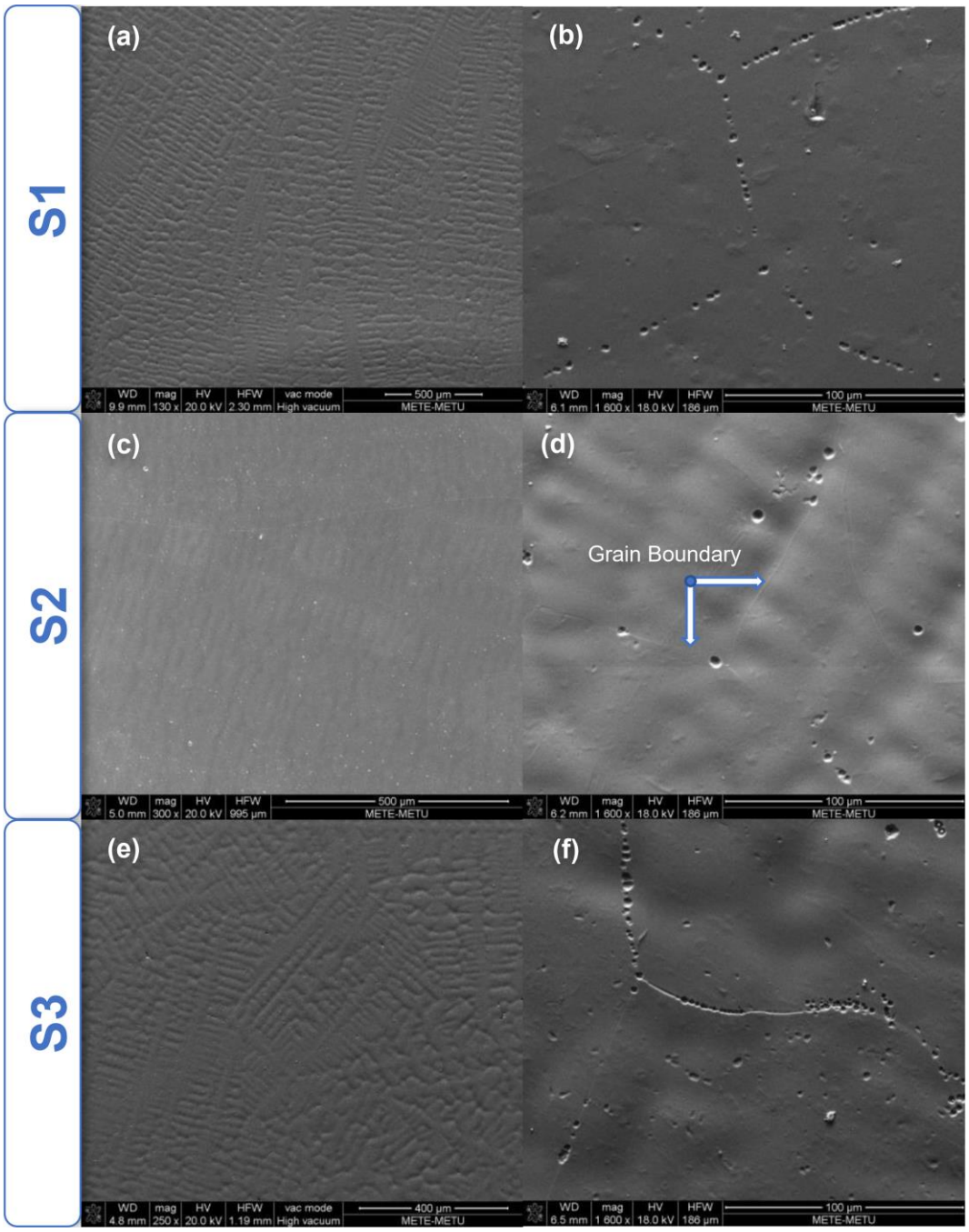

Figure 4.3 FESEM images of as-cast (a, b) S1 (Ti-23.8Nb-2Zr-1.2O), (c, d) S2 (Ti-23Nb-0.93V-2Zr-1.2O) and (e, f) S3 (Ti-25Nb-0.7Ta-2Zr-2Al-1.2O) alloys.

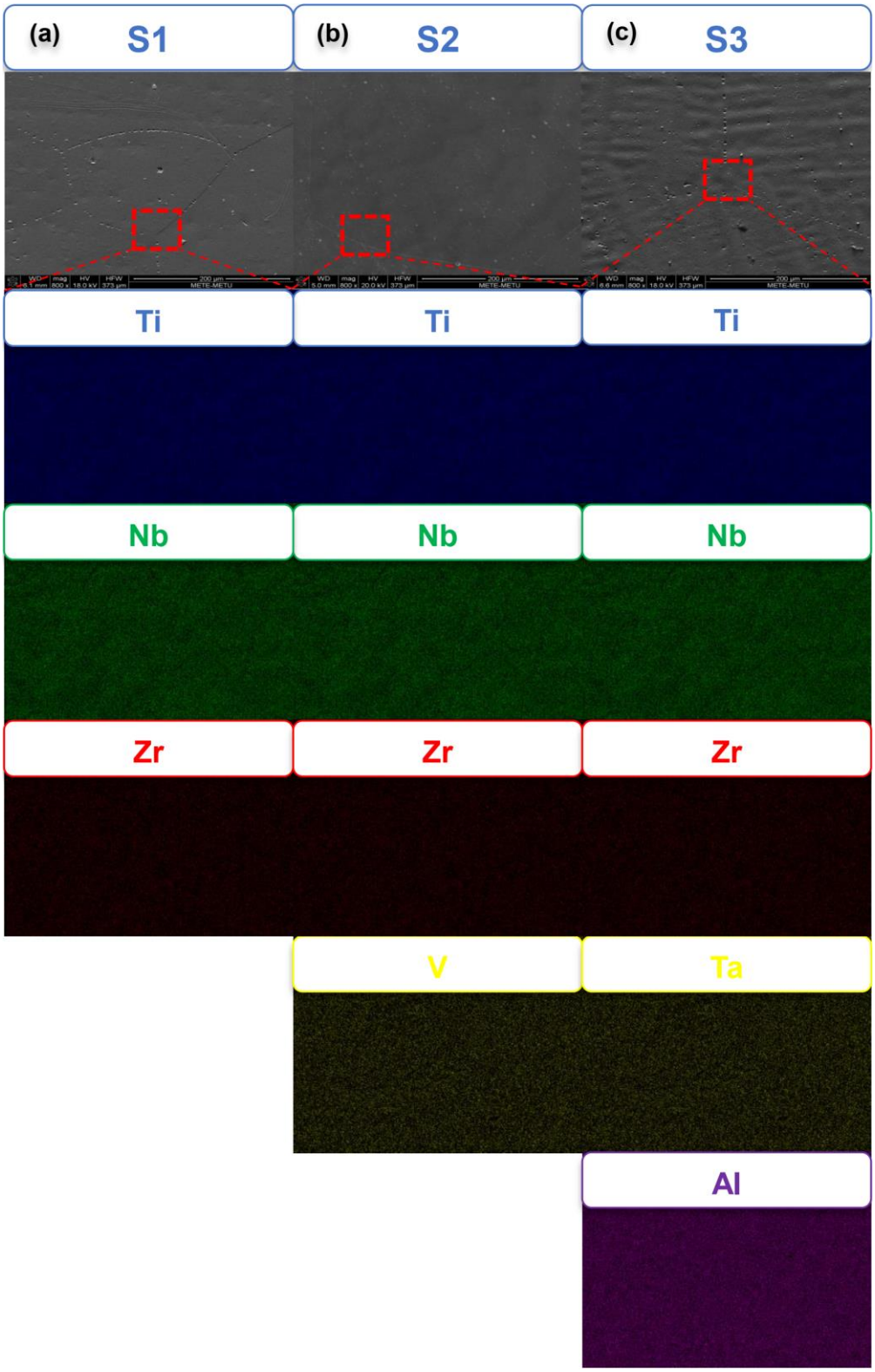

Figure 4.4 EDS mapping analysis of as-cast (a) S1 (Ti-23.8Nb-2Zr-1.2O), (b) S2 (Ti-23Nb-0.93V-2Zr-1.2O) and (c) S3 (Ti-25Nb-0.7Ta-2Zr-2Al-1.2O) alloys.

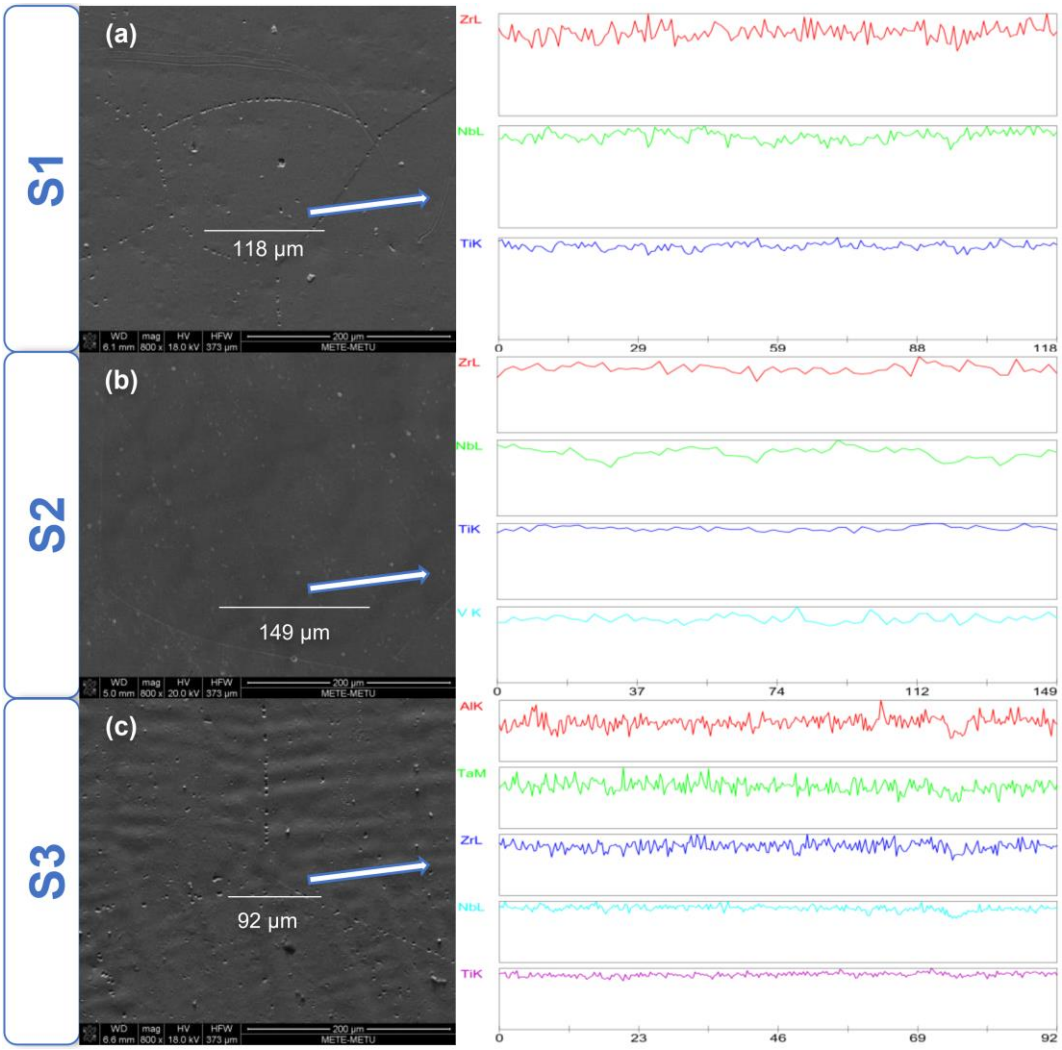

Figure 4.5 EDS line analysis of as-cast (a) S1 (Ti-23.8Nb-2Zr-1.2O), (b) S2 (Ti-23Nb-0.93V-2Zr-1.2O) and (c) S3 (Ti-25Nb-0.7Ta-2Zr-2Al-1.2O) alloys.

The result of the EDS analysis on the mapping line is given in Table 4.1. The amount of oxygen in the structure could not be measured because the EDS detector could not detect light elements such as O, C, B. Therefore, there is a slight deviation in the ratio of elements in the structure. However, according to the results of the EDS analysis, it is seen that the ratio of the elements is close to the desired alloy ratio, and since the microstructure is distributed homogeneously, it can be said that alloy preparation and casting process was realized successfully by using arc melting furnace.

Table 4.1 *EDS analysis of as-cast S1 (Ti-23.8Nb-2Zr-1.2O), S2 (Ti-23Nb-0.93V-2Zr-1.2O) and S3 (Ti-25Nb-0.7Ta-2Zr-2Al-1.2O) alloys.*

Alloy	Ti (at%)	Nb (at%)	Zr (at%)	V (at%)	Ta (at%)	Al (at%)
S1	73.29	24.39	2.31	-	-	-
S2	73.22	23.43	2.36	0.99	-	-
S3	67.97	25.69	2.98	-	0.76	2.60

Although the microstructures of three distinct as-received alloys seem to be homogeneously distributed and contain only single-phase, XRD has been utilized for the detection of possible phases. Prior to deformation, as-cast alloys consist of only the beta phase, as shown in the X-ray diffraction pattern (Figure 4.6). However, it has been reported that orthorhombic α" martensite phase could appear in metastable β titanium alloys due to β to α" phase transformation during quenching or deformation [67, 68]. The formation of the α" phase in our samples could have been suppressed by the presence of β stabilizer alloying elements "Nb, Zr" with the help of interstitial oxygen.

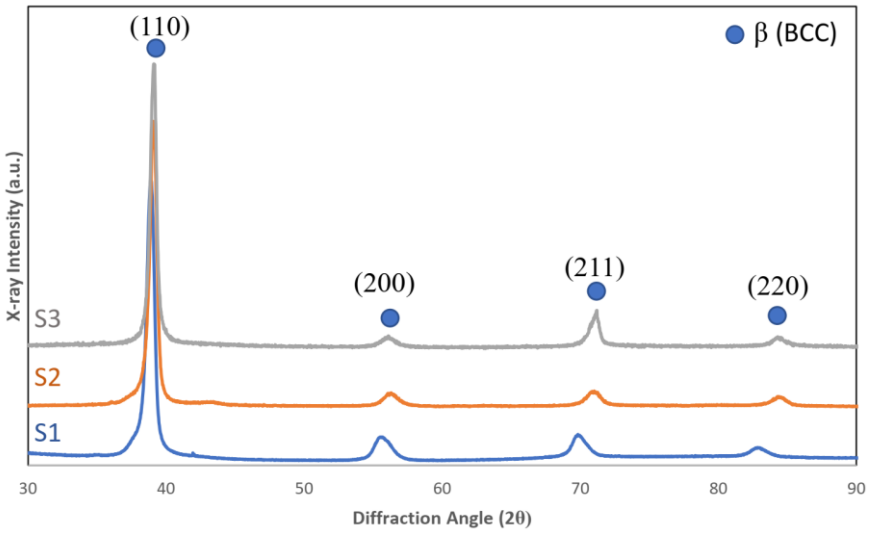

Figure 4.6 XRD patterns of as-cast S1 (Ti-23.8Nb-2Zr-1.2O), S2 (Ti-23Nb-0.93V-2Zr-1.2O) and S3 (Ti-25Nb-0.7Ta-2Zr-2Al-1.2O) alloys.

It is evident from XRD peaks of the base alloy (S1) that have been shifted to a high 2θ diffraction angle.

The main reason why there is a shift on peaks may be alloying elements such as aluminum, tantalum, and vanadium makes a lattice distortion on the structure. Thus, the change of lattice parameters may have increased the diffraction angle. To obtain exact results, lattice parameters, crystallite size, and microstrain values of the three samples were calculated after Rietveld refinement and listed in Table 4.2. Since crystal structures of all samples are body-centered cubic, lattice constants (a,b, and c) are the same as each other and were listed in the same column.

Table 4.2 *XRD characteristics of as-cast S1 (Ti-23.8Nb-2Zr-1.2O), S2 (Ti-23Nb-0.93V-2Zr-1.2O) and S3 (Ti-25Nb-0.7Ta-2Zr-2Al-1.2O) alloys.*

Alloy	Lattice Constant (Å)	Crystallite Size (Å)	MicroStrain (%)
S1	3.312	112	0.512
S2	3.300	124	0.507
S3	3.299	154	0.408

As can be seen in the table, a slight change of lattice constants changes the diffraction angles. Moreover, sample 3 (S3) has the lowest strain (%) value, and the highest crystallize size due to the presence of aluminum-tantalum alloying elements.

Aluminum addition to the base alloy leads to an increase in the intensity of the third peak from (211) plane, which may be attributed to Al atom distribution in the BCC structure of alloys.

Samples 1 and 2 consists of only beta stabilizer elements, while sample 3 contains aluminum, which stabilizes the alpha phase on titanium alloy. However, according to the XRD result, there is no alpha phase peak or aluminum related phase peak. Aluminum can be in solid solution form with other alloying elements in BCC titanium-niobium lattice. Since the alloying elements are added according to the magic number rule, the structure is expected to have a single beta (BCC) phase. Thus, empirical and experimental results are found to be consistent with each other.

DSC analysis was performed to investigate the effect of alloying elements on phase transition temperature. Given that the main alloying element in the beta isomorphous alloy system is the phase stabilizing Nb, the phase diagram of prepared alloys would probably form with very similar trends. Therefore, the Ti-Nb phase diagram represented in Figure 4.7 can be assumed as the skeleton structure of the present alloys, and it could shed light on the understanding of the phase stability of these alloys and its neighboring compositions. Therefore, the β-α phase transition temperature is expected to be between 600 and 850 degrees.

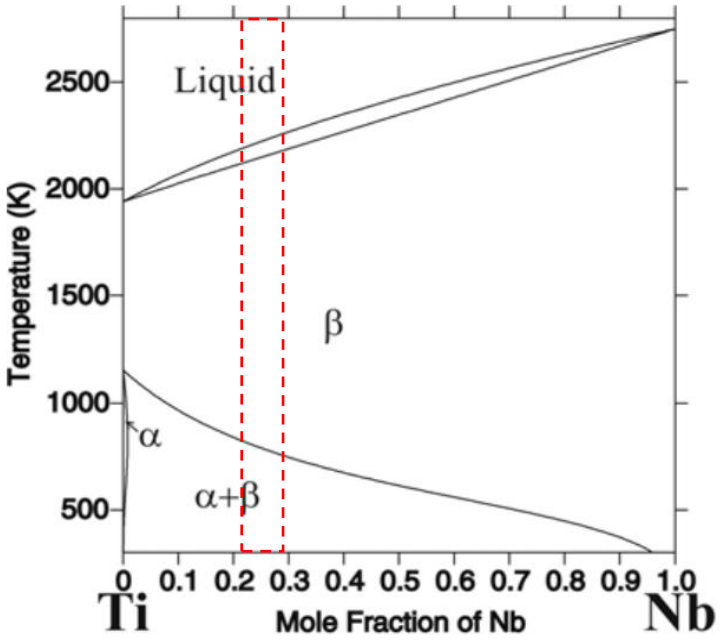

Figure 4.7 Ti-Nb binary phase diagram [69].

All alloys are in the beta phase at room temperature. Phase transformation may not occur during the heating curve since it will move from the beta phase to the beta phase region again. The cooling curve can show us the phase transformation as the transition from the beta phase to the alpha phase will take place. However, in titanium alloys, reverse β to α transformation is known to be slower than a direct one. Furthermore, it has been mentioned that cooling is problematic to identify phase transition temperatures due to slow kinetics [70]. Therefore, the phase transition temperature curve may not be seen during both heating and cooling.

When looking at the DSC curve of S1 (Figure 4.8), during heating exothermic peak at approximately 1050 ^{o}C and endothermic peak at 1150 ^{o}C are observed. This peak possibly is caused by lattice strain due to fast cooling. However, the cooling curve does not give any peak. DSC may not be able to detect phase transformation.

DSC heating curve of the second alloy (S2) (Figure 4.9) shows an exothermic peak at approximately 850 ^{o}C. It is seen that the cooling curve gives a minimal exothermic peak at the same temperature, 850 ^{o}C. This temperature can be α to the β phase transition region. Moreover, the DSC heating curve shows a broad endothermic peak at 1150 ^{o}C could be related to stress relief as seen on S1.

In the third alloy (S3) DSC heating curve gives only a small peak at 1150 ^{o}C, and another peak is not observed during the cooling and heating curve (Figure 4.10).

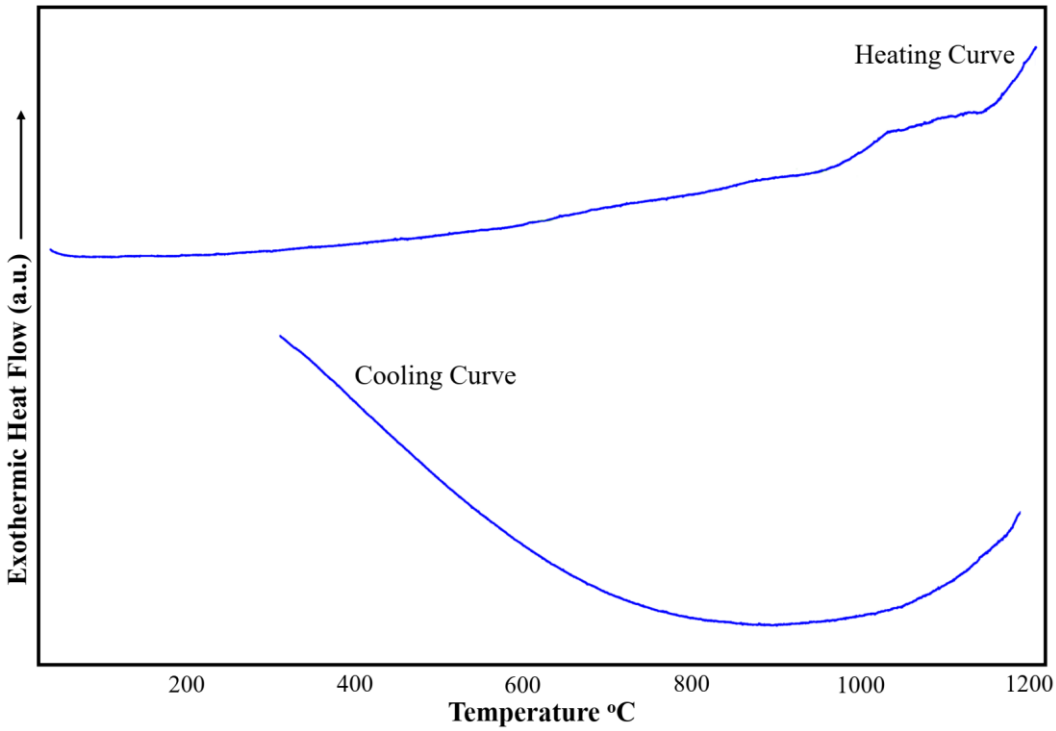

Figure 4.8 DSC curve of S1 (Ti-23.8Nb-2Zr-1.2O) alloy.

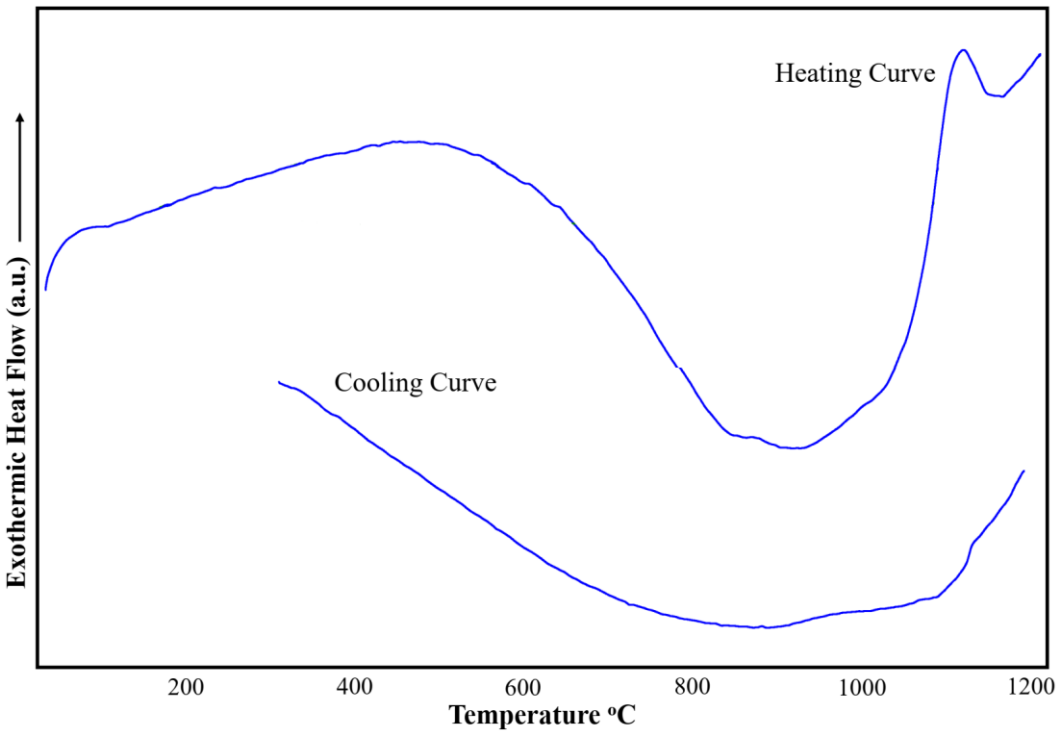

Figure 4.9 DSC curve of S2 (Ti-23Nb-0.93V-2Zr-1.2O) alloy.

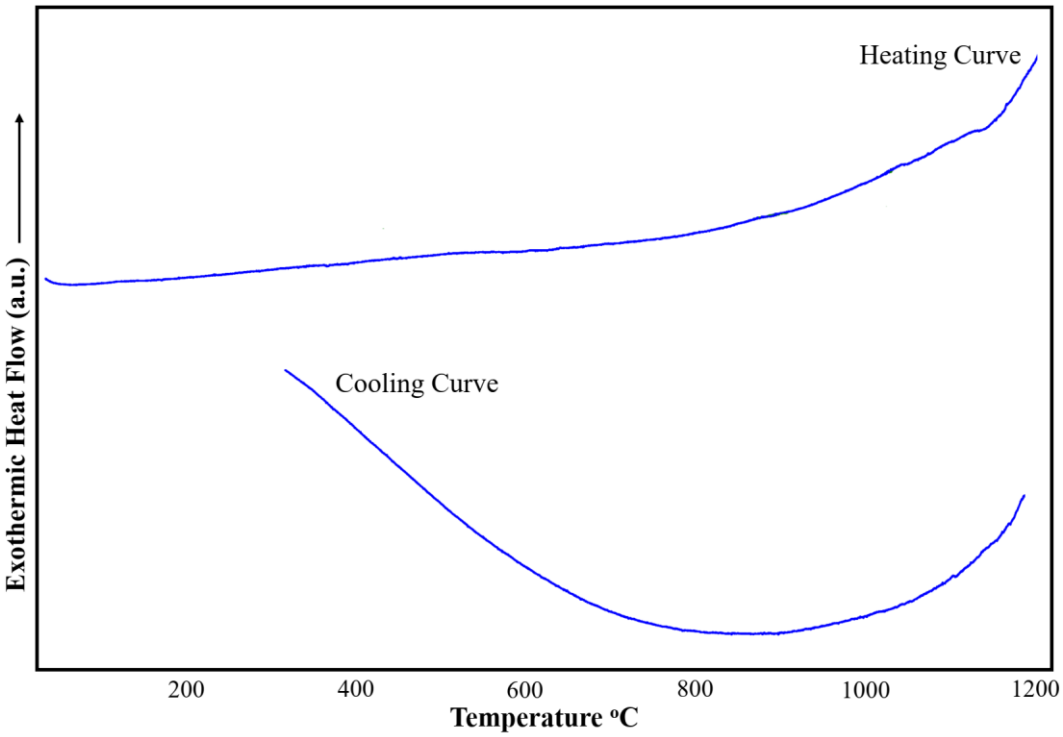

Figure 4.10 DSC curve of S3 (Ti-25Nb-0.7Ta-2Zr-2Al-1.2O) alloy.

DSC analysis could not give us exact information. Since DSC samples are very small (20 mg), XRD analysis could not be performed. Instead, in situ XRD analysis of as-received samples were performed to see crystalline structural changes (Figure 4.11). Moreover, after the DSC analysis, microstructure, and mechanical properties (hardness) of heat-treated samples have been analyzed in order to determine phase transformation effects on these phases.

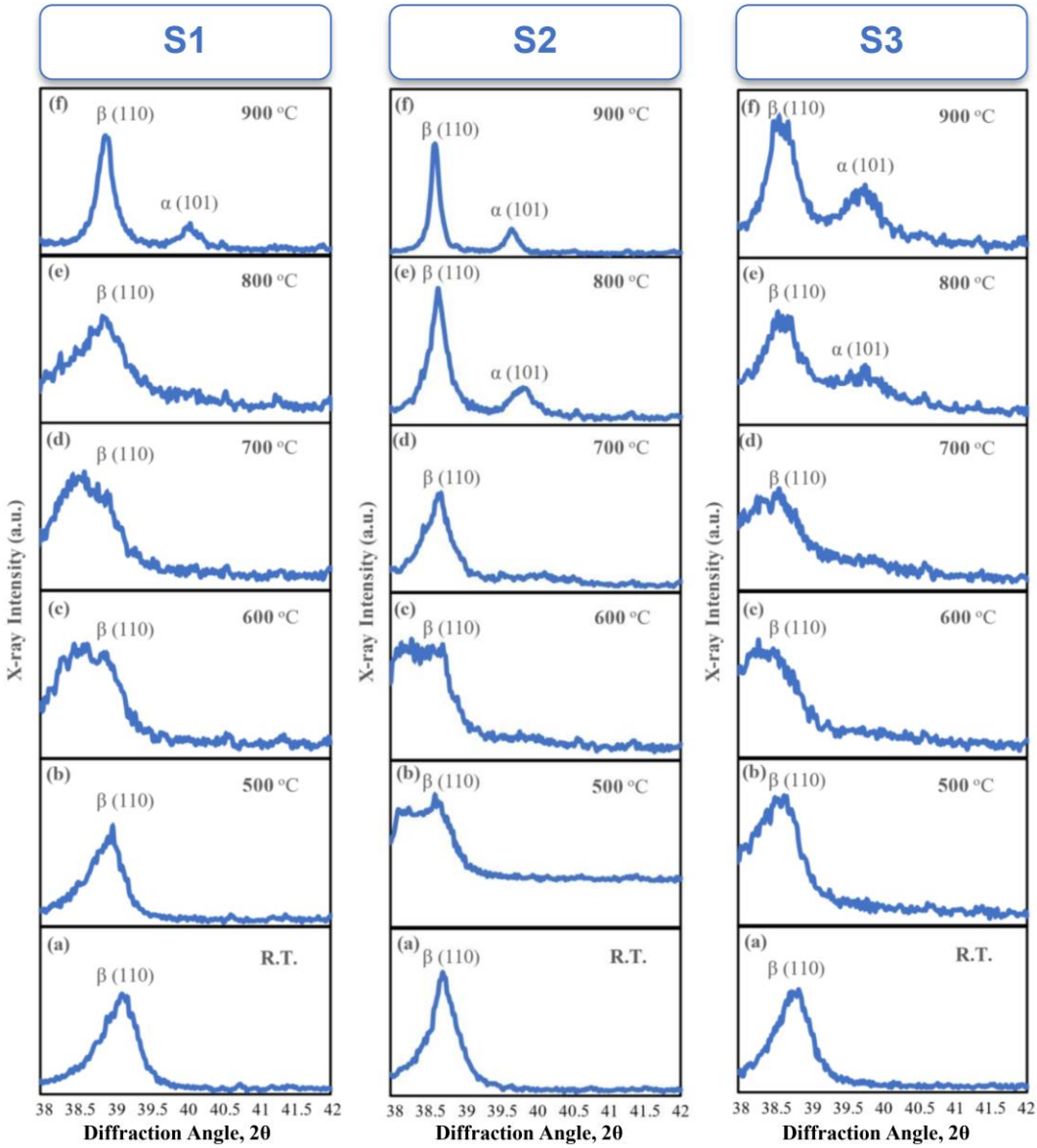

Figure 4.11 In-situ thermal XRD analysis of 85% cold deformed S1 (Ti-23.8Nb-2Zr-1.2O), S2 (Ti-23Nb-0.93V-2Zr-1.2O) and S3 (Ti-25Nb-0.7Ta-2Zr-2Al-1.2O) alloys at different temperature.

The formation of the α phase for S1 occurs at 900 ºC; on the other, this phase for S2 and S3 occurs at 800 ºC. The α peak of S3 is larger than the other samples, which is expected due to the existence of the α phase stabilizer aluminum element. Thus, alloying element addition (Vanadium and Aluminum with Tantalum) decreases the α to β phase transition temperature. In Figure 4.1, it was emphasized that aluminum

and vanadium addition might have a thermal effect on the candidate alloys due to the higher planar zone of S2 and S3. This thought was supported by in situ XRD analysis.

Since the vanadium alloying element is a beta stabilizer, it is expected to lower the beta transition temperature as seen in in-situ XRD analysis; however, aluminum is an alpha stabilizer element. Sample 3 (S3) includes tantalum and aluminum other than niobium, zirconium, and oxygen. S3 has the most niobium content alloys in three candidate alloys. S3 has 25% niobium and 0.7% tantalum contents which are beta stabilizer elements, while S1 has 23.8% niobium content, and S2 has 23% niobium and 0.93% vanadium content. The presence of tantalum and a higher amount of niobium can decrease the beta transition temperature despite the presence of the alpha stabilizer element of aluminum. According to the in-situ XRD analysis, it is seen that the alpha phase (HCP) is formed below 1000 ^{o}C. Therefore, the phase transition is expected since the temperature rises to 1400 ^{o}C during the DSC analysis.

Furthermore, SEM and optical images of alloys which are heat-treated during DSC analysis are given in Figure 4.12. According to micrographs, all three alloys contain a needle-like α (HCP) phase on the β (BCC) matrix. Slow cooling could affect the formation of the unwanted α phase. Furthermore, the hardness comparison of heat-treated samples with as cast was made. While the as-cast samples have an average of 240-260 HV hardness, the hardness value of the heat-treated samples has reached up to 440 HV hardness (Figure 4.13). These results prove that there is a phase transformation in the structure during DSC analysis.

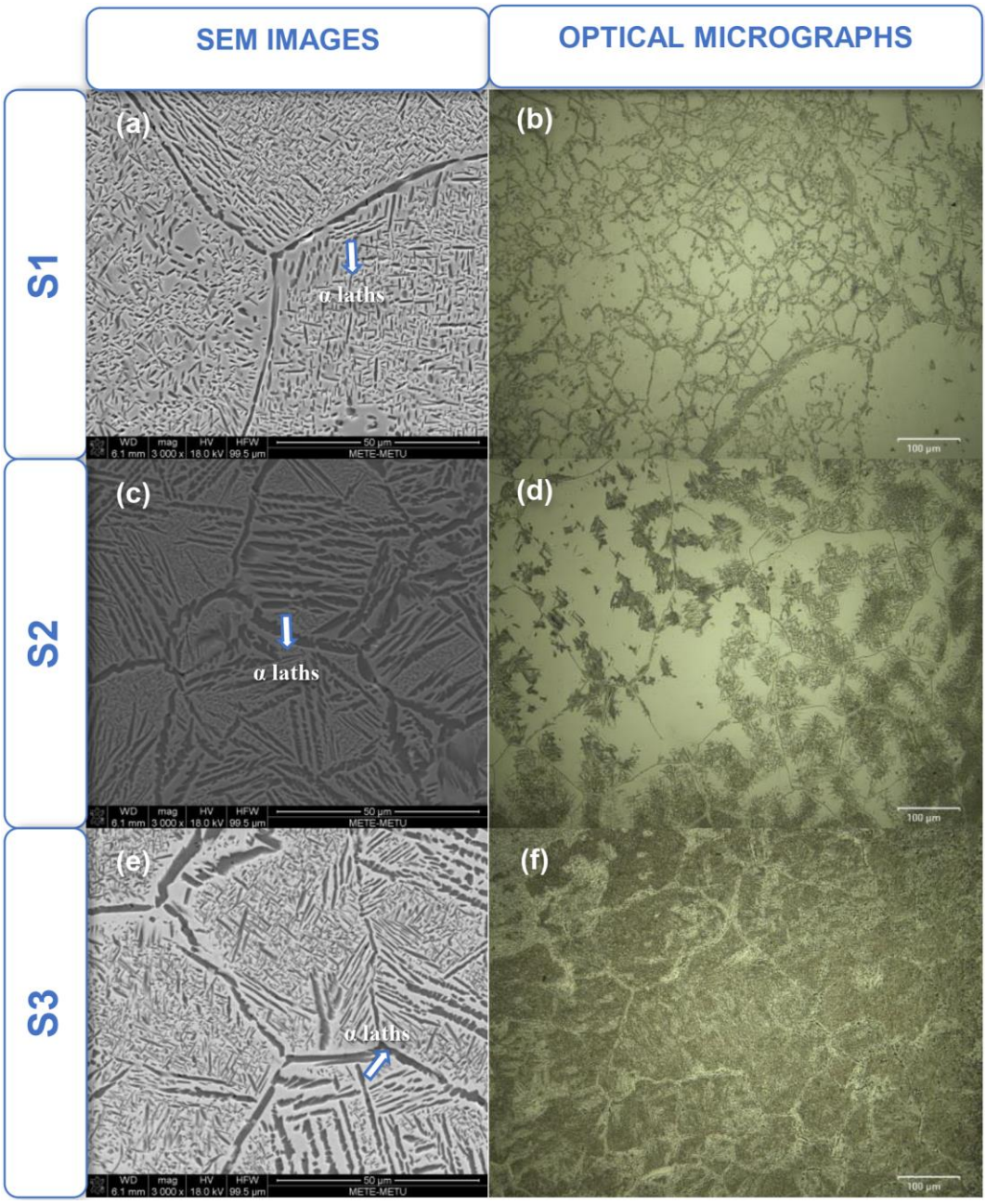

Figure 4.12 Alpha laths in a matrix of beta. The microstructure was formed by DSC analysis from an elevated temperature below the beta transus.

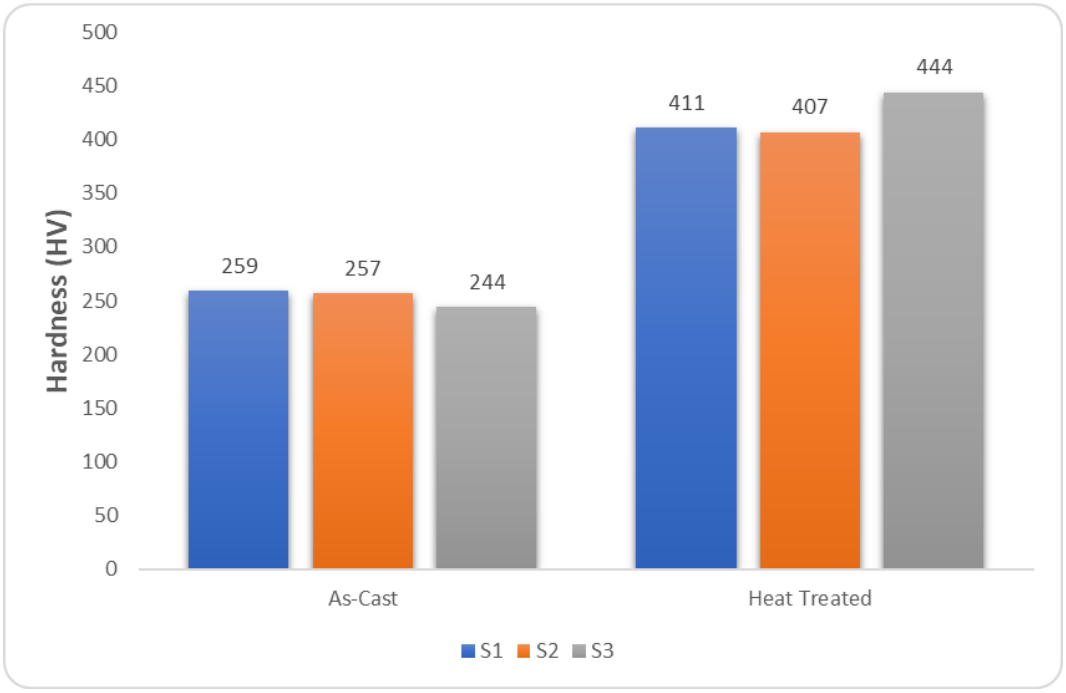

Figure 4.13 Micro Hardness comparison of as cast and heat treated S1 (Ti-23.8Nb-2Zr-1.2O), S2 (Ti-23Nb-0.93V-2Zr-1.2O) and S3 (Ti-25Nb-0.7Ta-2Zr-2Al-1.2O) alloys.

4.2 Mechanical Properties

4.2.1 Microhardness Test

The most important feature of gum metal is the absence of strain hardening. In order to determine whether the alloys cast homogeneously in the arc furnace had the property of gum metal or not, the samples were subjected to cold deformation process. Microhardness test was performed before and after deformation, and results were compared. Thus, hardness changes due to the cold deformation were observed. In order to have gum metal property, the hardness value before and after deformation should not change. Microhardness test results are given in Figure 4.14. S3 has the lowest hardness value in as-cast alloys due to aluminum-tantalum addition. However, as deformation increases, the hardness value of S3 increases linearly. The

hardness value of S1 and S2 alloy is almost not increased after 30% deformation. The reason for that the first deformation process up to 30% in thickness, the formation of twin and SIM α" or dislocation movement can be responsible for deformation, and after dislocations are completely inhibited, deformation may be continued with a giant fault like mechanism. Hence, the increased deformation ratio does not cause an increase in hardness for S1 and S2, but the same situation cannot be said for S3. In addition, in order to compare the effect of cold working on candidate alloys and common alloys, the copper alloy was also cold worked, and changes in the hardness value were observed. Copper alloy initially has 80 HV hardness value. Cold working increased the hardness value of copper alloy to 150 HV, which is almost twice the initial value; on the other hand, cold working was able to increase the hardness of candidate alloys (S1, S2, and S3) from 250 HV to 280 HV. After 60% cold worked, the hardness value of S1 and S2 were almost unchanged.

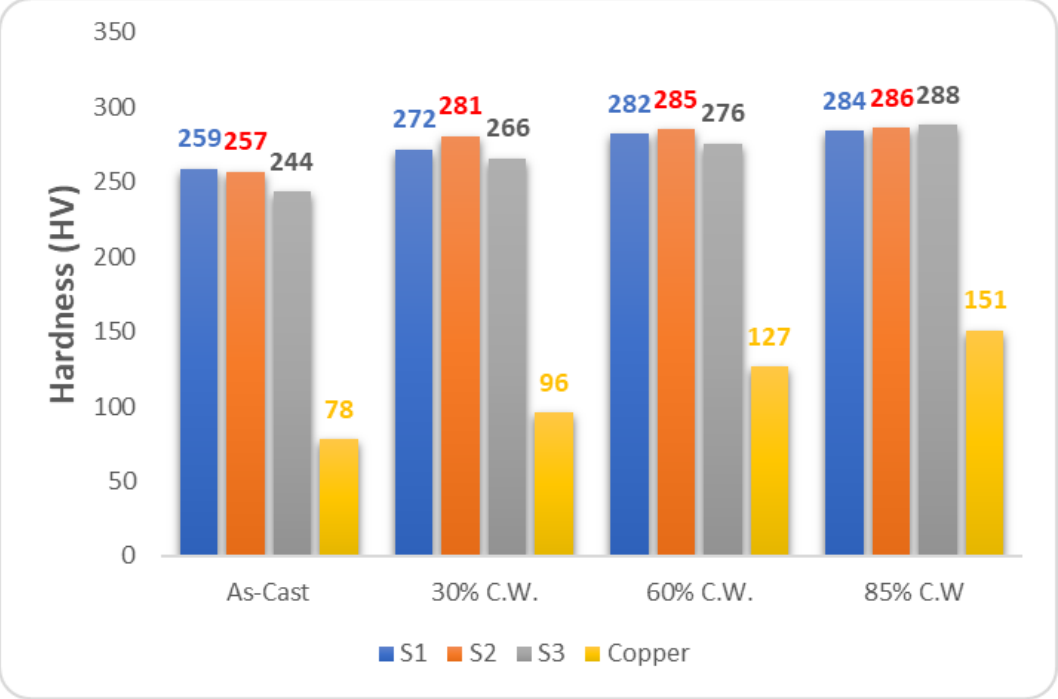

Figure 4.14 Micro Hardness comparison of 0%, 30%, 60%, 85% cold worked and α phase (DSC) S1 (Ti-23.8Nb-2Zr-1.2O), S2 (Ti-23Nb-0.93V-2Zr-1.2O) and S3 (Ti-25Nb-0.7Ta-2Zr-2Al-1.2O) alloys.

4.2.2 Compression Test

Cold deformation process and physical tests were done with a compression test in accordance with the ASTM E9 standard. Materials have been compressed under the constant strain rate of 10^{-4} s^{-1} and 100 kN load. Furthermore, friction conditions of all samples are the same due to the identical conditions. Each sample has the same dimensions, same surface smoothness, and no lubricant was used between the device and samples. Compressive engineering strength vs. strain graphs for all samples are drawn and shown in Figure 4.15. The dimensions of the samples before and after the compression test are shown in Table 4.2. None of the samples were broken during the compressive test, which shows that alloy has very high deformation capacity.

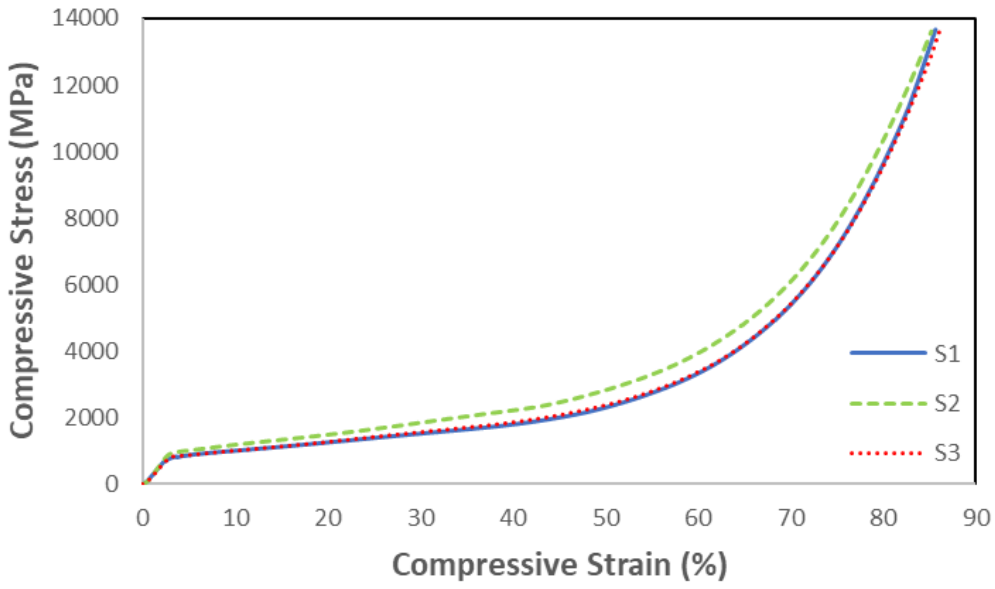

Figure 4.15 The compressive engineering stress-strain behavior of S1 (Ti-23.8Nb-2Zr-1.2O), S2 (Ti-23Nb-0.93V-2Zr-1.2O) and S3 (Ti-25Nb-0.7Ta-2Zr-2Al-1.2O) alloys at higher values of strain.

Table 4.3 *Dimensions before and after the compression test of S1, S2, and S3.*

	R_i (mm)	H_i (mm)	R_f (mm)	H_f (mm)	Reduction in H. at 100 kN load(%)
S1	3	6	7,85	1,00	83,3
S2	3	6	7,65	1,05	82,5
S3	3	6	7,9	0,95	84,2

The relationship between the compressive strength and the tensile strength varies according to the material. The compressive and tensile strength of materials with low elastic modulus is close to each other, whereas the compressive strength of materials with high elastic modulus is greater than the tensile strength (Figure 4.16) [71]. Since the alloys produced in this thesis have a low elastic modulus, the compressive strength is very close to the tensile strength, so it can be said that yield strength be calculated by using the offset method.

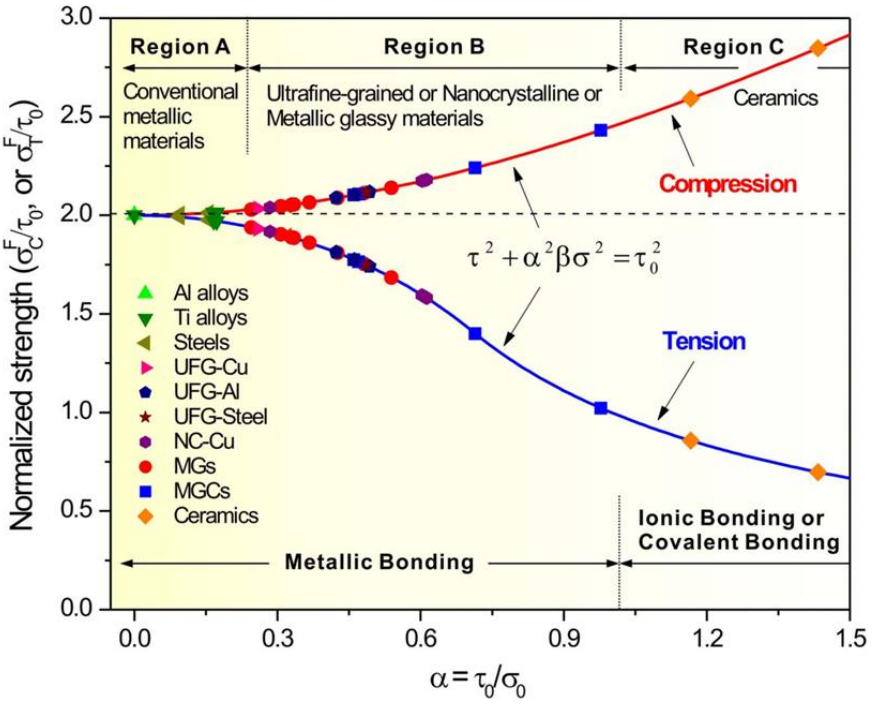

Figure 4.16 Normalized tensile strength and compressive strength of various metals [71].

As the samples which were cast in the laboratory-scale arc furnace could not meet the tensile test measurement standards, samples were subjected to the compression testing to observe their mechanical properties. The 0.2% compressive yield strength was calculated from the engineering stress-strain graph by using a 0.2% offset method, which is used in tensile stress-strain graphs. The yield points, which are determined by the offset method, are on the necking point. Moreover, to confirm the accuracy of the results, a single beta phase titanium alloy with known yield strength was compressed under the same conditions, and it was found that the yield strength was close to the expected value. Thus, the calculated yield strength of candidate samples can be considered as reasonable. The engineering stress-strain graph obtained from the compression test of each alloy is given in Figure 4.17-4.19.

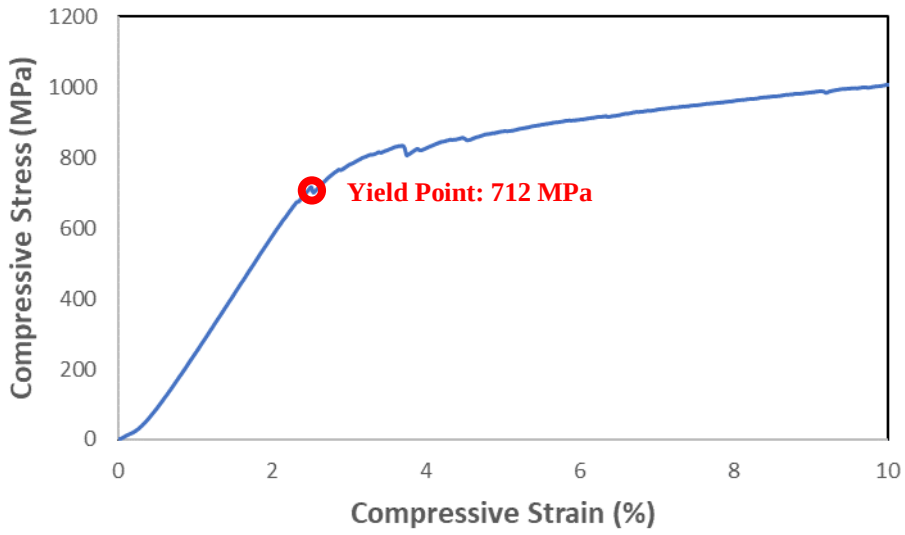

Figure 4.17 The compressive engineering stress-strain behavior of S1 (Ti-23.8Nb-2Zr-1.2O) up to 10% strain limit.

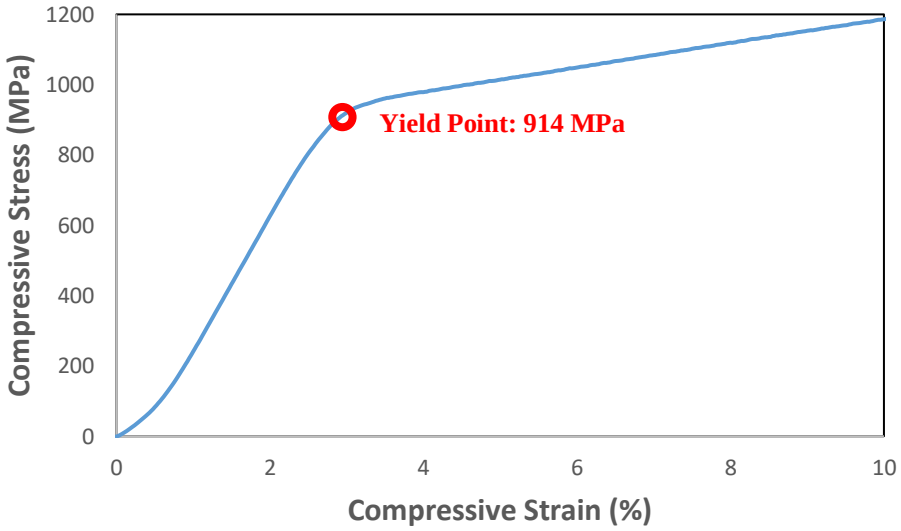

Figure 4.18 The compressive engineering stress-strain behavior of S2 (Ti-23Nb-0.93V-2Zr-1.2O) up to 10% strain limit.

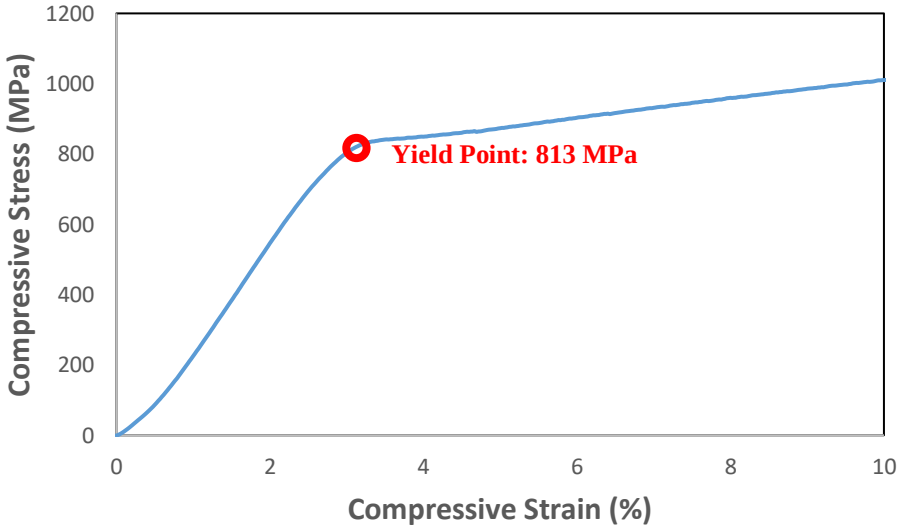

Figure 4.19 The compressive engineering stress-strain behavior of S3 (Ti-25Nb-0.7Ta-2Zr-2Al-1.2O) up to 10% strain limit.

Elastic deformation of most of the metals is limited up to 0.005 strain. When an alloy is strengthened, ductility is sacrificed. Almost all reinforcement techniques are based on restricting or preventing dislocation, making the material harder and stronger. Alloys are stronger than pure metals because impurity atoms entering the solid solution typically apply lattice strains to surrounding host atoms. Interference between dislocations and these impurity atoms results in the lattice strain field, and consequently, dislocation motion is restricted, and deformation capability is limited [72]. However, as shown in the compression test graphs, yield strengths are higher than 700 MPa, and plastic strain exceeds nearly 85% since alloys did not break under 100kN. These alloys have not only high yield strength but also have high deformation capacity.

According to results, S1 has the lowest yield strength. The alloy with the highest yield strength is S2. It is seen that the addition of alloying elements vanadium and aluminum with tantalum increases the yield strength of the base alloy.

4.3 Characterization of Deformed Alloys

The most important feature that distinguishes gum metal from other metals is its extraordinary deformation mechanism and superior mechanical properties. This section will explain whether the produced alloys have gum metal properties or not.

After the as-cast alloys were subjected to cold compression up to 30%, 60%, and 85% in thickness reduction, cold-worked alloys were divided by two pieces. One-piece was cut parallel to the deformation direction, and the other part was cut vertically. Optical and SEM analyzes of two pieces were done and evaluated.

Briefly explaining the deformation mechanisms (gum metal, slip, twinning, kink band, and stress-induced martensite (α")) related to gum metal and beta phase titanium alloy can be useful for understanding the deformed structure observed in this thesis. As mentioned early, deformation mechanisms rather than giant faults such as twin, slip, and stress-induced martensite could be observed in the gum metal

[49-56]. Twin and giant fault are similar in appearance. Both of them are thick and extend from the grain boundary. The difference is that twin glides on a single axis while giant fault glides on two perpendicular axes. Giant fault formation is illustrated in Figure 4.20 [11, 37]. According to Yang's article [46] if the lines extending from the grain boundary is thick, they are called as deformation twins (Figure 4.21 (a)), if extending lines are thin, they are called as a slip or SIM α" (Figure 4.21 (b)). When the lines are homogeneously distributed and parallel to each other, the deformation mechanism is SIM α" (an orthorhombic phase which occurs after the diffusionless deformation process), and if it is scattered and passes through each other, it is slip. Formation of band structures induced by dislocation free deformation causes strain softening and the formation of kink bands [46, 73]. Kink bands can be seen on surfaces perpendicular to the deformation direction (Figure 4.21 (c)). As the deformation rate increases, the deformation mechanism changes from kink or twins to shear bands (Figure 4.21 (d)) [46].

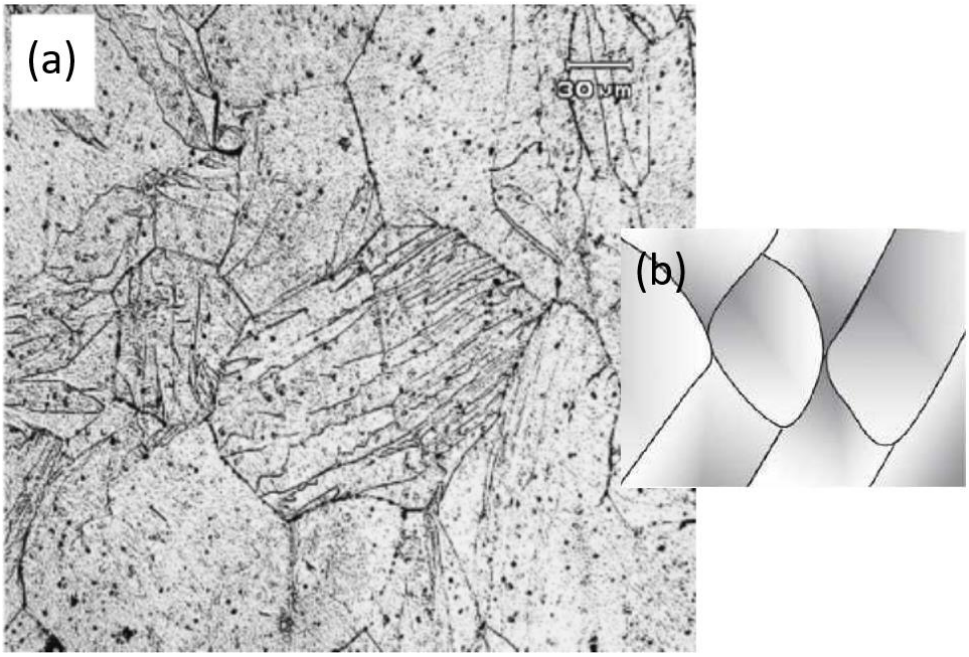

Figure 4.20 Giant faults on the %40 deformed Gum Metal (a) and subgrain form (b) [11, 37].

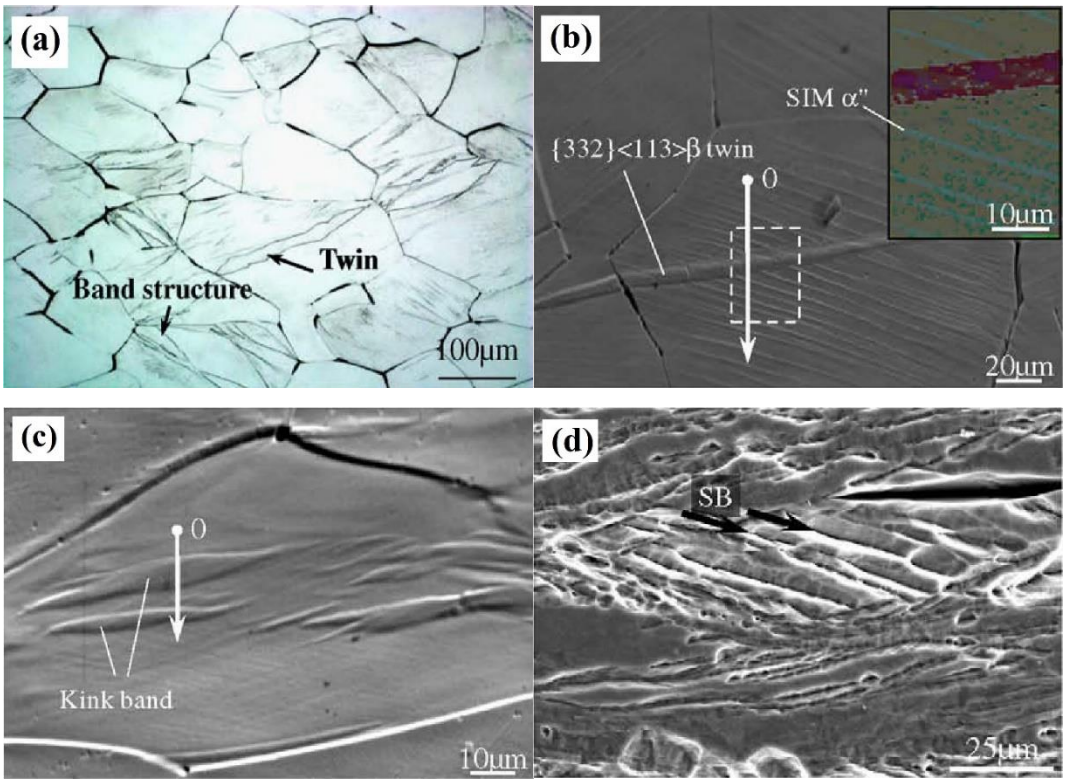

Figure 4.21 Microstructure of cold-compressed specimen deformation twinning (a), stress induced martensite (b), kink band (c) and shear bands (d) [46].

The XRD patterns of 85% cold-worked samples given in Figure 4.22 reveal that cold deformation leads to an increase in the intensity of (200) BCC and (211) BCC diffraction peaks. This result provides that there is no phase transformation during the compression test. As the stress applied causes the atoms to be ordered in a certain direction and plane, the intensity of the second and third peaks increases. Furthermore, reflection peaks are observed to broaden. There may be two reasons for the broadening of peaks. One of them is the reduction of crystallite size. As it is known, when the alloys having dynamic recovery or recrystallization are subjected to severe plastic deformation, the line defects (dislocations) turn into surface defects (grain boundaries) without any failure. This transformation creates a new subgrain. Therefore, the grain size becomes smaller and produces nano-sized grains that are too small to be obtained by heat treatment. In other words, severe deformation reduces the grain size to nano size in special metals [74]. Since gum metal is a special metal which does not cold worked and does not show dislocation activity, a similar

process except dislocation activity could have taken place. The formation of giant faults or shear bends may have caused subgrain by disrupting grain boundaries. Severe plastic deformation may have reduced the grain size of these produced alloys. The other reason for broadening peak is the presence of stress-induced martensite α" (SIM α") phase. The peaks of the α" phase shown in Figure 4.23 is very close to the peaks of the β phase, and it is difficult to determine the α" peaks between the broad β peaks [75]. Although only the beta phase peaks appear in the XRD pattern, there may be stress-induced α" phases due to the broadening of β phase peaks. Crystallite size, lattice parameters, and strain (%) values of the three samples were calculated after Rietveld refinement and listed in Table 4.4. It is interestingly seen that strain values of sample 2 (S2) almost do not change after the deformation process; but, sample 1 (S1) and sample 3 (S3) slightly increased. Furthermore, the crystallite size seems to decrease due to the cold working process. Thus, it can be said that subgrain formations decreased grain size. Almost no changes in strain values could indicate that the candidate alloys exhibit gum metal properties.

Table 4.4 *XRD characteristics of as-cast and deformed S1 (Ti-23.8Nb-2Zr-1.2O), S2 (Ti-23Nb-0.93V-2Zr-1.2O) and S3 (Ti-25Nb-0.7Ta-2Zr-2Al-1.2O) alloys*

Alloy	As-Cast			Deformed		
	Lattice Constant (Å)	Crystallite Size (Å)	Micro Strain (%)	Lattice Constant (Å)	Crystallite Size (Å)	Micro Strain (%)
S1	3.312	112	0.512	3.299	84	0.753
S2	3.300	124	0.507	3.284	83	0.592
S3	3.299	154	0.408	3.292	68	0.926

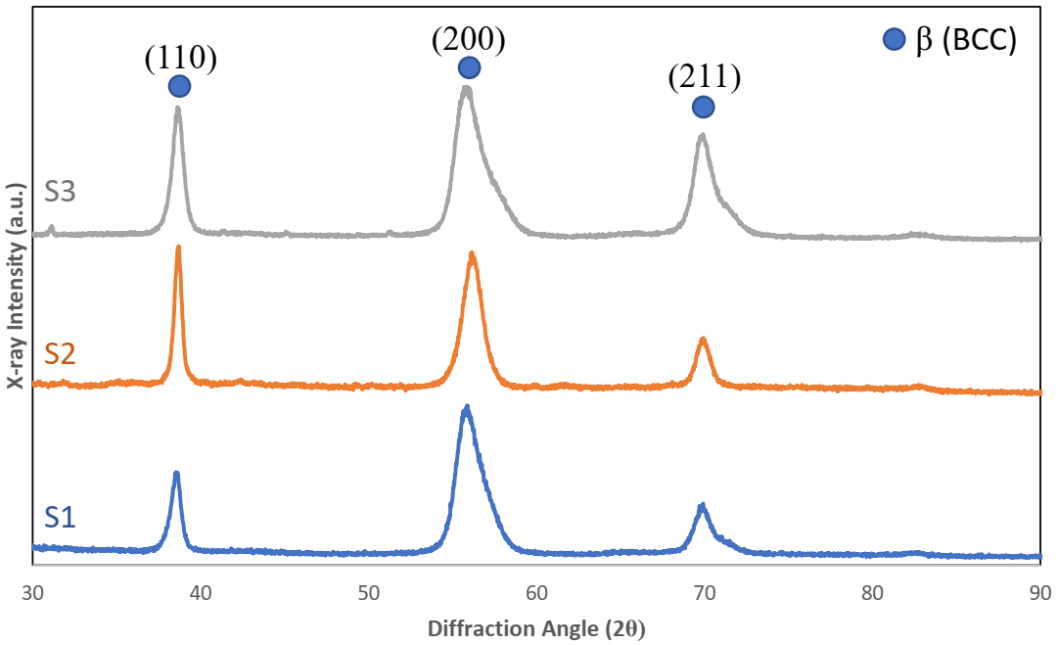

Figure 4.22 XRD patterns of 85% cold deformed S1 (Ti-23.8Nb-2Zr-1.2O), S2 (Ti-23Nb-0.93V-2Zr-1.2O) and S3 (Ti-25Nb-0.7Ta-2Zr-2Al-1.2O) alloys.

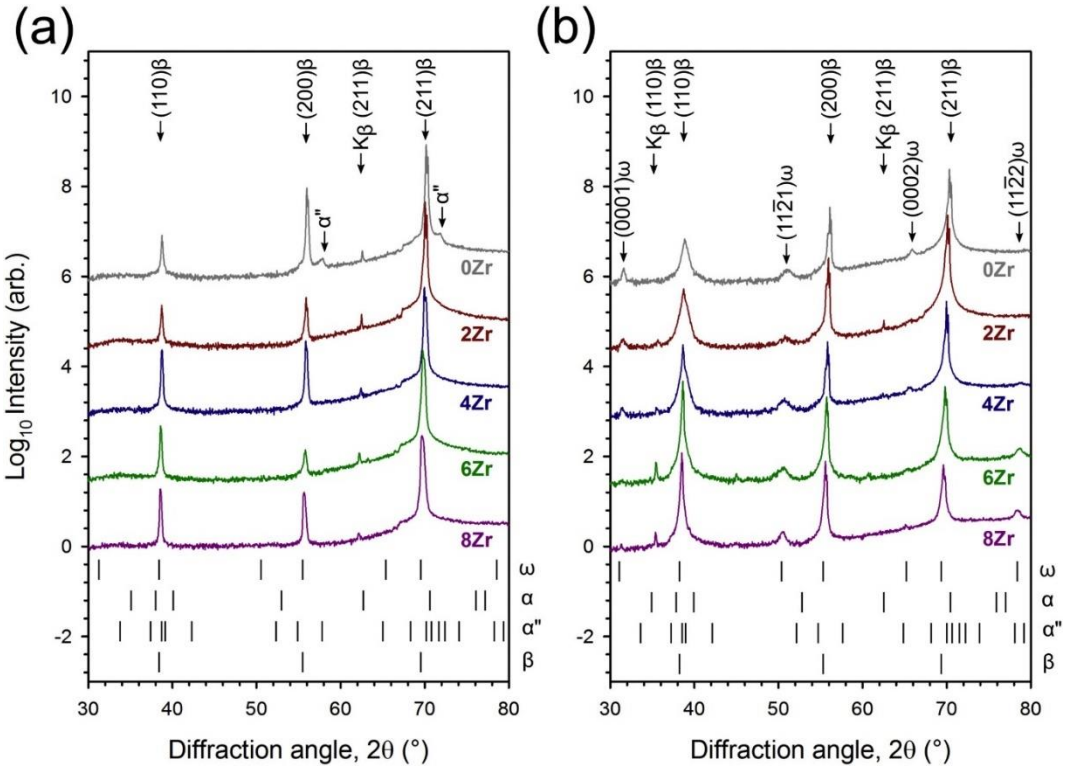

Figure 4.23 X-ray diffraction (XRD) patterns for Ti-24Nb-(0–8)Zr alloys (a) in the as-recrystallized (AR) state and (b) after aging at 300 °C for 100 h [75].

Sample 2 (S2) has the minimum broadening peaks; hence, the probability of having an α" phase is very low. On the other hand, sample 1 (S1) and sample 3 (S3) may contain α" phase. Cold deformation leads to the formation of stress-induced α" and ω phases. It has been reported that diffusionless phase transformation after deformation process, such as β→ α" (bcc to orthorhombic) or β→ω (bcc to hexagonal) in metastable β titanium alloys results in twin formation [68] Thus, the presence of deformation twinning suggests that α" and ω phases exist in the structure. It is necessary to look at the SEM results in order to make a final decision.

The microstructure of each alloy dramatically changes after the cold working in which deformation 'lamella' bands are observed mainly in the planar growth zone (Figure 4.24-4.29). It is complicated to determine the deformation mechanisms such as giant fault, twin, and slip by looking at the optical micrographs. In order to determine the deformation mechanisms correctly, it is necessary to determine the plane and direction of the deformation mechanism. In this study, deformation mechanisms were determined by comparing the optical micrographs and SEM images given in the literature (Figure 4.20 - 4.21).

The microstructure of the S1 at different cold worked amount is shown in Figure 4.24-4.25. When the cold working ratio (C.W.) is 30%, deformation mechanism could be a giant fault which is seen on the perspective of perpendicular to deformation direction, twin and SIM α", which are visible on parallel to deformation direction. When the deformation rate increases to 60 percent, giant faults form subgrain seen in Figure 4.24 (c). Furthermore, twins also exist at a 60% deformation rate. An increase in the cold working ratio increases the deformation bands. When the cold working ratio reaches 85%, twins and SIM α" transforms to shear bands. Shear bands are characterized by a mesoscopic orientation that does not have a specific crystallographic direction, such as a slip and twinning system. Furthermore, slip and twinning systems are located within the grain boundaries; however, shear bands often penetrate multiple grains. Therefore, they are also referred to as noncrystallographic deformation zones [76]. Kink band is also seen at 85% C.W.

The presence of twins and SIM α" reinforces the likelihood that the reason for broadening beta peak in the XRD could be caused by α" phase.

The deformation mechanism of sample 2 (S2) does not show SIM α," as seen in XRD analysis and optical micrographs. Niobium is known to inhibit the formation of SIM α"; on the other hand, although the amount of niobium content is less than the sample 1 (S1), SIM α" does not observe in S2. It is said that the presence of vanadium with the help of niobium prevents the formation of SIM α". When the C.W. ratio is 30%, giant faults become visible. Furthermore, from Figure 4.26 (b), deformation bands nucleated at the grain boundary and propagated into the grain interior. These bands could be giant faults or twins. Bands are likely to be twins since they have a certain deformation direction and planes. Shear bands are formed as the deformation rate increases as in sample 1 (S1). Furthermore, the increase in the C.W. ratio increases the complexity and band's number.

Aluminum-tantalum addition seems to increase the number and complexity of deformation bands. From Figure 4.28 (a) and (b), deformation bands are similar to each other. For Figure 4.28 (a), deformation bands are not entirely parallel to each other, and it looks like they do not have a specific direction. Thus, it could be considered as giant faults. However, from Figure 4.28 (b), deformation bands seem to have a precise orientation or direction, so they were evaluated as a twin. When the C.W. ratio reaches 60%, the cluster of SIM α" makes subgrain.

As mentioned earlier, it is quite challenging to determine slip deformation by using optical micrographs. If segregation occurs as a result of slip deformation, the etching effect becomes more visible, and the surface may appear darker under the optical micrographs. When we look at the third sample (S3), dark regions can be considered as a slip so dislocation activity could exist in sample 3. Oxygen and zirconium increase the critical shear stress required for the slip. Although oxygen and zirconium contents are the same for all three alloys, the addition of aluminum may have reduced the critical shear stress. The presence of the SIM α" on the micrograph proves that the peak of the XRD belongs to SIM α".

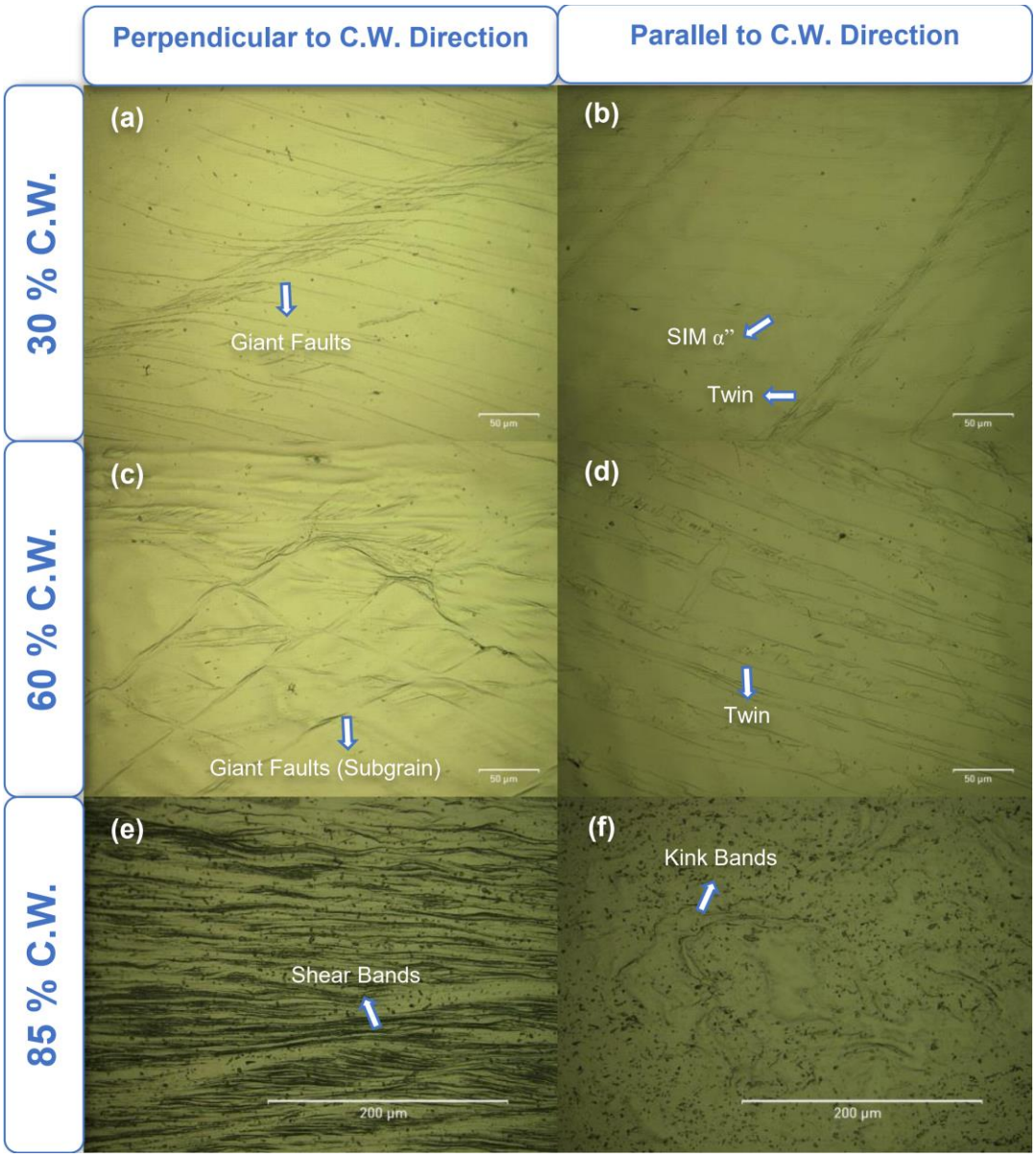

Figure 4.24 Optical micrographs of 30% (a, b), 60% (c, d), and 85% (e, f) cold deformed S1 (Ti-23.8Nb-2Zr-1.2O) alloy. (Micrographs of (a), (c), and (e) are perpendicular to the compression direction; (b), (d), and (f) are parallel to the compression direction).

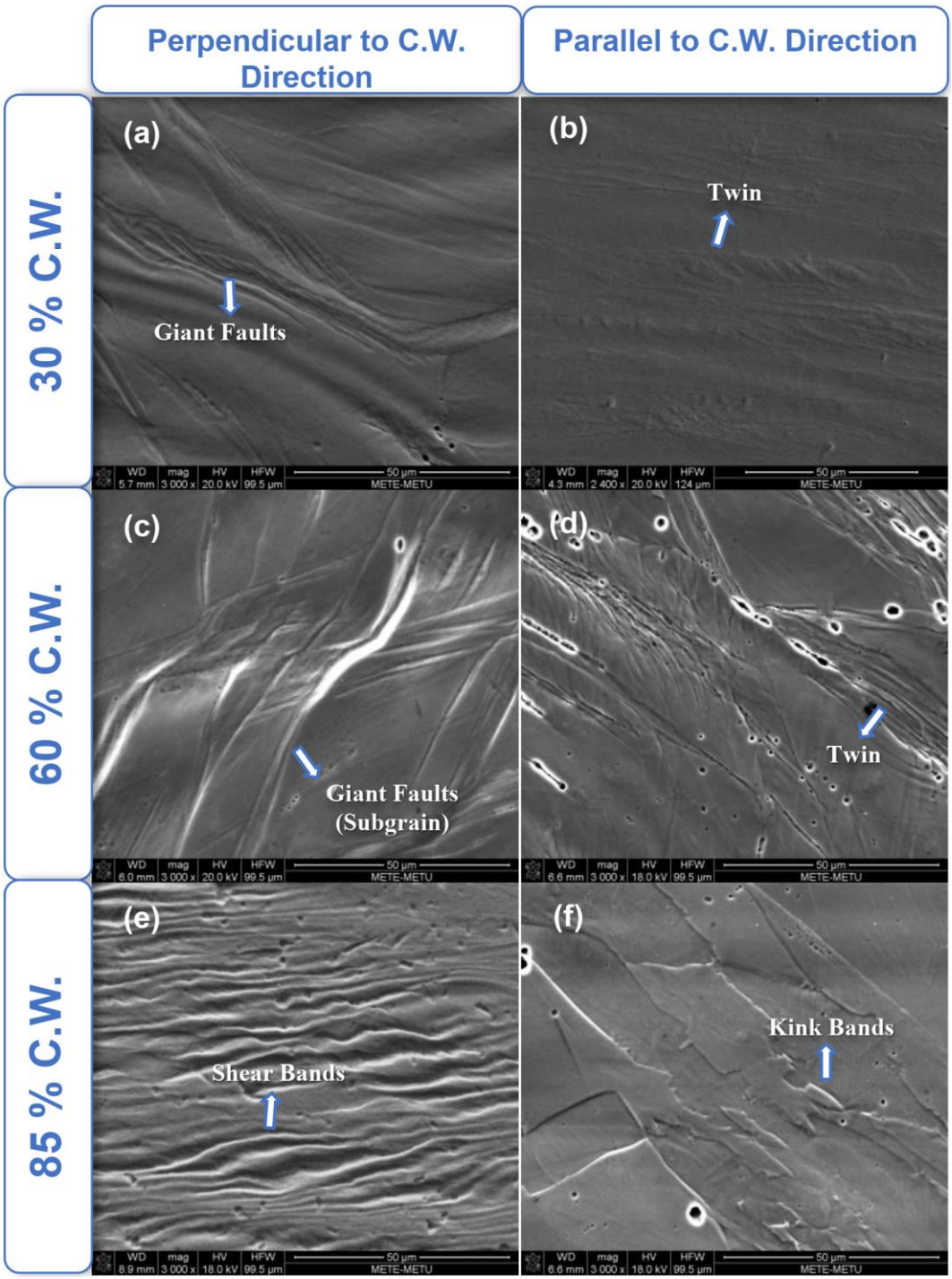

Figure 4.25 SEM images of 30% (a, b), 60% (c, d), and 85% (e, f) cold deformed S1 (Ti-23.8Nb-2Zr-1.2O) alloy. (Micrographs of (a), (c), and (e) are perpendicular to the compression direction; (b), (d), and (f) are parallel to the compression direction).

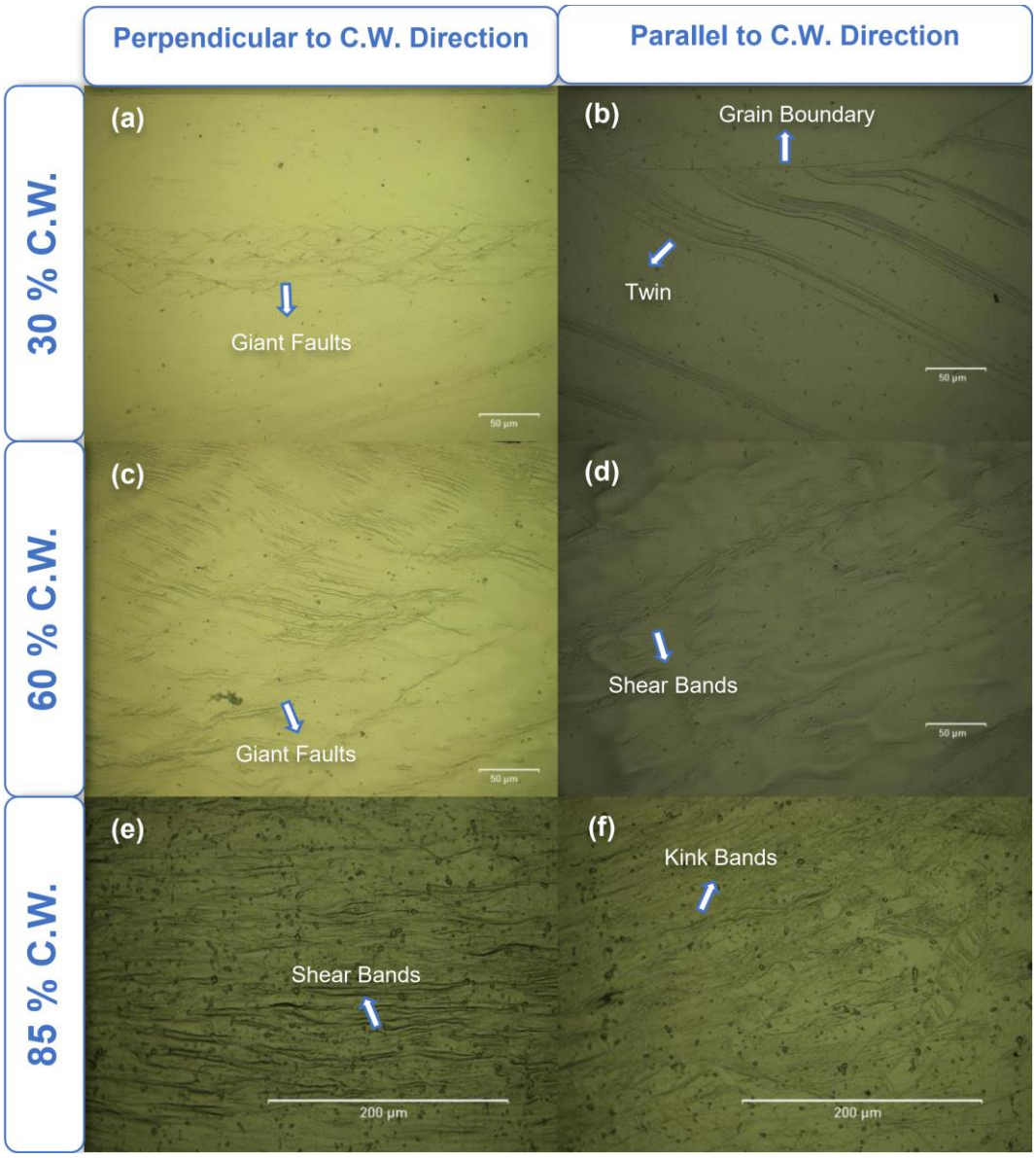

Figure 4.26 Optical micrographs of 30% (a, b), 60% (c, d), and 85% (e, f) cold deformed S2 (Ti-23Nb-0.93V-2Zr-1.2O) alloy. (Micrographs of (a), (c), and (e) are perpendicular to the compression direction; (b), (d), and (f) are parallel to the compression direction).

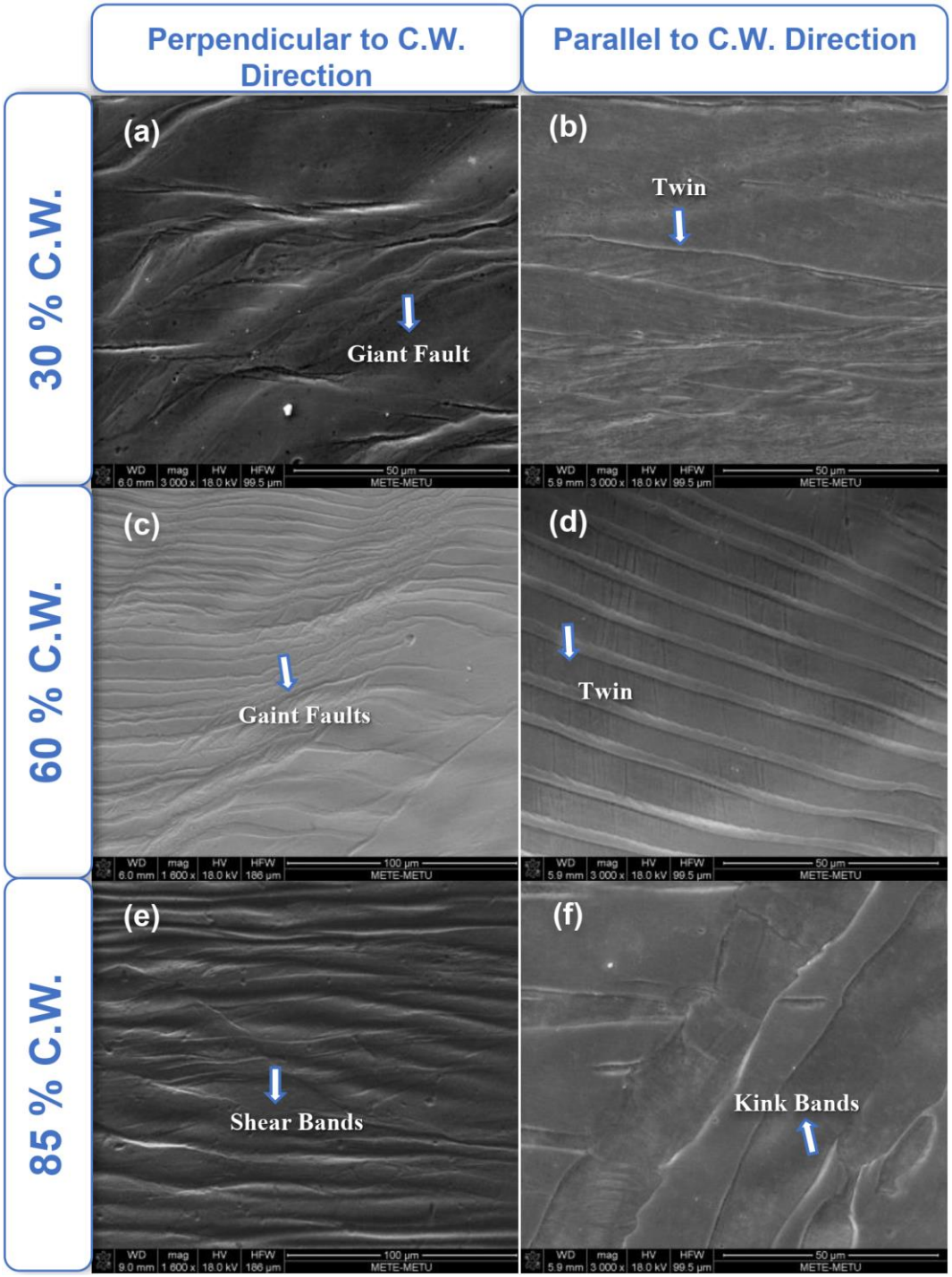

Figure 4.27 SEM images of 30% (a, b), 60% (c, d), and 85% (e, f) cold deformed S2 (Ti-23Nb-0.93V-2Zr-1.2O) alloy. (Micrographs of (a), (c), and (e) are perpendicular to the compression direction; (b), (d), and (f) are parallel to the compression direction).

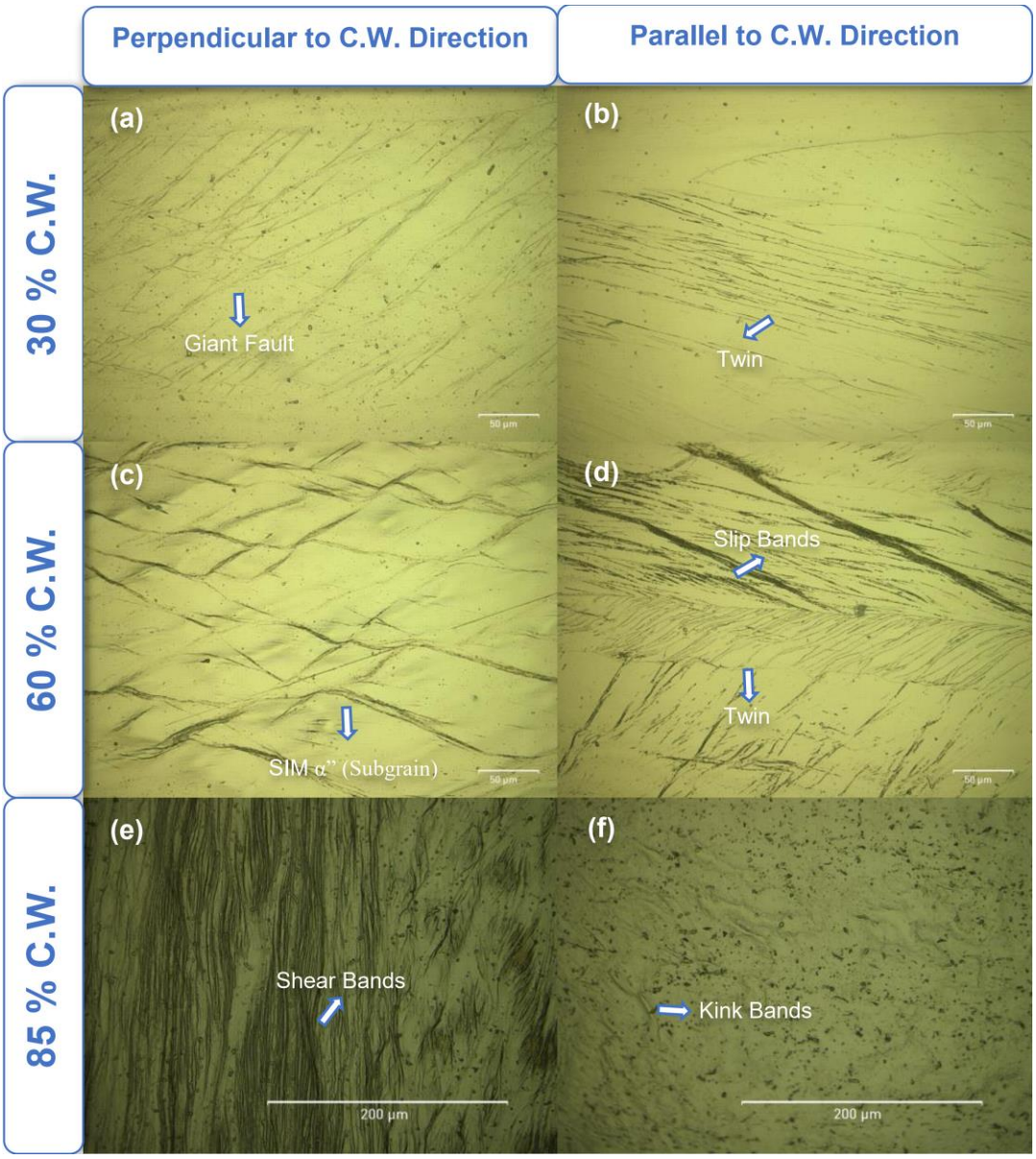

Figure 4.28 Optical micrographs of 30% (a, b), 60% (c, d), and 85% (e, f) cold deformed S3 (Ti-25Nb-0.7Ta-2Zr-2Al-1.2O) alloy. (Micrographs of (a), (c), and (e) are perpendicular to the compression direction; (b), (d), and (f) are parallel to the compression direction).

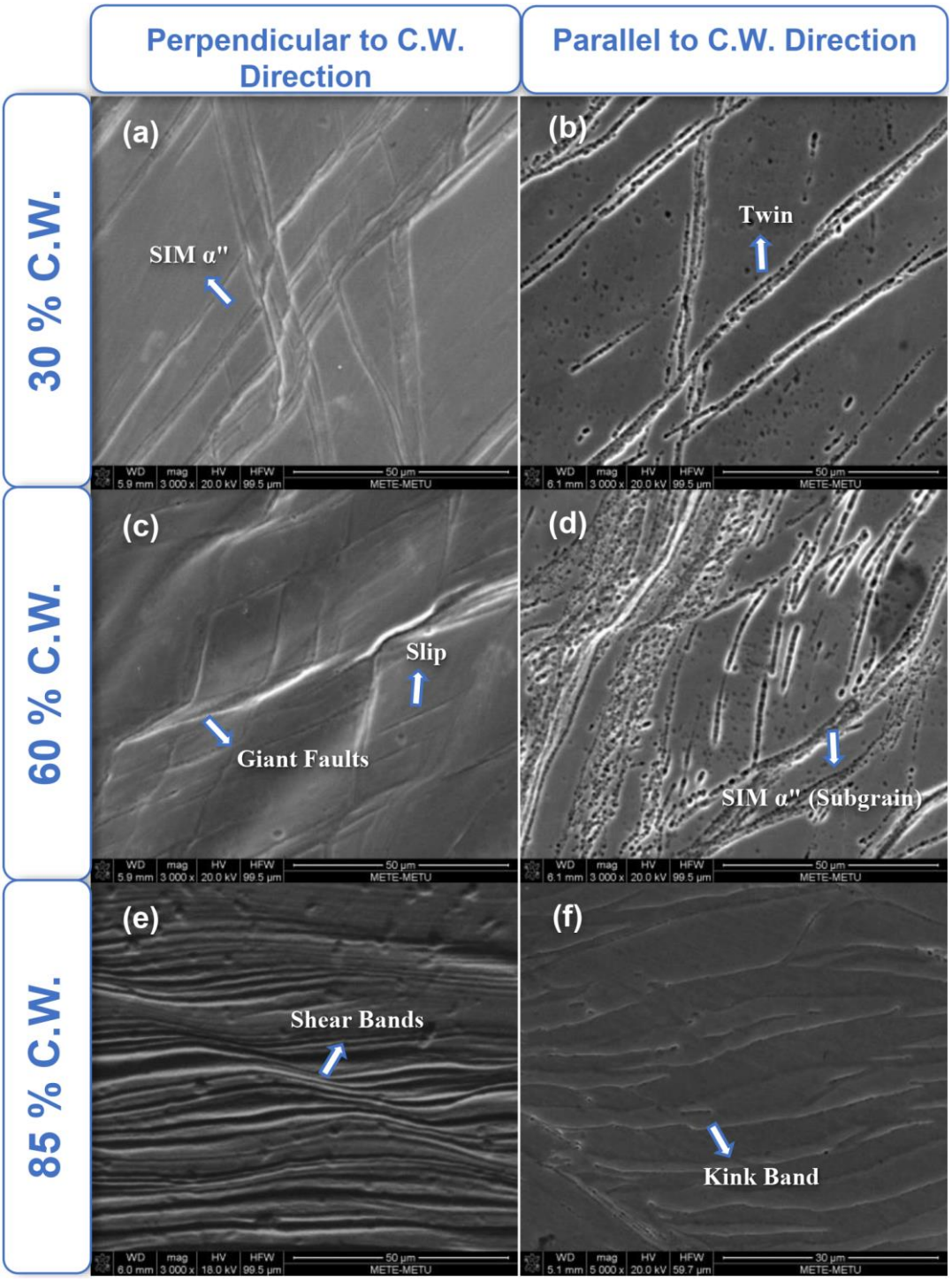

Figure 4.29 SEM images of 30% (a, b), 60% (c, d), and 85% (e, f) cold deformed S3 (Ti-25Nb-0.7Ta-2Zr-2Al-1.2O) alloy. (Micrographs of (a), (c), and (e) are perpendicular to the compression direction; (b), (d), and (f) are parallel to the compression direction).

CHAPTER 5

CONCLUSIONS AND FUTURE SUGGESTIONS

5.1 Conclusions

Within the scope of this work, three unique compositions were selected to adhering magic numbers differing from the original gum metal composition. The selected compositions are (S1) Ti-23.8Nb-2Zr-1.2O (at %), (S2) Ti-23Nb-0.93V-2Zr-1.2O, and (S3) Ti-25Nb-0.7Ta-2Zr-2Al-1.2O (at %). These alloys were produced successfully in the arc remelting method rather than the inconvenient powder metallurgy method.

The following conclusions are drawn from the thorough microstructural characterization, phase analysis, thermal analysis, and mechanical tests of as-cast state and deformed state. The crucial points of the as-cast state can be summarized as follows:

- Three as-cast alloys consist of only the beta phase due to the presence of β stabilizer alloying elements “Nb, Zr” and with the help of interstitial oxygen. It is seen that the addition of alloying elements of vanadium, aluminum, and tantalum affects the lattice, thus increasing the diffraction angle due to the change in the lattice parameters. Furthermore, aluminum addition to the base alloy leads to an increase in the intensity of the third peak from (211) plane, which may be attributed to Al atom distribution in the BCC structure of alloys.

- Differential scanning calorimetry (DSC) analysis was performed to determine the thermal behavior of the alloys. However, the exact phase transition temperature curve could not be observed during both heating and cooling due to incredibly slow kinetics.
- In-situ thermal XRD analysis was performed for thermal analysis of deformed alloys due to insufficient information from DSC analysis. Phase transition α to β is seen at 900 ^{o}C for S1, 800 ^{o}C for S2, and S3. Vanadium and Tantalum with aluminum addition decrease the β transition region, which means increase the beta stability of titanium alloy.
- During solidification, the solid-liquid interface undergoes morphological instability because of the changing growth velocity; thus, there is a structural transition from planar growth to dendritic solidification as the solidification rate decreases moving away from the contact surface. Planar growth areas of S2 and S3 are higher than the base alloy (S1) due to the effect of alloying element differences. The presence of vanadium could have decreased the melting point or beta transition temperature. Furthermore, it decreases the grain size, and grain becomes more equiaxed owing to vanadium addition. Aluminum and tantalum addition to alloy may have decreased the viscosity, melting point, or beta phase transition temperature. All three candidate alloys are homogeneously distributed. In micrographs, alloys were observed only in the beta phase.

The crucial points of the deformed state can be summarized as follows:

- After severe deformation (200)bcc and (211)bcc reflection peak intensity of three alloys increased. Furthermore, reflection peaks are observed to broaden. One of the reasons for broadening peaks is that the presence of SIM α" due to cold deformation. Another reason is that crystallite size decreases due to severe deformation. S1 and S3 contain SIM α" phase; on the other hand, S2 includes only the β (BCC) phase. Vanadium addition could have inhibited the formation of SIM α".

- Deformation changes the microstructure dramatically. Lamella bands are observed for three alloys. It is seen that giant fault formation is seen on the only perpendicular to deformation direction, Twin, SIM α" and kink bands are seen on parallel to deformation direction. Giant faults are observed at S1 and S2, while slip bands are seen at S3. Aluminum addition distortion the giant fault mechanism to SIM α" and slip bands. On the other hand, vanadium increases the beta stability due to inhibition of SIM α" and twin deformation. When the deformation ratio increases, twins transform to shear bands.
- The hardness value of S1 and S2 almost do not change with the deformation process after a 30% reduction in thickness. However, the hardness value of S3 and copper alloy increases linearly with the deformation ratio. Moreover, an increase in the hardness ratio of all candidate alloy is below 15%, while increasing hardness ratio copper alloy is almost 100%. There are almost no noticeable changes in the hardness values for all of the candidate alloys. S1 and S2 behave like gum metal properties, but S3 does not. Except for those, the hardness value can be twofold of the BCC phase when it changes to the alpha phase.
- Original as-cast gum metal alloys, produced by the powder metallurgy method, generally have 750-950 MPa yield strength values [25, 78]. In this study, as-cast candidate alloys which were produced by arc melting method have almost the same yield strength value as original gum metal. Alloying elements increases the yield strength of the alloys. S1 has only 712 MPa, while S2 has the most yield value of 914 MPa, and S3 has 813 MPa. Furthermore, all candidate alloy have enormous plastic strain values (>80%). The yield strength value and plastic strain level of the three alloys are close to the original gum metal.

5.2 Future Suggestions

After the cold working operation, optical examination and XRD analysis were performed. However, it is better if in-situ tensile XRD and optical examination were done during the tensile test, it can give better information about the deformation mechanism.

In order to determine the deformation structures, it is necessary to know the direction and planes of the deformation bands. Therefore, TEM analysis is essential for deformation mechanism determination. TEM analysis should be used for the examination of the microstructure and deformation mechanism.

Within the scope of this work, a compression test was performed to observe the mechanical properties. The compression test does not give an accurate result about elastic strain and modulus. The tensile testing method could be better instead of the compression test.

Using a dilatometer instead of DSC analysis may be more useful in seeing phase transformation.

The effect of zircon and oxygen on the deformation mechanism is known. However, this is explained by the cluster mechanism in the literature. Zircon and oxygen may have a different effect on the deformation mechanism other than the clustering mechanism. The tetragonal phase zirconia undergoes a higher volume monoclinic phase under force. This mechanism is used to stop the crack propagation in ceramics and is described as a fracture transformation toughening mechanism [77]. The gum metal contains zircon and oxygen. During melting, zircon atoms can combine with the oxygen in the structure to form the zirconia and remain in the tetragonal phase at room temperature via rapid cooling. During cold work, zirconia, whose crystal structure changes by 4% in volume, can create lattice strain to help prevent dislocating activity. Therefore, whether zircon and oxygen have this mechanism should be examined in later studies.

In this thesis, the thickness of the sample becomes very thin as the cold working process was made by the compression method. Consequently, the cold-worked alloys had no possibility of mechanical testing other than hardness test. In the literature, cold deformation is performed by the cold swaging method [6]. The suggestion of this thesis is that a cold working process should be applied by equal channel angular pressing method using in severe plastic deformation method, which will not change the total shape for cold deformed alloys. With this method, the shape integrity of the alloy will not be disturbed, and it will allow mechanical tests.

It is noteworthy that no crack formation has not been observed on candidate alloys after the compression test, and their hardness values almost remained the same. It was also supported by optical micrographs where giant faults formed subgrain. The severe plastic deformation technique, used to produce nano-size grain alloys to improve their mechanical properties, can be applied to this material. Different deformation mechanisms or mechanical properties may occur.

REFERENCES

[1] K. Nitta, S. Watanabe, N. Masahashi, H. Hosoda and S. Hanada: Structural Biomaterials for 21st Century, ed. by M. Niinomi, T. Okabe, E. M. Taleff, D. R. Lesuer, H. E. Lippard, (TMS, Warrendal, 2001) pp. 25–34.

[2] M. Niinomi: Metall. Mater. Trans. A 33A (2002) 477–486.

[3] T. Ahmed, M. Long, J. Silvestri, C. Ruiz and H. J. Rack: Titanium '95 Science and Technology, ed. by P. A. Blankinsop, W. J. Evans, F. H. Flower, The Material Society, London, (1996) pp. 1760–1767.

[4] M. Niinomi: Mater. Sci. Eng., A 243 (1998) 231–236.

[5] D. Kuroda, M. Niinomi, K. Fukui, A. Suzuki and J. Hasegawa: Tetsu–to-Hagane 86 (2000) 610–616.

[6] T. Akahori, M. Niinomi, T. Maekawa, K. Fukui and A. Suzuki: J. Japan Inst. Metals. 66 (2002) 715–722.

[7] M. Niinomi, T. Akahori, T. Yabunaka, K. Fukui and A. Suzuki: Tetsu– to-Hagane 88 (2002) 553–560.

[8] M. Niinomi, T. Akahori, S. Nakamura, K. Fukui and A. Suzuki: Tetsu–to-Hagane 88 (2002) 567–574.

[9] T.Saito, T.Furuta, J.H.Hwang, S.Kuramoto, K.Nishino, N.Suzuki, R.Chen, A.Yamada, K.Ito, Y.Seno, T.Nonaka, H.Ikehata, N.Nagasako, C.Iwamoto, Y.Ikuhara, T.Sakuma, Multifunctional alloys obtained via a dislocation–free plastic deformation mechanism, Science, V. 300(18), (2003), p. 464.

[10] M.Y. Gutkin, T. Ishizaki, S. Kuramoto, and I.A. Ovid'ko, Acta Mater. 54, (2006), p. 2489.

[11] Kuramoto S, Furuta T, Hwang J, Nishino K, Saito T., Plastic Deformation in a Multifunctional Ti-Nb-Ta-Zr-O Alloy, Metall Mater Trans A, Vol. 37, (2006), p.657.

[12] C.R. Krenn, D. Roundy, J.W. Morris Jr., M.L. Cohen, Mater. Sci. Eng. A 319-321, (2001), p.111–114.

[13] Kuramoto S, Furuta T, Hwang J, Nishino K, Saito T. Mat Sci Eng A, (2006), p. 442-454.

[14] Gutkin MY, Ishizaki T, Kuramoto S, Ovid'ko IA, Skiba NV. Int J Plast, (2008), p.24-1333.

[15] R.J. Talling, R.J. Dashwood, M. Jackson, D. Dye, On the mechanism of superelasticity in gum metal, Acta Mater, V. 57, (2009), p. 1188–1198.

[16] M. Tane, T. Nakano, S. Kuramoto, M. Niinomi, N. Takesue, H. Nakajima, X Transformation in cold-worked Ti–Nb–Ta–Zr–O alloys with low bodycentered cubic phase stability and its correlation with their elastic properties, Acta Mater, V.61, (2013), p. 139–150.

[17] H.Y. Kim, L. Wei, S. Kobayashi, M. Tahara, S. Miyazaki, Nanodomain structure and its effect on abnormal thermal expansion behavior of a Ti–23Nb–2Zr–0.7Ta–1.2O alloy, Acta Mater, V. 61. (2013). P. 4874–4886.

[18] X. Mao, Titanium Microalloyed Steel: Fundamentals, Technology, and Products, (2007), p. 2-57.

[19] W. Sha and S. Malinov, Titanium alloys: modelling of microstructure, properties and applications, (2009), p. 1-258.

[20] G. Lütjering and J. C. Williams, Titanium 2nd edition, (2007), p. 175-337.

[21] C. Leyens and M. Peters, Titanium and Titanium Alloys Fundamentals and Applications, (2003), p.1-230.

[22] Boyer, R. Materials properties handbook titanium alloys. Materials Park, OH: ASM International. (1994).

[23] ASM Material Data Sheet. (n.d.). Retrieved May 22, 2016, from http://asm.matweb.com/search/SpecificMaterial.asp?bassnum=MTP641

[24] Guo, W., Quadir, M., Moricca, S., Eddows, T., & Ferry, M. Microstructural evolution and final properties of a cold-swaged multifunctional Ti–Nb–Ta–Zr–O alloy produced by a powder metallurgy route. Materials Science and Engineering: A, (2013) 206-216.

[25] T.Furuta, S.Kuramoto, J.H.Hwang, K.Nishino, T.Saito, Elastic deformation behavior of multi-functional Ti–Nb–Ta–Zr–O alloys, Materials Transactions, Vol. 46, (2005), p.3001-3007.

[26] C. E. Guillaume, Proc. Phys. Soc, Vol. 32, (1920), p. 374.

[27] Y. Nakamura, IEEE Trans. Magn, Vol. 12, (1976), p. 278.

[28] T.Furuta, S.Kuramoto, R.Chen, J.H.Hwang, K.Nishino, T.Saito, M.Ikeda, Effect of oxygen on phase stability and elastic deformation behavior in Gum Metal, Journal of the Japan Institute of Metals, Vol. 70, (2006), p. 579-585.

[29] H. Ikehata, N.Nagasako, T. Furuta, A. Fukumoto, K. Miwa, and T. Saito, First-principles calculations for development of low elastic modulus Ti alloys, Phys. Rev. B 70, (2004).

[30] H. Ikehata, N. Nagasako, S. Kuramoto, and T. Saito, Designing New Structural Materials Using Density Functional Theory: The Example of Gum Metal, V. 31, (2006), p. 688-692.

[31] M. Morinaga, A Quantum Approach to Alloy Design, Materials Today, (2019), p. 19-94.

[32] Y. Yi, L. Geping, W. Songquan, L. Yulan, Y. Ke, Progress in Research of Gum Metal, V. 25, (2011).

[33] S. Shin, C. Zhang, K. S.Vecchio, Phase stability dependence of deformation mode correlated mechanical properties and elastic properties in Ti-Nb gum metal, V. 702, (2017), p. 173-183.

[34] M.Abdel-Hady, K. Hinoshita and M. Morinaga, General approach to phase stability and elastic properties of b-type Ti-alloys using electronic parameters, Scripta Mater, V. 55, (2006), p. 477-480.

[35] R.J. Talling, R.J. Dashwood, M. Jackson, S. Kuramoto and D. Dye, Determination of (C11-C12) in Ti–36Nb–2Ta–3Zr–0.3O (wt.%) (Gum metal), Scripta Mater, V. 59, (2008), p. 669-672.

[36] T. Li, J. W. Morris, Jr., N. Nagasako, S. Kuramoto, and D. C. Chrzan, "Ideal" Engineering Alloys, Phys. Rev. Lett. 98, (2006), p. 105503.

[37] J. Hwang, S. Kuramoto, T. Furuta, K. Nishino, and T. Saito, Phase-Stability Dependence of Plastic Deformation Behavior in Ti-Nb-Ta-Zr-O Alloys, V. 14, (2005), p. 747-754.

[38] S. Hanada, O. Izumi, Met. Trans. A, V. 17A, (1986), p. 1409.

[39] J.G. Niu, W.T. Geng, Oxygen-induced lattice distortion in β-Ti_3Nb and its suppression effect on β to α" transformation, Acta Mater, V. 81, (2014), p. 194-203.

[40] E.W. Collings, The Ph Physical Metallurgy of Titanium Alloys, ASM, Metals Park, O. H (1984).

[41] P. Castany, M. Besse, T. Gloriant, Dislocation mobility in gum metal b-titanium alloy studied via in situ transmission electron microscopy, Phys. Rev. B, V. 84, (2011), p. 020201.

[42] E. Plancher, C.C. Tasan, S. Sandloebes, D. Raabe, On dislocation involvement in Ti–Nb gum metal plasticity, Scripta Mater, V. 68, (2013), p. 805–808.

[43] Guo WY, Xing H, Sun J, Li XL, Wu JS, Chen R. Metall Mater Trans A, (2008), p. 672.

[44] E. Withey, M. Jin, A. Minor, S. Kuramoto, D.C. Chrzan, J.W. Morris Jr., The deformation of ''Gum Metal" in nanoindentation, Mater. Sci. Eng., A 493, (2008), p. 26–32.

[45] H. Xing, J. Sun, Q. Yao, W.Y. Guo, R. Chen, Origin of substantial plastic deformation in gum metals, Appl. Phys. Lett., V. 92, (2008), 151905.

[46] Yang Y, Wu SQ, Li GP, Li YL, Lu YF, Yang K, Ge P. Acta Mater, Evolution of deformation mechanisms of Ti–22.4Nb–0.73Ta–2Zr–1.34O alloy during straining, V. 58, (2010) p. 2778-2787.

[47] R. Talling, M. Jackson, R. Dashwood, D. Dye, Deformation of Ti–36Nb–2Ta–3Zr–0.3O (Gum Metal), in: M. Ninomi, S. Akiyama, M. Ikeda, M. Hagiwara, K. Maruyama (Eds.), Titanium-2007 Science and Technology, The Japanese Institute of Metals, Sendai, (2007), p. 631–634.

[48] M. Besse, P. Castany, T. Gloriant, Mechanisms of deformation in gum metal TNTZ-O and TNTZ titanium alloys: a comparative study on the oxygen influence, Acta Mater, V. 59, (2011), p. 5982–5988.

[49] T. Yano, Y. Murakami, D. Shindo, S. Kuramoto, Study of the nanostructure of Gum Metal using energy-filtered transmission electron microscopy, Acta Mater, V. 57, (2009), p. 628–633.

[50] J.W. Morris Jr, Y. Hanlumyuang, M. Sherburne, E. Withey, D.C. Chrzan, S. Kuramoto, Y. Hayashi, M. Hara, Anomalous transformation-induced deformation in <110> textured gum metal, Acta Mater, V. 58, (2010), p. 3271–3280.

[51] E.A. Withey, A.M. Minor, D.C. Chrzan, J.W. Morris Jr, S. Kuramoto, The deformation of gum metal through in situ compression of nanopillars, Acta Mater. 58 (2010) 2652–2665.

[52] T. Yano, Y. Murakami, D. Shindo, Y. Hayasaka, S. Kuramoto, Transmission electron microscopy studies on nanometer-sized x phase produced in gum metal, Scripta Mater. 63 (2010) 536–539.

[53] M. Tane, T. Nakano, S. Kuramoto, M. Hara, M. Niinomi, N. Takesue, T. Yano, H. Nakajima, Low Young's modulus in Ti–Nb–Ta–Zr–O alloys: Cold working and oxygen effects, Acta Mater. 59 (2011) 6975–6988.

[54] H. Xing, J. Sun, Mechanical twinning and omega transition by <111> 112 shear in a metastable beta titanium alloy, Appl. Phys. Lett. V. 93, (2008), p. 031908.

[55] Yang Y, Li GP, Cheng GM, Wang H, Zhang M, Xu F, Yang K. Scripta Mater,V. 58, (2008), p. 9.

[56] D. Vanderbilt, Phys, Rev. B, Vol. 41, (1990), p. 7892.

[57] K. Laasonen, A. Pasquarello, R. Car, C. Lee, D. Vaderbilt, Phys, Rev. B, Vol. 47, (1993), p. 10142.

[58] P. Hohenberg, W. Kohn, Phys. Rev, Vol. 136, (1964), B864.

[59] W. Kohn, L. J. Sham, Phys, Rev, Vol. 140, (1965), A1133.

[60] C.R. Krenn, D. Roundy, J. W. Morris Jr., M. L. Cohen, Mater, Sci. Eng. A, Vol. 319-321, (2001), p. 111.

[61] S.Kuramoto, T.Furuta, J.H.Hwang, K.Nishino, T.Saito, EBSP analysis on microstructure of gum metal after plastic deformation, Journal of the Japan Institute of Metals, Vol. 69, (2005), p. 952-961.

[62] Gutkin MY, Ishizaki T, Kuramoto S, Ovid'ko IA, Skiba NV. Int J Plast, (2008), p.1333-1359.

[63] Mitsuo Niinomi, Encyclopedia of Biomedical Engineering, (2019), p.213-224.

[64] M.J. Lai, C.C. Tasan, J. Zhang, B. Grabowski, L.F. Huang and D. Raabe, Origin of shear induced β to ω transition in Ti–Nb-based alloys, Acta Mater, V. 92 (2015), p. 55-63.

[65] A. Gysler, G. Lütjering, V. Gerold, Deformation behavior of age-hardened Ti–Mo alloys, Acta Metall, V. 22 (1974), p. 901–909.

[66] Hong-Chao Kou, Han-Lei Zhang, Yu-Dong Chu, Dong Huang, Hai Nan, Jin-Shan Li. , Microstructure Evolution and Phase Transformation of Ti-6.5Al-2Zr-Mo-V Alloy During Thermohydrogen Treatment, Acta Metallurgica Sinica(English Letters), V. 28, (2015), p. 505-513.

[67] M.J. Lai**, C.C. Tasan*, D. Raabe, On the mechanism of {332} twinning in metastable b titanium alloys, Acta Meter, V.111, (2016), p. 173-186.

[68] S. Hanada, O. Izumi, Correlation of tensile properties, deformation modes, and phase stability in commercial β phase titanium alloys, Metall. Trans, V. 18, (1987) p. 265-271.

[69] M.M. Gasik, H. Yu, Phase Equilibria and Thermal Behaviour of Biomedical Ti-Nb-Zr Alloy, 17th Plansee Seminar, Vol. 1, (2009), p. 2-5.

[70] M.M. Gasik, H. Yu, Phase equilibria and thermal behaviour of biomedical Ti-Nb-Zr alloy, V. 1, (2009).

[71] R. T. Qu & Z. F. Zhang, A universal fracture criterion for high-strength materials, Chinese Academy of Sciences, (2013), p. 5.

[72] W. D. Callister, D. G. Rethwisch, Fundamentals of Materials Science and Engineering: An Integrated Approach, 9th Edition, (2013), p. 217-250.

[73] Zhang YT, Qi DX, Gao J, Huang T. Int J Eng Sci, V. 46, (2008), p. 1077.

[74] R.Kapoor, Materials Under Extreme Conditions, Ch. 20, Severe Plastic Deformation of Materials, (2017), p. 717-754.

[75] E.L. Pang, E.J. Pickering, S.I. Baik, D.N. Seidman, N.G. Jones, The effect of zirconium on the omega phase in Ti-24Nb-[0e8]Zr (at.%)alloys, Acta Meter, V. 153, (2018), p. 62-70.

[76] D. E. Laughlin and K. Hono, Physical Metallurgy (Fifth Edition), Recovery and Recrystallization: Phenomena, Physics, Models, Simulation, V. 3, (2014), p. 2291-2397.

[77] N.Claussen, A.H.Heuer, Concise Encyclopedia of Advanced Ceramic Materials, Transformation Toughening, (1991), p. 494-497.

[78] Yang Y., 2, Li G., Wu S, Li Y, Yang K, Effect of Nb content on flow behavior of Ti-Nb-0.7Ta-2Zr-1.4O alloy during cold compression, The Chinese Journal of Nonferrous Metals, V. 20, (2010), p. 495-499.